Thomas Auer

The Electron-Nuclear Spin System in (In,Ga)As Quantum Dots

The Electron-Nuclear Spin System in (In,Ga)As Quantum Dots

Dissertation

presented to the Faculty of Physics
of the
Technische Universität Dortmund, Germany,
in partial fulfillment of the requirements
for the degree of Doktor rer. nat.

presented by

Thomas Auer

Dortmund, September 2008

Accepted by the Faculty of Physics
of the
Technische Universität Dortmund, Germany.

Day of the oral exam: 29th August 2008

Examination board: Prof. Dr. Manfred Bayer
Prof. Dr. Metin Tolan
Prof. Dr. Bernhard Spaan
Dr. Ilya Akimov

Contents

1 Introduction

1.1 Overview

The objects studied in this work are so called semiconductor *quantum dots*. The method used to study them is *optical spectroscopy*.

Giving the most general definition, a quantum dot is an artificially fabricated semiconductor solid state formation which provides a three dimensional confinement for charge carriers. In semiconductors these charge carriers are electrons and so called "holes". When illuminating a *bulk* semiconductor with laser light of energy above the band gap of the semiconductor, the photon's energy may be absorbed by valence band electrons which are then excited to the energetically higher conduction band. The electron leaves a vacancy in the valence band, the hole. The hole is positively charged with respect to its electronic surrounding. Due to the Coulomb attraction between the electron and the hole, the electron-hole pair may form a bound state, the "exciton".

Electrons, holes or pairs of them can be filled into quantum dots and kept there. Due to the quantum dot's confinement potential which restricts the movement of the carriers in all three spatial dimensions on a nanometre scale, quantum dots are also referred to as zero dimensional semiconductor structures. In quantum dots, the dimensions of the confinement region become comparable to the de-Broglie-wavelength of the trapped carriers. Therefore, inescapably quantum mechanical effects have to occur. The most important consequence of the zero dimensionality of quantum dots is the existence of discrete energy levels of the contained carriers. If a conduction band electron and a valence band hole occupy discrete quantum dot energy levels, the electron may consequently recombine with the hole under emission of a photon of well-defined energy.

First observations of such quantum size effects have been made in semiconductor microcrystals in the early and mid eighties [1–4]. Later, arrays of quantum dots were fabricated by self organised growth. In this work I study ensembles of such self-assembled quantum dots which in our case consist of indium arsenide (InAs) embedded in gallium arsenide (GaAs). In ensembles of quantum dots grown by self organised assembling the intrinsic quantum dot properties like the emission of well-defined wavelength are hidden in the ensemble emission which is broadened due to the fluctuations, predominantly in size, of the self-assembled quantum dots. In the early nineties, however, discrete emission lines from single self-assembled quantum dots were discovered for the first time [5, 6].

Since then quantum dots have inspired a huge amount of work and a lot of effort has been made in order to understand the phenomena related to quantum dots. Quantum dots have gained interest of the physical community due to two reasons:

(i) Quantum dots are particularly suitable to produce quantum opto-electronic devices [7]. As man made structures the properties of quantum dots can be relatively easily tailored in order to meet specific requirements concerning e. g. the emission energy. Furthermore, they are stable and safely embedded inside their crystal. The samples are easy to handle and can thus be easily incorporated in technical devices. The macroscopic samples allow the experimentalist to conveniently study the quantum dots in a well defined manner, optically or electrically excite them, fill them with a fixed number of electrons and holes, create elementary excitations inside them and keep these excitations in the dot, expose them to electric or magnetic fields and put them into environments of defined temperature. The progress that has been made in the last 15 years empowers physicists now to produce structures with several quantum dots arranged in a well defined manner so that coupled quantum dots emerge which can possibly interact with one another, and to embed quantum dots e. g. into microresonators which allows to control the spontaneous photon emission rate of the quantum dots. The fact that the behaviour of charge carriers inside a quantum dot is governed by quantum theory makes it an ideal candidate for the future technology of devices exploiting the quantum nature of the nano-world. Examples are single photon emitters with defined photon energy, quantum cryptography by quantum mechanically entangled photons, information storage by using the spin of electrons trapped inside a quantum dot as a "qubit" and in the future possibly even the realisation of quantum dot based quantum gates as a first step to nano scale semiconductor based quantum information processing.

(ii) On the other hand, quantum dots are interesting by themselves as objects which can be exploited in order to study fundamental physics and to search for new physical phenomena. To have with quantum dots an isolated quantum mechanical object at hand enables scientists to study processes like light-matter interaction, spin related phenomena and electro-magnetic field induced phenomena.

Optical spectroscopy is one of the major experimental means to study quantum dots. In the case of a quantum dot sample, electron-hole pairs can be optically excited in the bulk material in which the quantum dots are embedded. An electron-hole pair can become trapped by the quantum dot potential. The carriers quickly relax to the lowest energy level of the quantum dot, the quantum dot ground state. From there, the electron recombines with the hole under reemission of a photon having the energy of the quantum dot electron-hole ground state transition energy. The light emission from the quantum dots, the photoluminescence, can be detected and used in order to investigate processes occurring with the spin and charge carriers inside the quantum dots. The photolumines-

cence may be studied in dependence on many parameters which influence the behaviour of the carriers, such as excitation density, temperature or magnetic field. Additionally, the photoluminescence can be studied time resolved in order to obtain inside into the dynamics of the radiative decay.

Despite the fact, that single electrons, holes or elementary excitations as electron-hole pairs may be kept inside a quantum dot, the dot yet is composed out of thousands of atoms. They are regularly arranged in the quantum dot lattice which is in turn embedded inside a crystal with different properties. This leads e. g. to the interaction with elementary crystal excitations, phonons. In addition, the nucleus of each atom constituting the quantum dot generally inheres a nuclear spin. Already in the simplest atom, the hydrogen atom, the energy of the electron is influenced by the interaction between the electron spin and the spin of the nucleus. This hyperfine interaction is also present in quantum dots where the interaction between the spin of an electron inside the quantum dot and the entirety of the nuclear spins leads to various effects.

In the seventies it was already shown that for bulk semiconductors the nuclear spins in the vicinity of a a donor trapped electron may be polarised by transfer of angular momentum from the optically oriented electron [8–11]. It was observed that the electron spin and the nuclear spins are highly interdependent. Polarised nuclear spins create a magnetic field acting on the electron spin. In turn, they may themselves be influenced by small external magnetic fields. This inspired measurements where the dependence of the nuclear spin system on small external fields was exploited in order to reveal the processes occurring in the electron-nuclear spin system. The spin of the electrons was used as a sensitive detector for the state of the nuclear spin system [12–16].

In quantum dots the hyperfine coupling between electron and nuclear spins is further enhanced by the localisation of the electron in the dot. The aim of keeping a well defined spin state of the electron for a long time inside a quantum dot in order to use it e. g. for quantum information storage and processing was amongst other mechanisms hindered by the interaction of the electron spin with the randomly fluctuating nuclear spins [17, 18]. However, it could be shown that the nuclei do not only act destructively on the electron spin. Also in quantum dots the nuclear spins may be optically oriented. As each nuclear spin produces a magnetic field, the magnetic field of the sum of many oriented nuclear spins may be as large as several Tesla [19–23]. Such a strongly polarised nuclear spin system with a macroscopically large total spin can depress the electron spin relaxation and support long living electron spin polarisation in a quantum dot [24–26].

It was also shown that in a strong transverse external magnetic field in which the electron spins precess the nuclear spin system of the quantum dots in a ensemble is driven into a configuration so that the g-factor of electrons in different quantum dots is altered in a way that all electrons precess in phase ("mode locking", [27, 28]). This state of the nuclear spin system is very stable and lasts for hours [29]. While the general trend in the quantum dot community was going

towards single dot spectroscopy, this work also pointed out what great potential still lies in the use of quantum dot ensembles.

It might be possible to manipulate the nuclear spin system of quantum dots in a manner that magnitude and direction of the magnetic field produced by the nuclear spins inside could be controlled – optically and by application of small external magnetic fields. In doing so, the quantum dot could be turned into a "nuclear nanomagnet" [30] – a nanometer sized object containing a large magnetic field. This would open new possibilities concerning the tailoring of the environment the electron inside a quantum dot experiences.

It is thus important to obtain further insight into the complex interplay between a single electron spin and the nuclear spin system, not only in single quantum dots but also in quantum dot ensembles. With this work I wish to make a contribution to this task. We investigate the electron-nuclear spin system of the nuclear spin entirety and the spin of a single electron in quantum dots of an ensemble sample by optical means. We exploit optical orientation to polarise the electron and the nuclear spins. The electron spin polarisation is then used as a detector for the state of the nuclear spin system. The read out of the electron spin polarisation is performed measuring the circular polarisation of the photoluminescence.

In this chapter an introduction about quantum dot fabrication and the properties of quantum dots is given. In chapter 2 the studied samples are introduced and characterised. Chapter 3 contains the theoretical and experimental fundamentals of optical orientation of electron and nuclear spins and the introduction into the codependencies in the electron-nuclear spin system. The experimental setup of our experiments, schemes for excitation and detection and definitions and conventions used are described in chapter 4. The chapters containing the obtained results address two aspects of the electron-nuclear spin system: on the one hand the internal magnetic fields characterising the system and on the other hand the dynamics. In chapter 5 the internal magnetic fields acting on the nuclear spins are determined. The maximum nuclear polarisation is calculated using the measured values. Chapter 6 contains studies of the excitation power dependence of the nuclear polarisation and its behaviour in magnetic fields up to 1 T. In chapter 7 the accumulation dynamics of electron and nuclear spin polarisation are studied. Finally, chapter 8 presents the observation of hundreds of millisecond long spin memory times of the electron-nuclear spin system. These results are interpreted in terms of a self-consistent electron-nuclear spin complex in which the polarised electron spin and the nuclear spin ensemble mutually stabilise each other, the nuclear spin polaron.

1.2 Self-Assembled Semiconductor Quantum Dots

1.2.1 Fabrication of Self-Assembled Semiconductor Quantum Dots

As "quantum dot" is a general term for solid state structures which provide three dimensional confinement for electrons and holes, it compasses objects consisting of many different material systems and fabricated using various techniques, among them

- "natural quantum dots", isolated potential minima due to interface fluctuations in quantum well structures [31, 32].
- semiconductor lateral quantum dots, quantum dots obtained by patterning quantum well structures using electron beam lithography or wet chemical etching [33, 34].
- semiconductor nanocrystals, produced e. g. by precipitation out of organic liquids or incorporation in glasses [35–38].
- quantum dots obtained by cleaved-edge overgrowth, a method where by alternately growing quantum wells and cleaving the sample two quantum wires are produced at the intersection of which a single quantum dot is formed [39].

In the present work, I study *self-assembled* quantum dots grown in the Stranski-Krastanov mode [40] by molecular beam epitaxy. In the Stranski-Krastanov growth mode a thin layer is deposited on a host crystal of a different substance. From that layer islands form spontaneously [41]; it is therefore also known as "layer-plus-island" growth. In the case of the quantum dots studied here, the host crystal is composed of GaAs. On this substrate InAs is deposited monolayer by monolayer. The lattice constants of GaAs and InAs[1] differ by ≈ 7 %. The InAs monolayers are deposited so slowly that the InAs adopts the lattice structure of the substrate. This leads to a strain in the InAs layer which grows with increasing layer thickness. At a certain thickness of the InAs deposit, the point is reached where the strain energy due to the lattice mismatch becomes so large that it is energetically more favourable for a part of the InAs to form "islands" on the surface of the remaining InAs film. This InAs layer between the substrate and the islands is called "wetting layer". Figure 1.1 (a) schematically depicts the strain relaxation. The island formation occurs spontaneously which is why we speak of self organised quantum dots. For InAs quantum dot samples the wetting layer is typically three to five monolayers in thickness corresponding to ≤ 2 nm.

[1] Lattice constant InAs 6.0583 Å, GaAs 5.65325 Å at 300 K.

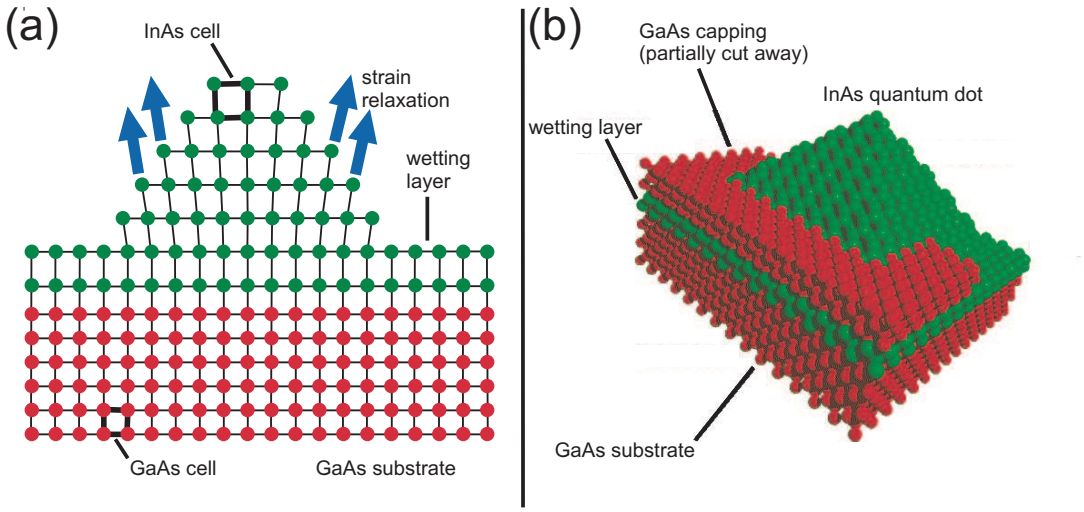

Figure 1.1: (a) Quantum dot formation from a strained epitaxial layer. InAs has a larger lattice constant than GaAs. The strain building up during the epitaxial deposition of InAs on the GaAs substrate is relaxed by the formation of InAs islands on a "wetting layer". (b) Composition of a self-assembled quantum dot sample. On a GaAs substrate a two dimensional InAs wetting layer is located on which the quantum dots form. On top a GaAs capping is grown (Picture: Materials Modelling Group, Newcastle University, UK.)

The indium islands are tens of nanometers in diameter and a few nanometers high and thus have the proper dimensions to evoke quantum effects. The crucial step to finally turn them into quantum dots is overgrowing the InAs islands with a capping layer of GaAs. InAs has a smaller band gap than GaAs so that sandwiching the InAs islands between GaAs brings about that they constitute potential minima in which charge carriers can be stored. Figure 1.1 (b) shows a model which illustrates the composition of a quantum dot and figure 1.2 (a) shows a transmission electron micrograph of a single quantum dot. In figure 1.2 (b) a micrograph of an InAs/GaAs quantum dot ensemble is shown. One can clearly see that the self assembling results in a non-uniformly distributed quantum dot array. Also the size obviously fluctuates from dot to dot.

Technically, the Stranski-Krastanov growth mode can be realised by molecular beam epitaxy (MBE) [42]. The layers are deposited extremely slowly in a high vacuum on a waver which is held at a high temperature – ≈ 600°C for the sample under study – so that *epitaxial* growth occurs. This means that the deposited material adopts the lattice structure of the substrate. The ultra pure elements, indium and arsenic, are separately evaporated by heating and do only react with each other when the vapours condense on the surface of the substrate. Like this, smooth defect free InAs monolayers are formed. Consequently, also the quantum dots emerging from the wetting layer are defect free when the growth

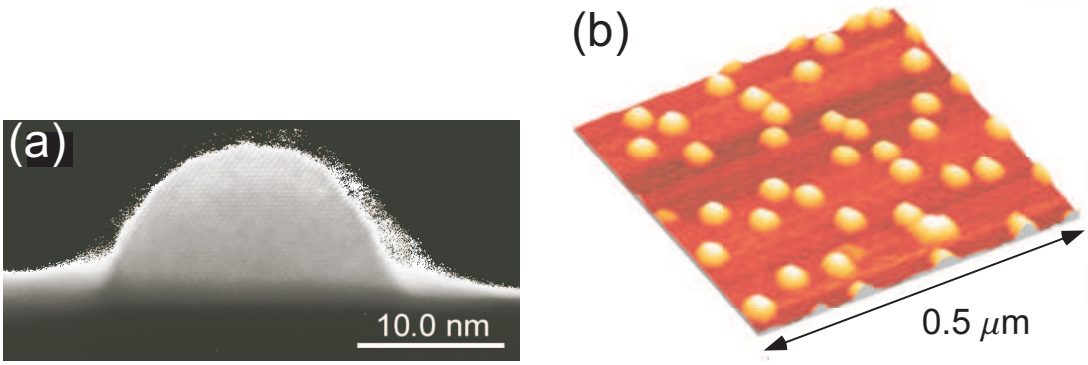

Figure 1.2: (a) Transmission electron micrograph of a single InAs/GaAs quantum dot (microscopy by J.P. McCaffrey, NRC Ottawa). (b) Micrograph of an InAs self-assembled quantum dot ensemble before capping. Note the non-uniform distribution and the fluctuations in size (Picture: A. Wieck, Angewandte Festkrperphysik, Ruhr-Universitt Bochum).

is terminated betimes.

Self-assembled quantum dots where produced from several III/IV semiconductor material systems[2]: In(Ga)As/GaAs, InP/InGaP, GaSb/GaAs, InSb/GaSb, (Si)Ge/Si, InAs/Si and InAlAs/AlGaAs[3]. Stranski-Krastanov growth has also been achieved for a number of II/VI semiconductors as (Zn)CdSe/ZnSe.

1.2.2 General Properties of Self-Assembled Quantum Dots and Thermal Annealing

The quantum dot arrays produced by strain induced self assembling typically exhibit a quantum dot density of $10^{10}/\mathrm{cm}^{-2}$ to $10^{11}/\mathrm{cm}^{-2*}$ corresponding to an average inter dot distance of 30 nm to 100 nm. The quantum dots are in the range of 10 nm to 30 nm in diameter and $\approx$ 5 nm high. However, during the formation of the quantum dots inevitably size fluctuations occur in the ensemble. The size distribution cannot be properly controlled, the typical size dispersion being $\approx$ 10 %. Quantum dots may be lens shaped, pyramidal or have the shape of a truncated pyramid. The shape and size of quantum dots can in fact be accurately determined using atomic force microscopy before the capping layer is deposited. They change, however, dramatically during the capping. Diffusion between the InAs islands and the GaAs capping occurs which changes the size, the shape and the composition of the quantum dots [7, 43]. InAs grown quantum dots therefore generally contain a significant fraction of GaAs which is why they

[2]The roman numbers refer to the main groups in the periodic table the elements belong to.

[3]See [7] and the references therein.

*Quantum dot ensembles locally having dot densities down to $10^{8}/\mathrm{cm}^{-2}$ have been produced using stationary instead of rotating substrate wavers in order to enable single dot spectroscopy.

are referred to as (In_x,Ga_{1-x})As quantum dots where x gives the indium fraction. The main characteristics of a quantum dot is the energy gap between the lowest electron state in the conduction band and the lowest hole state in the valence band. This transition energy determines the energy of the emitted photoluminescence. The transition energy is influenced both by the size of the quantum dot due to the size quantisation and by the gallium content due to the different band gaps of GaAs and InAs. The dispersion in quantum dot size and the possibly different composition of different dots leads to an inhomogenous broadening of the ensemble emission. Furthermore, the local distribution of gallium and indium inside a dot has a profound effect on the form and the localisation of the carrier wavefunctions inside the quantum dot. The basic quantum dot parameters, indium concentration, shape and size, strongly depend on the growth conditions, mainly growth temperature and deposition rate.

To date the epitaxial growth mode represents the best method to incorporate quantum dots in a wide range of structures and devices, such as microresonators. As an impressive example micro tube ring resonators may serve which were recently fabricated by letting a strained two dimensional quantum dot layer roll up to form a three dimensional tube with a diameter of a few micrometer and a wall thickness of 200 nm [44].

Furthermore, self-assembled quantum dots possess a large confinement potential of up to hundreds of milli-electronvolt. The intraband level spacing between ground state and first excited state is in the range of tens of milli-electron volt.

Additionally, the quantum dot transition energy may be tuned by so called *thermal annealing*. After the growth is finished, the sample is exposed to a high temperature for a well-defined time. This leads to a secondary interdiffusion between InAs from the quantum dots and the GaAs substrate and capping. The gallium content of the quantum dots increases which in turn decreases the confinement potential. We define the confinement potential as the energy difference between the wetting layer and the ground state. Generally, the emission shifts to higher energies with increasing annealing temperature [45]. By choosing different temperatures and exposition times, from the same sample a series with different confinement potentials can be produced. Figure 1.3 shows the annealing series to which the sample mainly studied in this work belongs. The emisson energies span a range of 360 meV between 1.063 eV (1166 nm) for the unannealed sample up to 1.422 eV (872 nm) for an annealing temperature of 980°C. Using this definition, the confinement potentials range from $\approx$ 250 meV for the unannealed sample to $\approx$ 80 meV for the sample annealed at 980°C. The grey spectrum in figure 1.3 belongs to the sample studied in this work. This band gap engineering and the fact that a lot of different materials are suitable in order to produce self-assembled quantum dots, leads to a wide span of emission wavelength between 300 nm and 1.5 μm [43]. Another effect of the thermal annealing is that the quantum dots become more homogeneous in size. This can be seen by a narrowing of the inhomogeneously broadened ensemble emission peaks which can also been observed for the annealing series of figure 1.3.

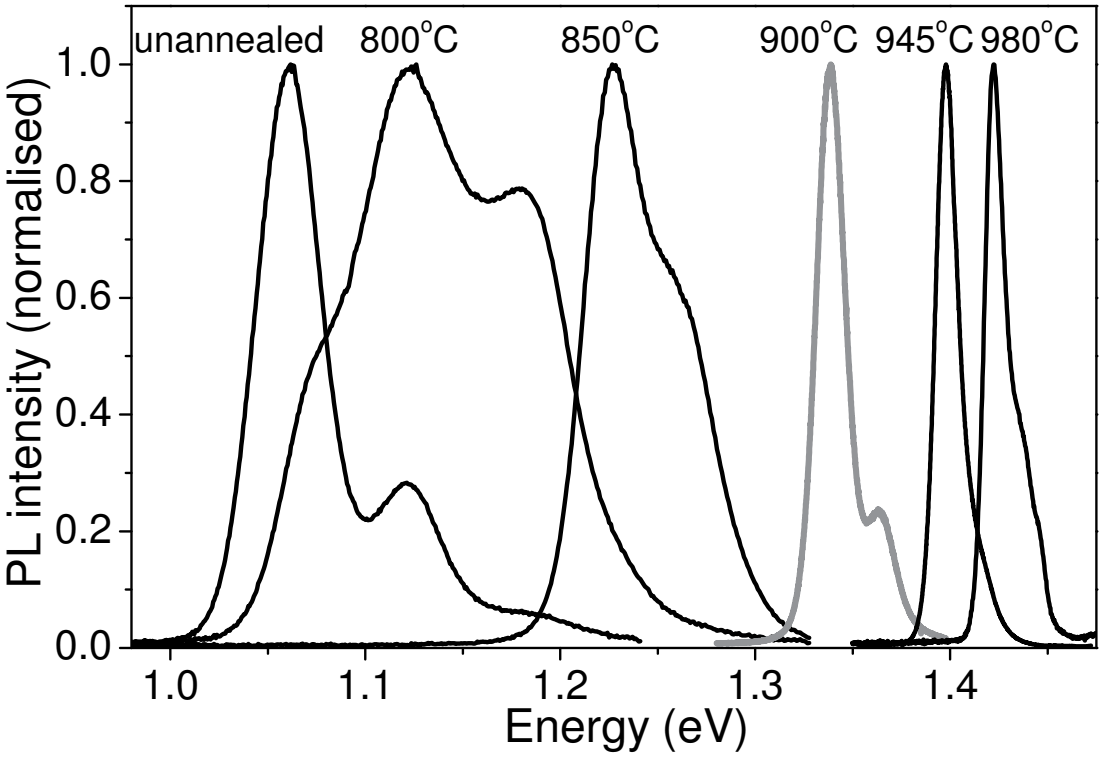

Figure 1.3: Photoluminescence of singly negatively charged quantum dot ensembles annealed at different temperatures after growth. Grey: The spectrum of the sample studied in this work.

1.3 Elementary Excitations in Quantum Dots

1.3.1 Excitons

Whenever the movement of particles is locally restricted to a scale comparable to their de-Broglie-wavelength this inevitably evokes quantum effects. Particularly, the density of states $D(E)$ of the particles becomes discretised. $D(E)$ expresses the number dN of states which are available per energy interval dE in a certain system, i. e. $D(E) = dN/dE$. In three dimensional structures the density of states of a free electron gas of non-interacting electrons is $\propto \sqrt{E}$ whereas in zero dimensional structures like quantum dots it is $\propto \sum_{l,m,n} \delta(E - E_{n,m,l})$ where $E_{n,m,l}$ are the energy levels of the single electron. $D(E)$ is depicted in figure 1.4 for the three dimensional and the zero dimensional case. The most prominent property of quantum dots thus is the fact that carriers inside them can only populate discrete energy levels due to the three dimensional confinement. In this chapter we will discuss the states of electrons and holes in quantum dots arising as a consequence of this size quantisation.

The bound state consisting of an electron in the conduction band and a hole in

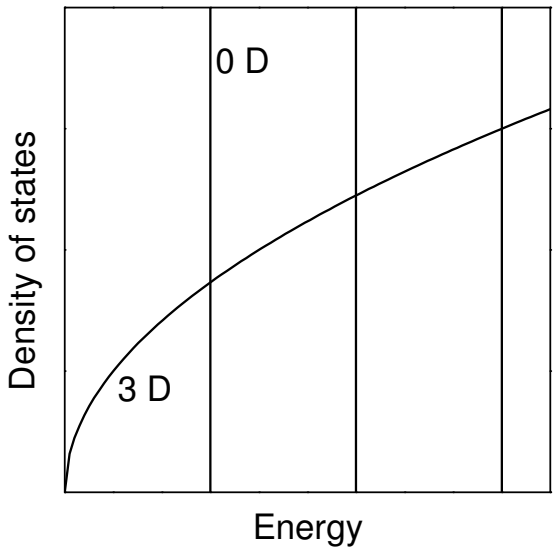

Figure 1.4: Density of states for a free electron gas per unit volume. Unrestricted translation ("three dimensional") and three dimensional confinement ("zero dimensional", vertical lines).

the valence band populating the discrete quantum dot energy levels is called an "exciton". The discrete energy levels of the quantum dot states are mainly governed by the size quantisation. We thus first determine the single particle states arising from the three dimensional confinement taking the rotational symmetry of the quantum dots into account. The exciton states can then be constructed from the single particle electron and hole states obtained in this way. Finally, we address the exciton finestructure induced by a reduction of the rotational quantum dot symmetry or the application of external magnetic fields.

In a first approach we can start to construct the quantum dot single particle electron and hole states on the basis of the quantum dot's symmetry[4]. Self-assembled quantum dots generally approximately display rotational symmetry[5]. Later we will discuss how the energy levels are altered when the rotational symmetry is partly broken. The height of the quantum dots is considerably smaller than their lateral extensions leading to a big confinement along the growth axis (the z axis) and a smaller in-plane confinement. The z and in-plane energies, E_z and E_{xy}, can thus be separated. The energies of the discrete states are then given by the two contributions

$$E = E_z + E_{xy}\,. \tag{1.1}$$

The confinement in z direction is so big that generally only one state fits in the quantum dot potential and thus only the lowest E_z state contributes to the quantum dot energy levels. The in-plane confinement can be approximated by a

[4]Derivation along the lines of [43].

[5]This can be verified analysing atomic force micrographs taken before capping. Although the capping process can alter the shape and the size of the quantum dots, the rotational symmetry of the quantum dots is still a good assumption to start with.

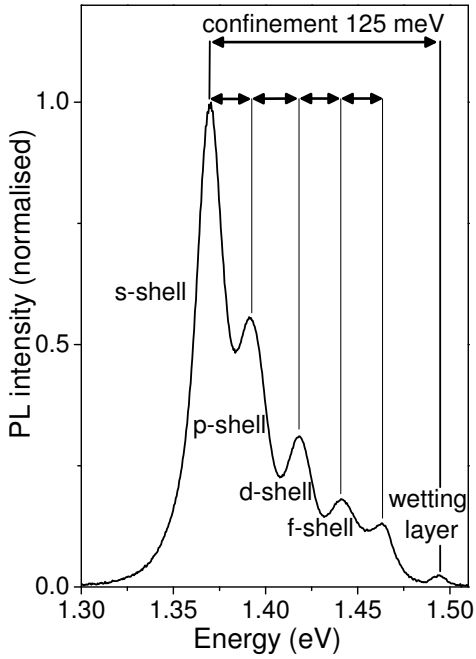

Figure 1.5: PL of a quantum dot ensemble for high excitation densities. Shell filling leads to emission from higher shells besides the ground state emission from the s-shell. Five shells fit into the quantum dot potential. The energy separation between the shells is approximately equidistant. The confinement is defined by the energetic distance between the wetting layer and the s-shell.

parabolic potential

$$V(r) = \frac{1}{2} m\omega^2 (x^2 + y^2) \tag{1.2}$$

leading to energy levels corresponding to a harmonic oscillator with the well known equidistant energy levels. That this assumption is justified is supported by the experimental finding that the energy spacing of the quantum dot energy levels is also equidistant. This can be seen in figure 1.5 which shows a photoluminescence spectrum of a quantum dot ensemble where several shells can be observed having approximately the same energy distance.

Due to the rotational symmetry, the in-plane energies can be characterised by a radial quantum number n_r and an orbital momentum quantum number n_φ, which leads to the energy eigenvalues of the quantum dot

$$\begin{aligned} E &= \hbar\omega(n+1) \\ &= \hbar\omega(2n_r + |n_\varphi| + 1)\,. \end{aligned} \tag{1.3}$$

Analogously to the atomic shell model, the states $|n, n_\varphi\rangle$ are then defined by the shell index $n = 2n_r + |n_\varphi| = 0, 1, 2, \ldots$ and the orbital angular momentum quantum number $n_\varphi = 0, \pm 1, \pm 2, \ldots$. Generally, the shells in quantum dots are labeled like in atomic physics by shell indices s,p,d,f,... corresponding to the angular momentum quantum numbers $0, \pm 1, \pm 2, \ldots$. Including the spin degree of freedom, the shell degeneracy is $2(n+1)$. The filling of the shells obeys the Pauli exclusion principle so that a state with else identical quantum numbers can only contain two carriers of opposite spin. The s-shell consequently may contain

two carriers, the p-shell four. The difference to atomic shells where the p-shell can be filled with six electrons is due to the reduced symmetry between z and in-plane direction.

Neglecting the Coulomb interaction, from the single particle electron and hole states the exciton states can be composed as electron-hole pair states

$$|eh\rangle = |n_e, n_{\varphi,e}\rangle |n_h, n_{\varphi,h}\rangle \,. \tag{1.4}$$

However, optical selection rules restrict the possible electron-hole state combinations which are optically active, i. e. which can be excited by absorption of a photon or decay radiatively under emission of a photon. The valence band has a p-type symmetry whereas the conduction band has a s-type symmetry. When an electron recombines with a hole, the angular momentum difference between the conduction and the valence band is carried over by the spin of the emitted photon. Therefore, the total orbital angular momentum of the decaying electron-hole pair state has to be zero, $n_{\varphi,e} + n_{\varphi,h} = 0$. Additionally, $n_e = n_h$ has to be fulfilled. Thus, there exist exciton states which are optically active ("bright excitons"), and states with $n_{\varphi,e} + n_{\varphi,h} = 0$ but which are optically not active ("dark excitons") because $n_e \neq n_h$.

Despite the fact that it already gives a good impression about the discrete energy levels in a quantum dot, the approach chosen above is obviously very approximative. The electron and the hole bare opposite charges and interact via the Coulomb interaction. The hole and the electron thus form a bound state. Consequently, the electron and the hole cannot be treated in a single particle picture. The Coulomb coupling makes it necessary to solve the full two-body problem of interacting distinguishable particles. The exciton states have to be constructed as linear combinations from all electron-hole pair states. Bright and dark states are mixed so that also dark states gain oscillator strength [43].

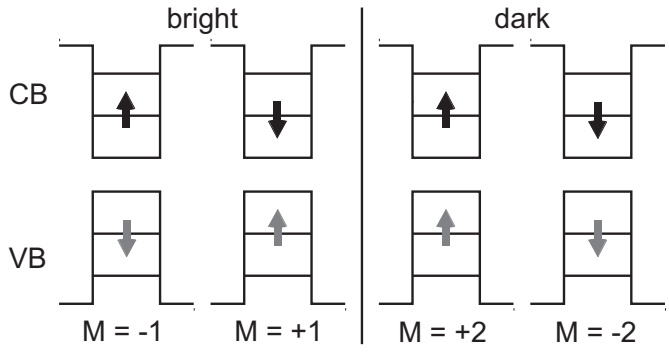

Figure 1.6: The four possible quantum dot ground state exciton configurations, electron spin $S_z = \pm 1/2$, heavy hole angular momentum $J_{h,z} = \pm 3/2$. Bright excitons: $J_{h,z} + S_z = \pm 1$. Dark excitons: $J_{h,z} + S_z = \pm 2$.

Let us now take a closer look at the exciton ground state with respect to optical activity. There $n_{h,\varphi} = n_{e,\varphi} = 0$ and radiative decay is allowed concerning the orbital momentum selection rule. However, also the angular momentum of the electron and the hole arising from the band structure have to be taken into account. The heavy hole bares angular momentum $J_{h,z} = \pm 3/2$ and the electron

its intrinsic spin $S_z = \pm 1/2$ where $J_{h,z}, S_z$ are the respective projections on the z axis. When the ground state decays radiatively, the emitted photon carries away an angular momentum of ± 1. Thus, only configurations with total spin $M = S_z + J_{h,z} = \pm 1$ are optically active. Therefore, four states do exist: two bright excitons with $J_{h,z} + S_z = \pm 1$ and two dark excitons with $J_{h,z} + S_z = \pm 2$. Figure 1.6 schematically depicts these four possible states.

Finally, we discuss the finestructure of the exciton ground state. There are mainly two causes leading to a splitting of the exciton states: (i) The anisotropic exchange interaction between electron spin and hole angular momentum which acts when a quantum dot is not perfectly rotationally symmetric but e. g. elongated along one direction. (ii) The Zeeman splitting induced by magnetic fields [46, 47].

Generally, not all quantum dots in an ensemble possess a perfect rotational symmetry. The reduction of this symmetry leads to a splitting of the else degenerate bright states by between 100 and 200 μeV. The splitting is induced by the *anisotropic exchange interaction* between electron and hole spins [47–50]. The Hamilton operator of the exchange interaction is given by [51]

$$\mathcal{H}_{exch} = -a_z J_{h,z} \cdot S_z + \sum_{i=x,y,z} \left(b_i J^3_{h,z,i} + S_{z,i} \right) . \tag{1.5}$$

With the exciton eigenstates being categorised by their total spin projection on the z axis, $M = J_{h,z} + S_z$, the matrix representation of $\mathcal{H}_{exch}$ can be constructed from a basis consisting of the bright excitons with $M = \pm 1$ and the dark excitons with $M = \pm 2$. In this basis, $(|+1\rangle, |-1\rangle, |+2\rangle, |-2\rangle)$, we obtain

$$\hat{H}_{exch} = \begin{pmatrix} +\delta_0 & \delta_1 & 0 & 0 \\ \delta_1 & +\delta_0 & 0 & 0 \\ 0 & 0 & -\delta_0 & \delta_2 \\ 0 & 0 & \delta_2 & -\delta_0 \end{pmatrix} ,$$

with

$$\begin{aligned} \delta_0 &= -\frac{3}{4}(a_z + \frac{9}{4} b_z) \\ \delta_1 &= \frac{3}{8}(b_x - b_y) \\ \delta_2 &= \frac{3}{8}(b_x + b_y) . \end{aligned}$$

The parameters $a_z, b_{x,y,z}$ characterise the dimensions of the quantum dot. The matrix is composed of two sub matrices corresponding to the bright excitons and the dark excitons, respectively. From the structure of $\hat{H}_{exch}$ it can be seen:

- $\hat{H}_{exch}$ has block diagonal form – bright and dark excitons thus do not mix and are split energetically by δ_0.

- For rotationally symmetric quantum dots $b_x = b_y$ and hence $\delta_1 = 0$. In this case $|+1\rangle$ and $|-1\rangle$ are eigenstates of $\hat{H}_{exch}$.
- If the rotational symmetry is broken, $b_x \neq b_y$. $|+1\rangle$ and $|-1\rangle$ mix and are no longer eigenstates of $\hat{H}_{exch}$; the new eigenstates $L_+ = 1/\sqrt{2}(|+1\rangle + |-1\rangle)$ and $L_- = 1/\sqrt{2}(|+1\rangle - |-1\rangle)$ are separated by δ_1.
- $\delta_2 \neq 0$ – the dark states always mix, they are separated by δ_2.

Figure 1.7 gives a schematic overview of the fine structure at zero magnetic field. In rotationally symmetric quantum dots the $|\pm 1\rangle$ states decay emitting circularly polarised light while the $L_{+/-}$ states in quantum dots with reduced symmetry decay emitting linearly polarised light.

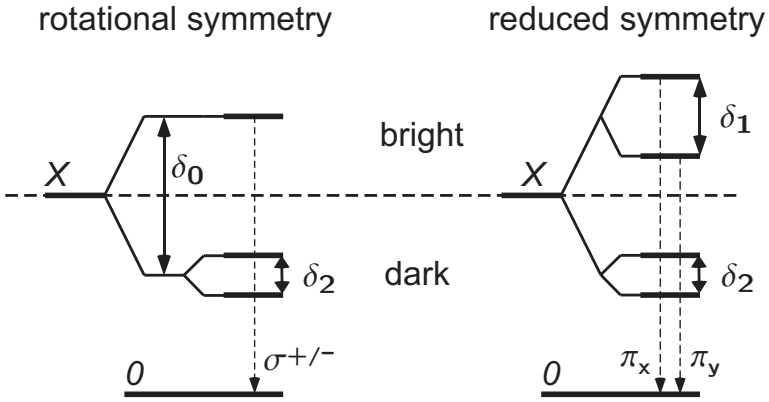

Figure 1.7: The exciton finestructure in quantum dots at $B = 0$. X: exciton states. 0: empty quantum dot state after exciton decay. Quantum dots with rotational symmetry: The dark states are split by δ_0 from the bright states, the dark states are split by δ_2. Each of the degenerate bright states $|\pm 1\rangle$, decays emitting circularly polarised light. Reduced symmetry: the anisotropic exchange interaction splits bright excitons by δ_1, emission of linearly polarised light.

At $B \neq 0$, the states experience an additional Zeeman spin splitting. The interaction of the electron and hole spins with a magnetic field $\mathbf{B} = (B_x, B_y, B_z)$ is expressed by the Hamiltonian

$$\mathcal{H}_Z = \mu_B \sum_i \left(g_{e,i} S_i - \gamma_{h,i} J_{h,i} + \Gamma_{h,i} J^3_{h,i} \right) B_i \,. \tag{1.6}$$

$g_{e,i}$ ($\gamma_{h,i}$) are the electron (hole) g-factors in the direction $i = x, y, z$. We construct the matrix representation of the Zeeman Hamiltonian using the basis

$$(|+1\rangle, |-1\rangle, |+2\rangle, |-2\rangle)$$

again. For a magnetic field $\mathbf{B} \,||\, \mathbf{e}_z$ ("Faraday geometry") with z parallel to the quantum dot growth direction only $i = z$ contributes to the sum in equation 1.6.

$J_{h,z}^2 = 9/4$ and we can thus replace $\gamma_{h,z} - \Gamma_{h,z} J_{h,z}^2$ in equation 1.6 by an effective hole g factor $1/3 g_{h,z}$. $\mathcal{H}_Z$ then becomes

$$\mathcal{H}_{Z,B||z} = \mu_B \left(g_{e,z} S_z - \frac{g_{h,z}}{3} J_{h,z} \right) B_z \,. \tag{1.7}$$

The matrix representation is hence given by

$$\hat{H}_{Z,B||z} = \frac{\mu_B B_z}{2} \begin{pmatrix} (g_{e,z} + g_{h,z}) & 0 & 0 & 0 \\ 0 & -(g_{e,z} + g_{h,z}) & 0 & 0 \\ 0 & 0 & (g_{e,z} - g_{h,z}) & 0 \\ 0 & 0 & 0 & -(g_{e,z} - g_{h,z}) \end{pmatrix} .$$

The total fine structure Hamiltonian is the sum of the Zeeman Hamiltonian and the exchange interaction Hamiltonian, $\hat{H}_{fs} = \hat{H}_Z + \hat{H}_{exch}$. In the case $\mathbf{B} \,||\, \mathbf{e}_z$ $\hat{H}_Z$ is diagonal, the rotational symmetry of the system is not violated. For non-symmetric quantum dots, a magnetic field in z direction can thus restore the symmetry when the off-diagonal elements originating from the exchange interaction are negligible compared to the Zeeman terms on the diagonal. The two Zeeman levels then decay under emission of circularly polarised light again [46, 47, 52]. The spin splitting of the Zeeman levels grows linearly with the magnetic field B_z for rotationally symmetrical quantum dots. For non-symmetric dots the dependence of the spin splitting on the magnetic field is non-linear.

Next, we want to study the influence of a transverse magnetic field. In a semi classical picture a purely transverse magnetic field leads to the precession of spins about the field axis which results in an oscillation between +1/2 and -1/2 for the electron spin and between +3/2 and -3/2 for the hole angular momentum. Consequently, the precession of the electron spin mixes the $|+1\rangle$ with the dark $|+2\rangle$ state and the $|-1\rangle$ state with the $|-2\rangle$ state while the hole spin precession couples the $|+1\rangle$ exciton with the $|-2\rangle$ exciton and the $|-1\rangle$ exciton with the $|+2\rangle$ exciton. In order to determine the matrix representation in the case of a purely transverse magnetic field ("Voigt geometry") we neglect the terms with higher powers of J_h. Their coefficients $\Gamma_{h,i}$ are negligible compared to $\gamma_{h,i}$ for structures of high symmetry. With this simplification the matrix representations of the Hamilton operator for $\mathbf{B} \,||\, \mathbf{e}_x$ and $\mathbf{B} \,||\, \mathbf{e}_y$ are then given by

$$\hat{H}_{Z,B||x} = \frac{\mu_B B_x}{2} \begin{pmatrix} 0 & 0 & g_{e,x} & \frac{3}{2} g_{h,x} \\ 0 & 0 & \frac{3}{2} g_{h,x} & g_{e,x} \\ g_{e,x} & \frac{3}{2} g_{h,x} & 0 & 0 \\ \frac{3}{2} g_{h,x} & g_{e,x} & 0 & 0 \end{pmatrix}$$

and

$$\hat{H}_{Z,B||y} = i\frac{\mu_B B_y}{2}\begin{pmatrix} 0 & 0 & g_{e,y} & -\frac{3}{2}g_{h,y} \\ 0 & 0 & \frac{3}{2}g_{h,y} & -g_{e,x} \\ -g_{e,y} & \frac{3}{2}g_{h,y} & 0 & 0 \\ -\frac{3}{2}g_{h,y} & g_{e,y} & 0 & 0 \end{pmatrix},$$

where $g_{e,x} = -g_{e,y}$ and $g_{h,x} = -g_{h,y}$ has to be fulfilled to assure that 90° rotations in the x-y- plane leave $\mathcal{H}_Z$ invariant. Obviously, the total angular momentum states $|\pm 1\rangle$ and $|\pm 2\rangle$ are no longer eigenstates of the system and the rotational symmetry is broken. Bright and dark excitons mix as expected from the semi classical picture of precessing spins.

So far, we have only addressed the discrete electron and hole energy levels arising from the size quantisation. The wave functions belonging to these energy eigenvalues represent only the envelope part of the electron and hole quantum dot wave functions though. The full wave functions are composed from the quantum dot envelope functions and the electron and hole Bloch functions

$$\Psi(\mathbf{r}) \propto u_e(\mathbf{r}_e)u_h(\mathbf{r}_h)\phi_{s_e,n_{\varphi,e}}\phi_{s_h,n_{\varphi,e}}\,. \tag{1.8}$$

While the envelope wave functions $\phi_{s_{e/h},n_{\varphi,e/h}}$ stem from the three dimensional carrier confinement, the periodic Bloch functions $u_{e/h}$ reflect the solid state nature of the quantum dots. It is a complicated task to calculate the carrier population densities taking influences as the strain in the quantum dot lattice, the composition of the dot, the spin-orbit coupling and the Coulomb interaction into account. To conclude, we thus only list the most important theoretical models which have been used in order to actually calculate the probability density of the electron and the hole inside a quantum dot.

- $\mathbf{k}\cdot\mathbf{p}$ theory: starting from band structure parameters, the Schrödinger equation is solved perturbatively taking up to eight bands into account, including the conduction band, light and heavy hole bands and the split off band [53, 54].

- tight binding: The assumption that the wavefunctions of the single atoms are vanishingly small for distances greater than the lattice constant allows to treat the lattice sites independently and to construct the bands from single atoms [55, 56].

- ab initio ("from first principles"): Diagonalisation of the Hamiltonian using a pseudo-potential representing the involved atoms, the local strain, the spin-orbit coupling via fitting parameters [57, 58].

Additionally to excitons also multiexcitons and charged excitons can be formed. Multiexcitons are complexes consisting of several excitons, e. g. the biexciton

with two electrons in the conduction band and two holes in the valence band. These complexes will not be important for the studies presented in this work and we therefore refer the reader to the literature [43, 59, 60]. In the present work, however, negatively charged quantum dots, i. e. quantum dots containing an additional single electron are studied. When an exciton is brought into such a negatively charged quantum dot, a negatively charged exciton, the so called *trion*, is formed. We discuss negatively charged quantum dots and trions in chapter 1.3.2.

1.3.2 N-Doped Quantum Dots and Trions

The decay time of an exciton in a quantum dot is of the order of a nanosecond. This limits the possibility to use the exciton for quantum information storage or quantum information processing. However, quantum dots can be produced which are permanently populated by a charge and spin carrier. This permanent spin can then be initialised, manipulated and read out.

While also quantum dots can be produced which permanently house a single hole ("p-doped quantum dots"), in this work we study n-doped quantum dots which are on average populated by a single electron throughout. In the case of self-assembled quantum dots the doping is achieved by growing a doping layer, e. g. a silicon layer, ≈ 20 nm beneath each quantum dot layer in a multi-layer quantum dot sample. Excess electrons from the doping layer tunnel into the quantum dot layer where they are trapped inside the quantum dots. The doping density can be controlled to be equal to the quantum dot density in the quantum dot arrays. The quantum dots are then populated by on average one electron. We call this residual electron the "resident electron".

If such a singly negatively charged quantum dot captures an additional electron-hole pair, a negatively charged exciton is formed, the *trion*, X^-, an elementary excitation consisting of two electrons and one hole. Concerning the orbital angular momentum, the electrons and the hole occupy the same single particle states as discussed in connection with the neutral exciton in section 1.3.1. The spin distribution of excited trion states, however, is obviously more complex as for the neutral exciton and gives rise to a finestructure of the trion caused by spin-spin interactions [61–64]. Let us first investigate the trion ground state. The ground state of the trion is formed by two electrons in the s-shell having paired, opposite spins and a hole in its s-shell. We label the trion configurations according to the scheme $carrier^{spin}_{shell}$ meaning e. g. $(e_s^{+1/2}, e_s^{-1/2}; h_s^{\pm 3/2})$ for the trion ground state. The total z projection of the electron spin $S_z = S_{z,1} + S_{z,2}$ in the trion ground state is zero. Thus, there is no electron-hole exchange interaction and irrespective of the quantum dot symmetry there is no splitting of the ground state. The trion consequently decays under the emission of circularly polarised light.

The excited trion state where one of the electrons is occupying the p-shell

displays more diverse spin configurations. We refer to this state as the "hot" or "excited-electron" trion. In the hot trion, the two electrons can have a non-vanishing total spin enabling the exchange interaction to split the states [61–65]. The interaction between the two electrons is about one order of magnitude stronger than the electron-hole exchange because identical particles experience a stronger exchange interaction than distinguishable ones [62].

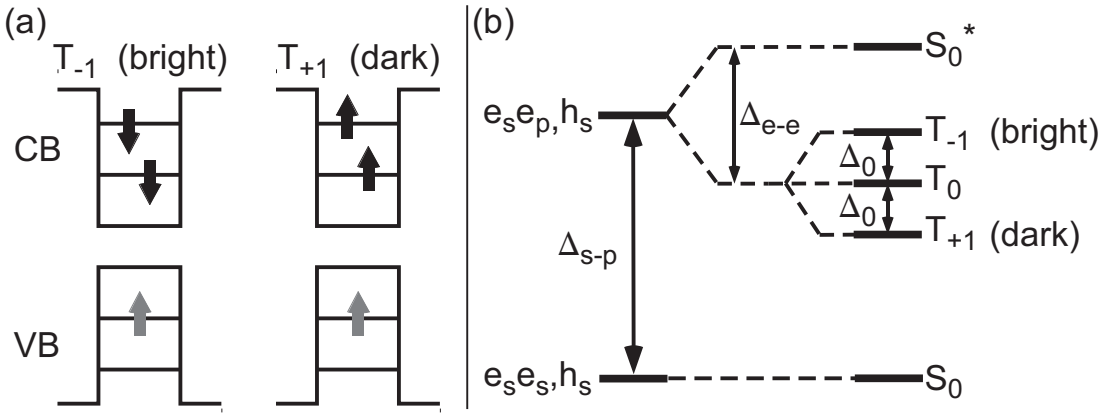

Figure 1.8: (a) The two states of the excited-electron trion triplet, $T_{M_\Sigma=\pm1}$, with total electron spin z projection $M_\Sigma = \pm1$, hole angular momentum $J_{h,z} = +3/2$. The states with $J_{h,z}$ parallel M_Σ are dark, the ones where $J_{h,z}$ antiparallel M_Σ are bright. Analogously for $J_{h,z} = -3/2$. (b) Fine structure of the excited-electron trion for $J_h = +3/2$. The energy difference between trion ground state and the excited-electron trion state is Δ_{s-p}. Electron-electron exchange splits the excited-electron trion in a singlet state $S_0^\star$ with $(\Sigma, M_\Sigma) = (0,0)$ and a spin triplet $T_0, T_{\pm1}$ with $\Sigma = 1$. The singlet-triplet splitting is Δ_{e-e}. Electron-hole isotropic exchange further splits the states of the triplet by Δ_0. The same set of states exists for $J_{h,z} = -3/2$ with the only difference that T_{-1} and T_{+1} are interchanged.

Figure 1.8 shows the finestructure of the excited-electron trion. Table 1.1 gives an overview of the typical energies playing a role in the trion [63, 66]. The electron-electron exchange interaction splits the hot trion into a singlet state $S_0^\star$ and a triplet $T_{0,\pm1}$. With the total spin quantum number Σ composed of the s-shell electron spin quantum number S_s and the p-shell electron spin quantum number S_p and the z projection of the total electron spin M_Σ, the electron spin configurations (Σ, M_Σ) of these four states are

$$\begin{aligned}
(\Sigma, M_\Sigma)_{S_0^\star} &= (0,0) \quad : \quad S_0^\star = e_s^{+1/2} \cdot e_p^{-1/2} - e_s^{-1/2} \cdot e_p^{+1/2} \\
(\Sigma, M_\Sigma)_{T_{-1}} &= (1,-1) \quad : \quad T_{-1} = e_s^{-1/2} \cdot e_p^{-1/2} \\
(\Sigma, M_\Sigma)_{T_0} &= (1,0) \quad : \quad T_0 = \tfrac{1}{\sqrt{2}}(e_s^{+1/2} \cdot e_p^{-1/2} + e_s^{-1/2} \cdot e_p^{+1/2}) \\
(\Sigma, M_\Sigma)_{T_{+1}} &= (1,+1) \quad : \quad T_{+1} = e_s^{+1/2} \cdot e_p^{+1/2}.
\end{aligned}$$

The typical energy range for the electron-electron exchange splitting Δ_{e-e} is of the order of 10 meV. The zero total spin states $S_0^\star$ and T_0 relax very quickly

Table 1.1: Typical energies of the excited-electron trion.

ground state - hot trion		Δ_{s-p}	tens of meV
e-e exchange	singlet-triplet splitting	Δ_{e-e}	a few meV
e-h isotropic exchange	triplet splitting	Δ_0	hundreds of μeV
e-h unisotropic exchange	$S_0^\star$-$T_{\pm 1,bright}$ coupling	Δ_1	a few μeV

to the ground state S_0 and thus do not decay radiatively. The behaviour of the $T_{\pm 1}$ states is more complicated due to the Pauli blockade of the s-shell. Its dynamics will be explained in detail in connection with the effect of negative circular polarisation in chapter 3.2.

The triplet is further split due to the isotropic electron-hole exchange interaction by $\Delta_0 < 1$ meV. Including the two directions of the hole angular momentum orientation, the excited-electron trion thus consists of eight states. The states of the triplet where the hole angular momentum $J_{h,z}$ is parallel to M_Σ are optically inactive (dark states), the ones with $J_{h,z}$ being antiparallel to M_Σ could recombine radiatively (bright states). In figure 1.8 the situation with $J_{h,z} = +3/2$ is shown. For $J_{h,z} = -3/2$ the bright state of the triplet is T_{+1}, the dark state is T_{-1}. Again, the bright state is located energetically above T_0, the dark one below T_0 so that in figure 1.8 only T_{+1} and T_{-1} are interchanged.

Additionally to the isotropic electron-hole exchange an anisotropic electron-hole exchange interaction is present in quantum dots with reduced symmetry. The anisotropic exchange Δ_1 is of the order of a few μeV. Its most important effect is that it couples the bright triplets $(T_{+1}, h_s^{-3/2})$ and $(T_{-1}, h_s^{+3/2})$ to the singlet $S_0^\star$ inducing spin flips between the p-electron and the hole[6].

1.4 Excitation, Capture, Relaxation, Decay

1.4.1 Optical Excitation and Recombination

The energy structure of an (In,Ga)As quantum dot sample with the quantum dots located on an InAs wetting layer and embedded in a GaAs substrate is governed by the contributions schematically depicted in figure 1.9 (a): The band gap of the substrate material, E_{GaAs}, the band gap of the InAs wetting layer E_{wl} and the band gap of the (In,Ga)As quantum dot material $E_{(In,Ga)As}$ modified by the discrete confined quantum dot energy states $E_{0,e}$ and $E_{0,h}$. For (In,Ga)As quantum dots at cryogenic temperatures, the GaAs substrate band gap is located at $\approx$ 1.5 eV and the wetting layer at $\approx$ 1.48 eV, the confined quantum dot states between 50 meV and hundreds of milli-electronvolt below the wetting layer, depending on the actual indium-gallium content and the size of the quantum dot.

[6]This will be discussed in detail in chapter 3.2.

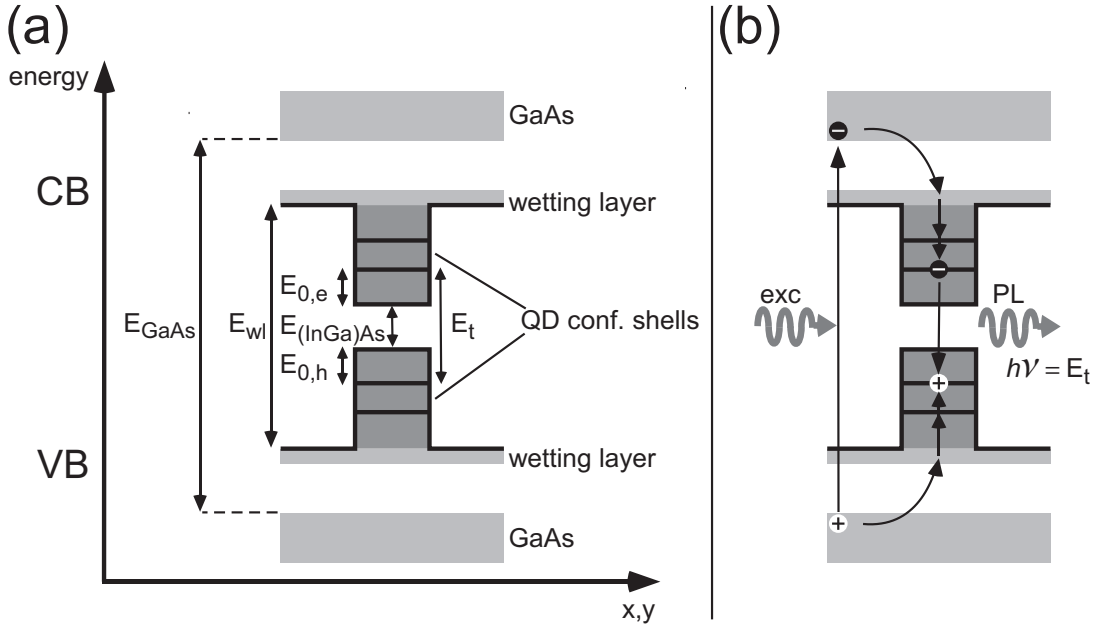

Figure 1.9: (a) The energy structure in an (In,Ga)As quantum dot sample. GaAs band gap E_{GaAs}, wetting layer transition energy E_{wl}, discrete confined quantum dot states with the ground state energies of the electron $E_{0,e}$ and the hole $E_{0,h}$, ground state transition energy E_t. (b) Optical excitation of an electron-hole pair above the GaAs band gap, capture by the quantum dot potential, relaxation to the quantum dot ground state, radiative recombination under emission of a photon with energy $h\nu = E_t$.

Quantum dots can be filled with electron-hole pairs by optical excitation. Depending on the energy of the exciting photons, excitons can be created in the GaAs substrate material, in the wetting layer or directly in the confined quantum dot shells. However, the absorption of light in the GaAs barrier is more effective than for light resonant to one of the confined quantum dot shells. This is due to the continuous density of states of the bulk material compared to the δ-distribution like density of states of quantum dots. An efficient way to fill the quantum dots with electron-hole pairs is therefore to create them energetically above the confined quantum dot states and let them be trapped by the quantum dots. If a quantum dot sample is illuminated with light of energy greater than the band gap of the bulk GaAs substrate, electrons are excited from the valence band to the conduction band leaving behind a hole which is positively charged with respect to its surrounding. The created electron-hole pairs are rapidly captured by the quantum dot potentials. The carriers quickly relax to the ground state of the quantum dots losing their excess energy by carrier-carrier scattering and the interaction with phonons. Having reached the ground state of the quantum dot, the exciton decays radiatively under emission of a photon. The capture and

relaxation typically occurs on a picosecond timescale while the radiative decay times of excitons in quantum dots are hundreds of picoseconds. The excitons thus generally relax to the quantum dot ground state before they recombine. The process of excitation, relaxation and recombination is shown schematically in figure 1.9 (b).

If a lot of carriers are created in the substrate, the quantum dots can be filled with more than one electron and hole. As capture and relaxation are generally much faster than the radiative decay and each shell can only house a finite number of particles due to the Pauli blockade, also higher lying shells are filled resulting in emission not only from the ground state but also from higher shells as can be seen in figure 1.5.

The transition energy E_t of the ground state emission is a combination of the valence band-conduction band energy gap of the quantum dot material, $E_{(In,Ga)As}$, and the energies of the lowest electron and hole states, $E_{0,e}$ and $E_{0,h}$ (c. f. figure 1.9):

$$E_t = E_{(In,Ga)As)} + E_{0,h} + E_{0,e}\,. \tag{1.9}$$

It is thus clear that the transition energy characteristic for a quantum dot sample is both governed by the indium and gallium content of the quantum dots via $E_{(In,Ga)As}$ and by the size of the quantum dots via $E_{0,e/h}$.

In the experiments presented in this work, optical excitation generally was performed in the wetting layer. For excitation in the wetting layer states, electron-hole pair creation, capture and relaxation occur analogously to the case of above band gap excitation in the GaAs substrate.

1.4.2 Radiative Decay Dynamics

The radiative recombination dynamics of quantum dots is typically analysed assuming that the quantum dot represents a two level system. In quantum dots the two levels are given by the lowest electron state in the conduction band and the lowest hole state in the valence band. Figure 1.10 (a) schematically depicts the level occupations in this case.

Labeling the occupation of the respective levels by electrons and holes with (n_e, n_h), it is obvious that the two level picture only allows the cases $(1,1)$ and $(0,0)$ to occur. There is thus always a one to one correlation between the electron and hole populations of the levels: An electron occupying the conduction band ground state correlates with a hole in the lowest valence band state. This inevitably leads to the decay of the exciton obeying a monoexponential decay law with a decay constant τ.

However, non-exponential decays were observed as well for quantum dot ensembles as for single quantum dots (see e. g. [67]). Various effects have been suggested in order to explain the non-exponentiality of the decays, such as state filling effects, carrier diffusion effects, inhomogeneities in the electron-hole overlap

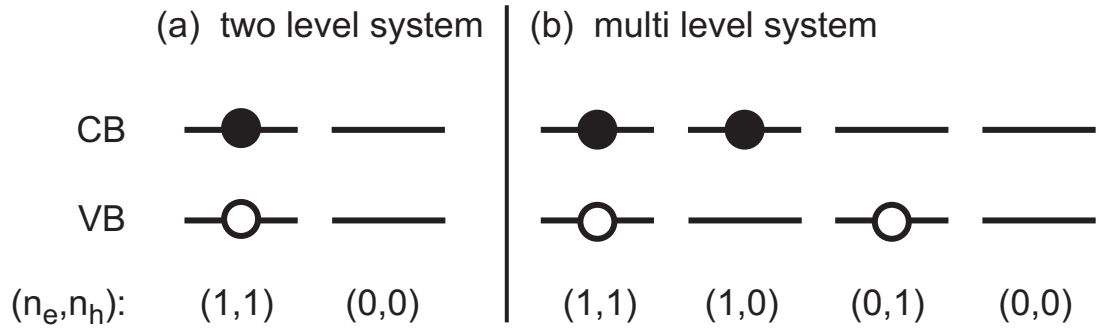

Figure 1.10: Possible carrier configurations (n_e, n_h) in the conduction band (CB) and valence band (VB) quantum dot ground states. (a) Quantum dot as a two level system. Electron and hole populations are fully correlated. (b) Multi level system. When the carriers can occupy different levels, the ground state population correlation is weakened. The occupations (1,0) and (0,1) have to be included.

or dark excitons. Only recently, however, the model predicting the exponential decay was questioned, the picture of quantum dots as two level systems. Generally, quantum dots do possess several confined shells. Upon excitation of an electron-hole pair above the confined quantum dot states (in the wetting layer or the barrier), the carriers could thus populate different shells. As shown in figure 1.10 (b) the one to one correlation between electron and hole population of the ground state is then weakened and the occupations $(n_e, n_h) = (1, 0)$ and $(n_e, n_h) = (0, 1)$ of the ground state have to be included.

It was recently argued how the electron-hole population correlations influence the exponentiality of the decay dynamics [68, 69]. A theoretical model [68] revealed that whenever the one to one population correlation between electron and hole is weakened, the radiative decay cannot be described by an exponential decay law anymore. Quantum dots do have more than two levels so that the non-exponentiality of the radiative decay is an intrinsic property of quantum dots. Thus, it is generally also not possible to unambiguously assign a time constant to a quantum dot decay transient.

We have thus systematically experimentally studied how quantum dot properties and experimental conditions influence the exponentiality of the ground state radiative recombination, i. e. to determine under which circumstances quantum dots may or may not be viewed as two level systems.

I wish to give a brief overview of these systematic experimental studies[7]. The experiments were performed by exciting different ensembles of (In,Ga)As quantum dots with linearly polarised picosecond pulses. The photoluminescence was detected time resolved with a time resolution of ≈ 20 ps using a streak camera. The samples were kept at a temperature of 10 K.

[7] For a detailed explanation of the underlying theoretical considerations and numerical results c. f. [68–70]

One expects an exponential decay dynamics when the carrier populations are fully correlated. When electron-hole pairs are created non-resonantly with the confined quantum dot states, in the barrier or the wetting layer, they may relax independently to their ground states. The build up of excitonic correlations can thus be hindered by carrier scattering. We probe the influence of the population correlations in two ways [70]:

- The photon energy of the exciting laser is changed in order to create electron-hole pairs above the GaAs band gap, in the wetting layer, resonantly with higher confined quantum dot states and finally resonantly with the quantum dot ground state.
- The electron population is varied by selecting n-doped quantum dots which are on average singly negatively charged, and comparing their emission dynamics with the one of nominally undoped quantum dots.

The excitation densities were kept small enough in all experiments so that the creation of multi-exciton complexes could be ruled out.

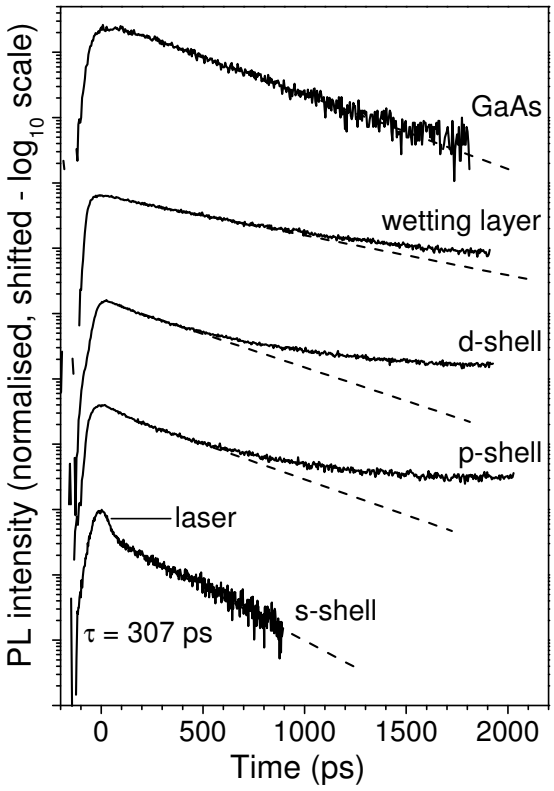

Figure 1.11: Time resolved photoluminescence of a nominally undoped (In,Ga)As quantum dot ensemble, confinement $\approx$ 80 meV. Excitation energies 1.550 eV (GaAs), 1.476 eV (wetting layer), 1.436 eV (d-shell), 1.414 eV (p-shell), 1.389 eV (s-shell). The dashed lines are exponential fits to the data in the range $200 < t < 500$ ps. Decay time for excitation resonant to the ground state transition energy: $\tau =$ 307 ps. $T = 10$ K.

Figure 1.11 shows transients of the ground state electron-hole recombination of an ensemble of undoped quantum dots having a confinement potential of $\approx$ 80 meV. From top to bottom, the traces correspond to above the GaAs band

gap excitation, excitation resonant with the wetting layer, resonant with the d-shell, the p-shell and finally the s-shell. One observes that the radiative decay of the ground state occurs on a time scale of 1 ns. The lines in figure 1.11 are exponential fits to the first part of the decay between $t = 200$ ps and $t = 500$ ps. Note that the traces are plotted on a logarithmic scale so that an exponential function is given by a straight line. A clear deviation of the measured decays from the exponential fits can be observed after a time of ≈ 1 ns for the excitation into GaAs and the wetting layer. Also for excitation resonant to higher lying confined quantum dot states, the d-shell and the p-shell, the decay does not follow an exponential decay law. For non-resonant excitation the optically generated polarisation transforms into a population in the quantum dot states by the scattering processes occurring during the relaxation to the lowest quantum dot state. The electron and the hole can occupy different levels so that an electron in its ground state does not necessarily mean that the hole ground state is also populated. The electron and hole populations are thus not fully correlated, the occupations $(n_e, n_h) = (1, 0)$ and $(n_e, n_h) = (0, 1)$ of the quantum dot ground state might appear. The bottom transient in figure 1.11 finally belongs to excitation resonant to the energy difference between valence band and conduction band ground states of the quantum dot. At $t \approx 0$ a peak is seen which is due to scattered laser light. After some tens of picoseconds, though, a decay becomes apparent which is monoexponential over the whole range up to where the signal becomes comparable to the noise background. For s-shell excitation the carriers are directly excited in the ground state. It is unlikely that they undergo scattering processes moving them to different shells. Thus, only the situations $(n_e, n_h) = (0, 0)$ and $(n_e, n_h) = (1, 1)$ occur. Strictly speaking, with resonant ground state excitation one does not have a *population* because the coherence with the light field is maintained until the radiative decay of the electron-hole pair. Hence, one does not observe a population decay but coherently driven luminescence [71, 72]. Still, we expect strong carrier correlations for resonant excitation in the s-shell of the quantum dots.

Next, we wish to study the influence of doping on the decay dynamics. By choosing n-doped quantum dots whose conduction band ground state is always occupied by on average one electron, we can keep the electron population approximately constant increasing the probability for $(n_e, n_h) = (1, 1)$. Figure 1.12 shows time resolved photoluminescence for a n-doped quantum dot sample for excitation into the wetting layer, the p-shell and the s-shell. For comparison, the transients of the nominally undoped sample from figure 1.11 are also shown. Irrespective the excitation energy, the decays of the charged quantum dots are closer to the straight line like decrease typical for an exponential decay on a logarithmic scale. Already for excitation into the wetting layer, the negatively charged quantum dots exhibit a decay coming closer to an exponential function as for the undoped sample. This behaviour becomes evident for p-shell excitation. There, the n-doped sample exhibits a decay which follows to a good approximation an

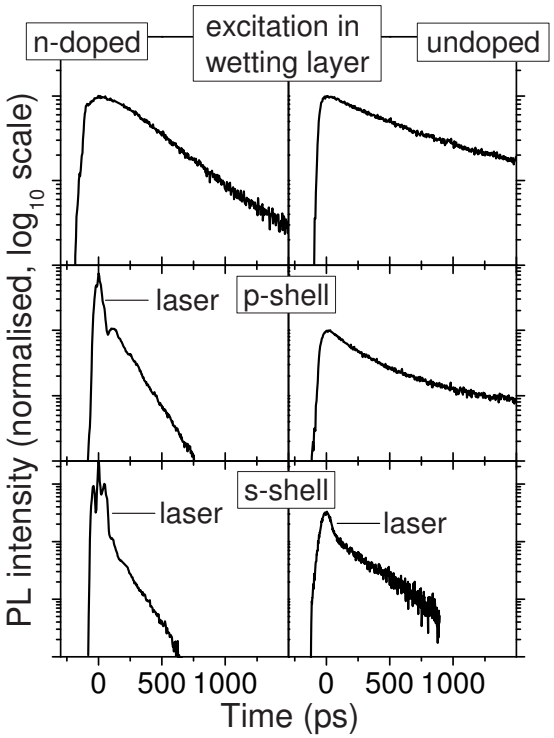

Figure 1.12: Time resolved photoluminescence of undoped (left) and n-doped (right) quantum dots with comparable confinement potential of $\approx$ 80 meV, excited at different energies. Excitation energies for the n-doped sample 1.476 eV (wetting layer), 1.417 eV (p-shell) and 1.397 eV (s-shell). $T = 10$ K.

exponential decay law. For s-shell excitation both samples show expectedly an exponential decay.

The degree of exponentiality may also be controlled via the confinement potential of the quantum dots. With increasing confinement the splitting between the shells also increases. This suppresses scattering of the carriers between the shells, the correlations are enhanced [70].

To conclude, we maintain that the radiative decay in quantum dots generally cannot be described by the picture of quantum dots as two level systems. The non-exponentiality of the recombination dynamics is an intrinsic property of quantum dots and related to the fact that carriers can populate different shells which breaks the one to one correlation between electron and hole populations. Therefore, it is generally also difficult to relate a time constant to a decay. We emphasise again, that the decays are generally genuinely non-exponential and not bi- or multi-exponential. A two level system and with it an exponential decay of the ground state emission can be approached though for specific conditions: Quantum dots possessing a deep confinement potential and a large energy difference between the shells and excitation into the quantum dot ground state. Charged quantum dots in general also exhibit a more exponential decay.

2 The Studied Sample

The studied sample was grown by the group of A. D. Wieck and D. Reuter, Angewandte Festkörperphysik, Ruhr Univerität, Bochum. It is a 20 layer (In,Ga)As self-assembled quantum dot ensemble grown on a (100) oriented GaAs substrate by molecular beam epitaxy (MBE)[1]. The dot density is approximately 10^{10} cm^{-2}.

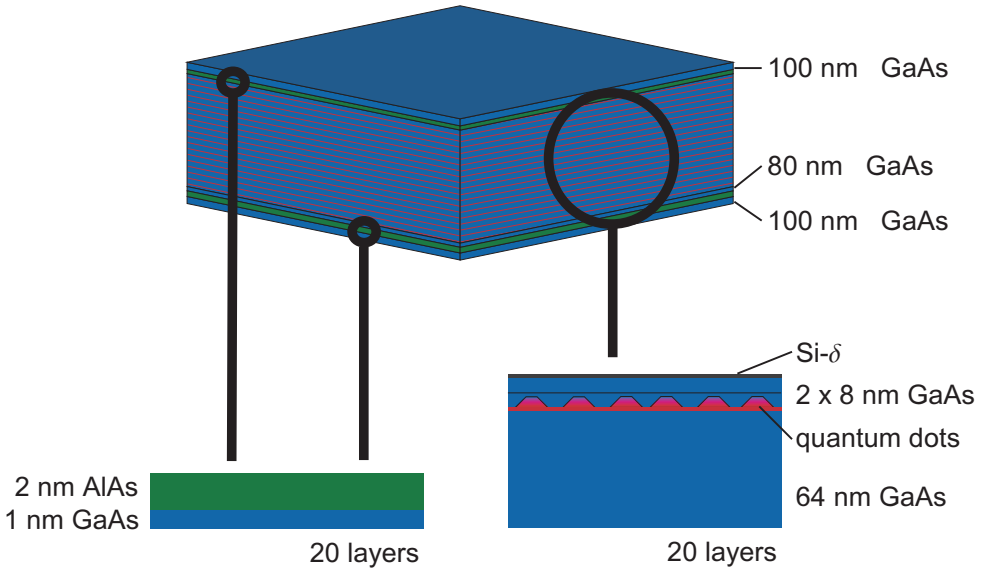

Figure 2.1: Schematic illustration of the composition of the studied sample.

The structure of the sample is schematically shown in figure 2.1. The quantum dot layers are separated by 64 nm wide GaAs barriers. 20 nm above each quantum dot layer a silicon δ-doping layer is located with a doping density about equal the dot density[2]. Thus each quantum dot is permanently populated with on average one "resident electron", as confirmed by pump and probe Faraday rotation measurements [28]. The structures have been thermally annealed for 30 seconds at 900℃. As mentioned above[3] this leads to interdiffusion of gallium ions into the InAs quantum dots, which shifts the ground state emission to 1.34 eV (925 nm) as compared to 1.063 eV (1167 nm) for an unannealed sample of the same series[4].

[1] c. f. chapter 1.2.1
[2] For a brief explanation of the fabrication of doped quantum dots c. f. chapter 1.3.2.
[3] For thermal annealing c. f. chapter 1.2.2.
[4] Photoluminescence of all samples of the annealing series figure 1.3.

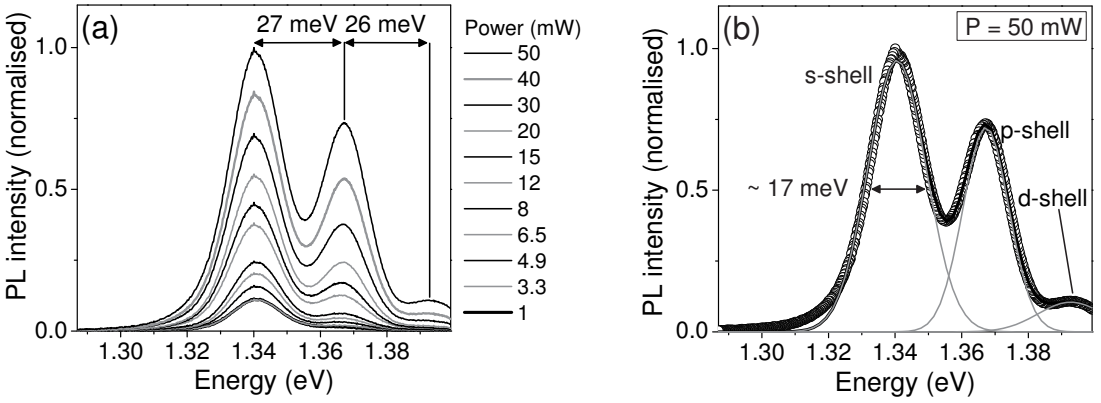

Figure 2.2: (a) Photoluminescence spectra for different excitation powers P. With higher excitation powers photoluminescence of higher quantum dot shells appears due to state filling of the lowest shells. Excitation into the wetting layer at 1.476 eV, $T = 2$ K. (b) Photoluminescence spectrum for excitation power $P = 50$ mW from (a) and a three peak Gauss fit of the spectrum revealing the energy distribution of the three levels. The width of the s-shell distribution is ≈ 17 meV.

In order to further characterise the quantum dots we study photoluminescence spectra which were obtained exciting the sample in the wetting layer at a laser energy of 1.476 eV. Figure 2.2 (a) shows photoluminescence spectra for different excitation densities. The maximum of the s-shell emission is located at an energy of 1.34 eV corresponding to 925 nm. At higher excitation densities state filling effects lead to emission also from the p-shell and the d-shell. The maximum of the p-shell photoluminescence is located at an energy of 1.367 eV or 907 nm. The average energetic level spacing is ≈ 26 meV. The confinement potential which we define by the energy difference between the wetting layer and the quantum dot ground state is ≈ 130 meV.

Figure 2.2 (b) shows the graph corresponding to the highest excitation power in (a) (black open circles). Also shown is a three peak Gaussian fit of the spectrum (black line). The spectrum is inhomogeneously broadened due to the size distribution and the inhomogeneities in composition of the quantum dots in the ensemble. The three single Gauss functions of the fit belonging to the s-shell, the p-shell and the d-shell (grey) show the spectral distributions of the three shells in the ensemble. The Gauss fit yields a width of the three distributions of ≈ 17 meV.

As we focus on the interaction between the nuclear spins and the resident electron spin in this work the properties of the nuclear isotopes involved play an important role. Table 2.1 compares the nuclear species composing the quantum dots we were studying.

Table 2.1: The properties of the nuclei of the studied sample. Line 3: Maximal magnetic moment in z direction. Line 4: Magnetic moment in units of the nuclear magneton $\mu_N = 5.0508 \cdot 10^{-27}$ J/T.

	Isotope	^{115}**In**	^{113}**In**	^{69}**Ga**	^{71}**Ga**	^{75}**As**
1	Abundance (%)	95.72	4.28	60.4	39.6	100
2	Nuclear spin I	9/2	9/2	3/2	3/2	3/2
3	Mag. moment μ_{I_z} (10^{-26} J/T)	2.795	2.790	1.018	1.294	0.727
4	Mag. moment μ_I (μ_N)	5.534	5.523	2.016	2.562	1.439

3 Electron and Nuclear Spins in Quantum Dots

3.1 Introduction

The negatively charged quantum dots investigated are on average always populated by one resident electron[1]. In its ground state the electron's wave function is extended over almost the whole quantum dot volume. The resident electron spin thus interacts with the majority of the spins of the quantum dot nuclei. The nuclear spin ensemble has a crucial effect on the resident electron spin polarisation. In this chapter we introduce the system studied in this work, the electron-nuclear spin system in negatively charged quantum dots. Firstly, it will be shown how the resident electron spin can be optically oriented by illumination of the sample with circularly polarised light and how the polarisation of the spin can be read out. We address the effect the randomly oriented nuclear spins have on the polarisation of the resident electron spin. Then, we explain how the nuclear spins may be polarised using the angular momentum transfer from spin polarised electrons to the nuclei and show in what way the polarised nuclear spin system acts on the resident electron spin compared to the case of unpolarised nuclear spins.

3.2 Negative Circular Polarisation and Optical Orientation of the Resident Electron Spin

In this section we discuss a mechanism which can be used in order to optically orient the resident electron spin in negatively charged quantum dots, the effect of "negative circular polarisation" (NCP). Further, we demonstrate how this effect may be at the same time exploited to read out the spin polarisation of the resident electrons.

After excitation of an electron-hole pair in the wetting layer and subsequent capture of the carriers into the quantum dots, in n-doped quantum dots a negatively charged trion X^- is formed out of the photoinjected exciton and the resident electron. The ground state of this trion consists of two electrons with antiparallel spins in the lowest conduction band state and a single hole. This means that the helicity of the light which is emitted upon the decay of the trion

[1] c. f. chapter 1.3.2,chapter 2.

ground state is fully governed by the spin orientation of the hole because for paired electrons all the spin information from the excitation is lost. If a well defined orientation of the spins is imprinted on the carriers by excitation with circularly polarised light, the emitted photoluminescence should have the same helicity as the exciting photons.

However, it is a well known feature with n-doped quantum dots, that the circular polarisation of the photoluminescence after circularly polarised excitation may be negative [63, 64, 73–76]. This means that the intensity of the photoluminescence having a circular polarisation which is opposite to the excitation polarisation is greater than the intensity of the photoluminescence with the same polarisation as the exciting light. Hereby we use the standard definition of circular polarisation

$$\rho_c = \frac{I^{\mathrm{co}} - I^{\mathrm{cross}}}{I^{\mathrm{co}} + I^{\mathrm{cross}}} , \tag{3.1}$$

where I^{co} denotes the intensity of the photoluminescence having the same circular polarisation as the excitation (co-polarised detection) and I^{cross} denotes the intensity of the photoluminescence polarised oppositely to the excitation (cross-polarised detection). The sign of ρ_c reflects whether the circular polarisation is positive or negative with respect to the circular polarisation of the excitation.

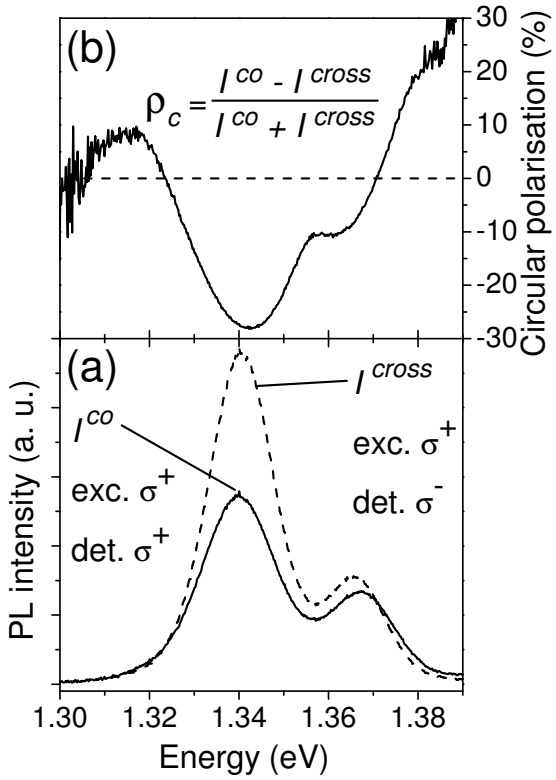

Figure 3.1: (a) Intensities of σ^+ and σ^- polarised photoluminescence after excitation with σ^+ polarised light. The emission of the ground state is predominantly oppositely polarised relative to the excitation polarisation. (b) Polarisation of the photoluminescence calculated according to equation 3.1. The circular polarisation is negative throughout the s-shell emission.

Figure 3.1 shows photoluminescence spectra of the studied quantum dot ensemble under σ^+ excitation with the detection being either co-polarised (σ^+) or

cross-polarised (σ^-). Both spectra show two inhomogeneously broadened photoluminescence peaks, corresponding to the emission from the first excited state (p-shell) at 1.37 eV and from the ground state (s-shell) at 1.34 eV. The intensity for cross-polarised detection is greater than that for co-polarised detection throughout the s-shell emission and hence the circular polarisation of the ground state photoluminescence is negative.

For negatively charged quantum dots the analysis of the relaxation and decay dynamics becomes involved as the additional electron allows a greater number of configurations concerning the occupation of the different quantum dot states and the spin distribution. The complex processes of carrier capture into the quantum dots, relaxation to the lowest quantum dot states and spin flips between electron and hole spins has therefore inspired different explanations of the negatively circularly polarised photoluminescence of n-doped quantum dots.

Negative circular polarisation was interpreted in terms of the higher probability of dark excitons[2] to be captured into the quantum dots when photogenerated in the wetting layer [74]: the bright excitons rapidly recombine radiatively in the wetting layer whereas the excitons whose holes have undergone a spin flip – and which thus have turned dark – live longer and so have a greater probability to become captured by the quantum dot potential. A significant fraction of dark excitons could be generated because the spin flip time of the heavy hole is much shorter than that of the electron in two dimensional structures due to the spin-orbit interaction between the hole states [77]. A trion formed out of a dark exciton and the resident electron decays emitting negatively circularly polarised light due to the spin orientation of the hole.

However, in reference [74] quantum dots were studied which were defined by monolayer steps at the interfaces of a GaAs/AlGaAs quantum well. With our self assembled (In,Ga)As quantum dot ensemble, the capture of photoexcited carriers into the dots is much more efficient: the radiative decay of the electron-hole pairs in the wetting layer takes long due to localisation of the carriers at potential fluctuations in the wetting layer. The capture times are thus much shorter than the radiative decay time of the wetting layer excitons. This is experimentally supported by the fact that the emission from the wetting layer is vanishingly small compared to the emission from the confined quantum dot states. This explanation of the negative circular polarisation effect thus does not hold in our case.

Other explanations of the negative circular polarisation effect were developed all of which have in common that the central mechanism is an electron-hole spin flip-flop [63, 64, 73, 75, 76, 78]. We describe the negative circular polarisation effect

[2]With dark excitons the sum of electron spin and hole angular momentum z projections is $M_\Sigma = \pm 2$. The radiative decay of dark excitons under emission of a photon is thus forbidden. c. f. chapter 1.6.

along the lines of [63, 64] but focus on the effect of negative circular polarisation on the polarisation of the resident electron.

The mechanism causing negative circular polarisation In order to explain the negative circular polarisation effect we assume that the carriers excited in the wetting layer are quickly captured in the quantum dots where the hole relaxes to the lowest valence band state. The hole angular momentum orientation is completely destroyed during the relaxation due to strong heavy-light hole mixing in the wetting layer [79–81]. Thus, the hole retains no angular momentum information from the excitation.

Note that some authors assume that the hole spin is conserved [75, 76, 82, 83]. In their work, however, they excite the quantum dots quasi-resonantly with an excitation energy corresponding to the high energy side of the inhomogeneously broadened ground state photoluminescence peak of their quantum dot ensemble. In this case, the spin of the holes may be retained until they have finally relaxed to the ground state. In our case, however, a spin memory of the hole is very unlikely as explained above.

Let the photoinjected electron at first relax to the first excited state p_e whereas the resident electron populates the lowest state in the conduction band, s_e. The photoinjected electron, the resident electron and the hole then initially form a "hot" trion[3]. Let us exemplarily consider the case of σ^+ excitation generating a photoinjected spin "down" electron. Figure 3.2 shows a simplified scheme of the hot trion configurations which are possible after excitation with positively circularly polarised light assuming that only the photoinjected electron spin keeps the information from the circularly polarised excitation.

The configurations with antiparallel electron spins (figure 3.2 (a.3) and (a.4)) allow direct electron relaxation to the ground state and formation of a ground state trion. No spin information is contained in the paired antiparallel electron spins. This trion state then decays producing unpolarised emission due to the random orientation of the holes.

The configurations with parallel electron spins are either bright (figure 3.2 (a.1)) or dark (figure 3.2 (a.2)). For both states, relaxation of the p-shell electron to the s-shell will not occur without a spin flip due to Pauli blocking which only allows two electrons to populate the same energy level when they have opposite spin.

The bright state could recombine radiatively leaving behind a spin down electron in the p-shell which then further relaxes to the ground state. However, the anisotropic exchange interaction between electron and hole [45, 47, 62, 84] enables also another process: it couples the bright hot trion state $(p_e^{\uparrow} s_e^{\downarrow}; s_h^{\Uparrow})$ to the hot singlet trion state $(p_e^{\uparrow} s_e^{\downarrow}; s_h^{\Downarrow})$ (figure 3.2 (b.2)). The admixture of light hole contributions to the heavy hole state allows the synchronous reversal of the p-shell

[3]For a detailed discussion of the hot trion finestructure see chapter 1.8.

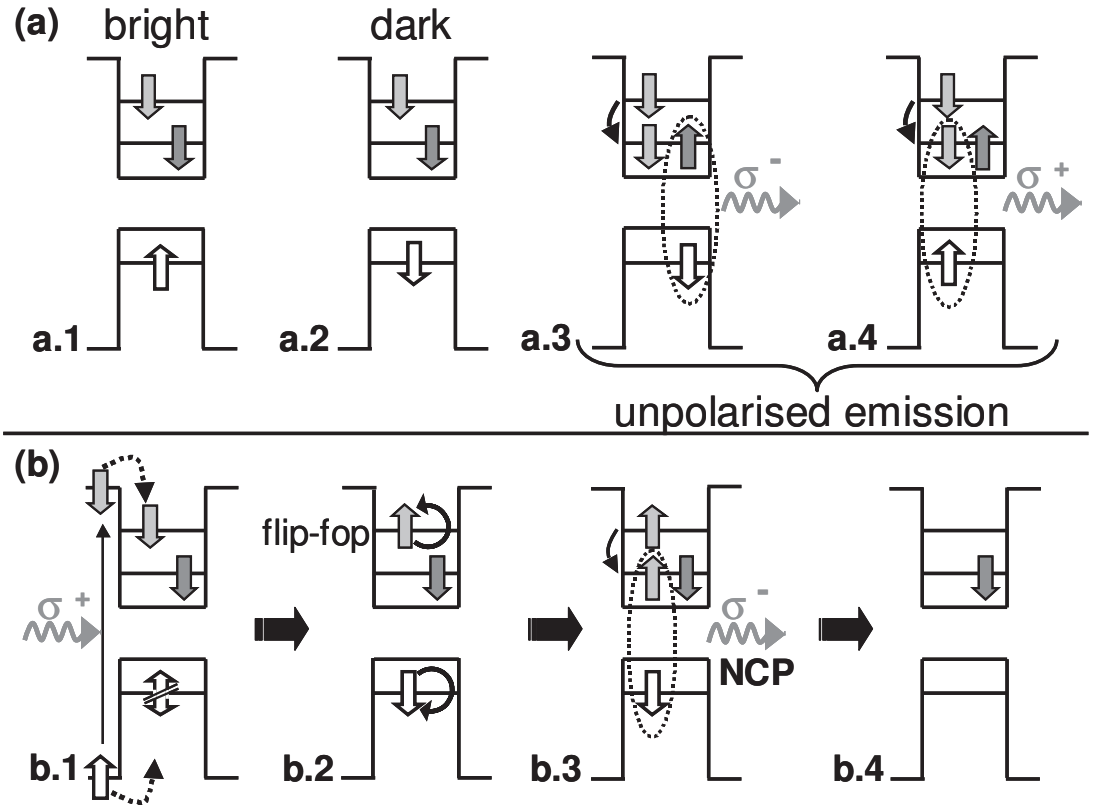

Figure 3.2: (a) Simplified scheme of the possible hot trion configurations for σ^+ excitation assuming that the hole spin is lost during relaxation whereas the electron spin is kept. The singlet states (a.3) and (a.4) together yield unpolarised emission due to the random orientation of the hole. (b) NCP emission from the bright trion: The electron-hole spin flip-flop (b.2) is followed by relaxation to the ground state. The ensuing radiative decay of the trion exhibits NCP (b.3). The resident electron is left behind polarised (b.4), maintaining its spin until the next excitation cycle (b.1). The dark trion eventually also exhibits NCP (see text).

electron spin and the angular momentum of the hole, an electron-hole flip-flop. After this, a fast relaxation to the trion ground state is possible. By the transfer of angular momentum from the electron to the hole, information about the circularly polarised excitation is transfered to the previously randomly oriented hole. The hole in the trion ground state is now polarised with angular momentum -3/2. The radiative decay therefore results in negative circular polarisation (figure 3.2 (b.3)) due to the orientation of the hole angular momentum.

The probability f of the spin flip-flop leading to negative circular polarisation is obviously governed by the competition between the radiative decay time τ_r of the bright hot trion state and the spin flip-flop time τ_{ff}. Figure 3.3 shows these two possible decay channels for the bright hot trion. f is given in terms of the flip-flop rate γ_{ff} and the radiative decay rate of the bright hot trion γ_r:

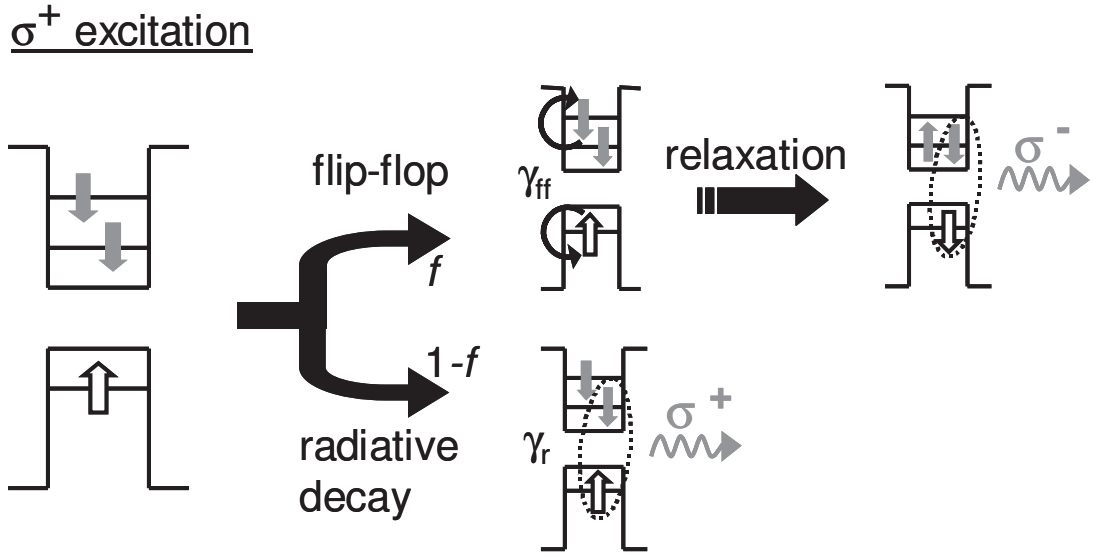

Figure 3.3: The two possible channels for the bright hot trion: there either occurs an electron-hole spin flip-flop with probability f, then relaxation to the ground state and decay emitting negative circular polarisation – or direct radiative decay. f is given in terms of the flip-flop rate γ_{ff} and the radiative decay rate γ_r (see text).

$f = \gamma_{ff}/(\gamma_{ff} + \gamma_r)$. In order to estimate f we take $\gamma_{ff} \approx \Delta_1/h$ [64] where Δ_1 is the magnitude of the anisotropic exchange interaction[4]. For the quantum dots under study it was measured that $\Delta_1 \approx 10$ μeV [45, 85]. With this value and $\tau_r \approx 300$ ps (c. f. chapter 1.4.2, [70]) we obtain $f \approx 0.42$.

An analogous mechanism for the dark hot trion would lead to the emission of positively polarised light. However, for the dark state this mechanism is thought to be by on average two orders of magnitude weaker than for the bright trion [47, 63, 64, 86]. Another possible process though is the phonon assisted spin flip of the p-shell electron which enables fast relaxation to the trion ground state. In this case the hole has not performed a spin flip and the hole spin remains in the spin down state. The ground state would therefore again decay emitting negatively polarised light. A fraction of the dark trions might also decay nonradiatively [64].

To summarise, we finally state that the bright hot trion state with parallel electron spins provides negative circular polarisation whereas the two states with antiparallel electron spins yield unpolarised emission. The dark hot trion also exhibits at least partially negative circular polarisation. The photoluminescence polarisation is therefore predominantly negative.

Accumulation of resident electron spin polarisation After the emission of negative circular polarisation, the resident electron stays behind with a well-

[4] c. f. chapter 1.3.2

defined polarisation. Its spin direction corresponds to that of the hole before the decay of the trion and is hence defined by the helicity of the emitted photon. Measured time integrated over the ensemble, σ^+ excitation predominantly leads to σ^- emission and leaves behind a spin down polarised resident electron as shown in figure 3.2 (b.4). In this way, the circular polarisation of the photoluminescence reflects the spin of the resident electron remaining in the quantum dots.

What is central to our experiment is, that the resident electron keeps a memory of its polarisation until the next excitation cycle of the quantum dot [63]. This leads to an accumulation of negative circular polarisation over several excitation events. Figures 3.2 (b.1) and (b.4) illustrate that in the quantum dots containing resident electrons which have already been polarised after the emission of negative circular polarisation, hot trions are formed after the next excitation with the spins of photoinjected and resident electrons being parallel. These trions eventually decay again emitting negatively polarised photoluminescence. At the same time, in each excitation cycle a fraction of the quantum dots which have housed a trion with antiparallel electron spins in the previous cycle also undergo the negative circular polarisation mechanism leading to the polarisation of their resident electrons [75, 87]. Thus, the negative polarisation increases from cycle to cycle until it saturates with the maximum resident electron spin polarisation achievable under the given conditions.

The degree of polarisation is consequently governed by three factors: (i) the average spin orientation retained by the photoinjected electron during capture into the quantum dot and relaxation to the p-shell, (ii) the average spin orientation of the resident electron and (iii) the probability of the electron-hole spin flip-flop in the bright hot trion necessary to obtain negative circular polarisation.

The negative circular polarisation thus is as much dependent on the spin memory of the photoexcited electron as on that of the resident electron. In order to show that the resident electron spin really retains a memory of its polarisation between two initialisations we study the power dependence of the negative circular polarisation. Figure 3.4 shows the polarisation of the photoluminescence as a function of excitation power. For low excitation densities, the polarisation is very low and even slightly positive for the lowest excitation densities, then the negative polarisation increases with power until it eventually saturates.

In order to explain why the circular polarisation possibly becomes positive at low powers we also have to take a closer look at the process of carrier capture. For excitation above the confined quantum dot states, holes and electrons might be captured independently of one another [70, 81, 88]. Particularly, holes may be captured before electrons by negatively charged quantum dots due to the attractive interaction of the resident electron [89]. This means that the quantum dots may contain a single hole and the resident electron for a certain time until an additional electron is also captured. This time increases when the excitation density is decreased. Therefore, for low excitation power, a captured hole may already recombine with the resident electron before the trion is formed [73]. The

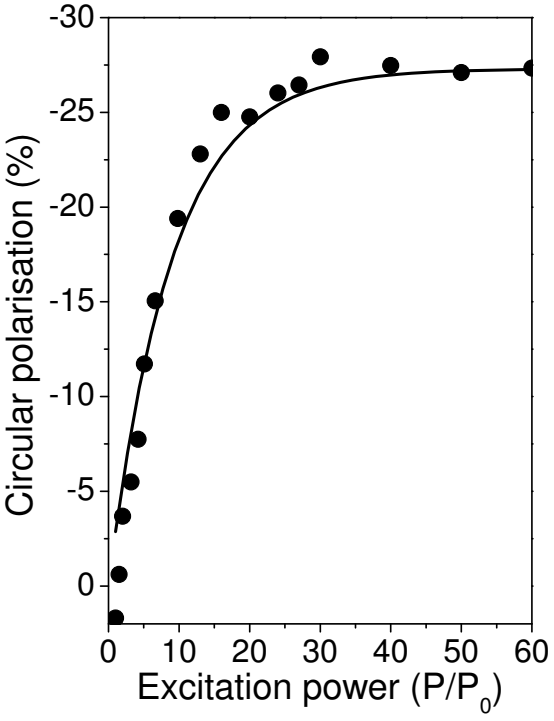

Figure 3.4: Excitation power dependence of the circular polarisation of the PL. At $P_0 = 0.5$ mW the polarisation is slightly positive, then it turns negative and the negative polarisation eventually saturates at high excitation powers. Solid line: asymptotic exponential fit.

emission of this decay may be weakly positively polarised.

The power dependence shows that the resident electron spin keeps a memory of its polarisation after the emission of negative circular polarisation until the spin is newly initialised. This can be explained as follows. The sample is excited by a pulsed laser with the pulses being separated by 13.2 ns. This gives the lower limit for the time between two excitations of a specific quantum dot. When the excitation density is high, the time between two excitations of a quantum dot is small. The resident electrons have less time to lose their spin orientation before their spin becomes reinitialised. Quantum dots whose resident electrons have already been polarised by the negative circular polarisation effect have a higher probability to exhibit negative circular polarisation again after the next excitation event. negative circular polarisation becomes accumulated. When the excitation density is small, however, each quantum dot is excited less frequently. The resident electron spin may have decayed before it is newly aligned. Every excitation event thus meets randomly polarised resident electrons and no accumulation takes place. The fraction of spin orientation retained by the *photoinjected* electron after relaxation, however, is very unlikely to exhibit a significant excitation power dependence. The potential influence of the excitation energy can be neglected as in all the measurements the excitation wavelength was kept constant to an accuracy of 0.1 nm.

Read out of the resident electron spin polarisation We now discuss the accumulation of electron spin polarisation by means of a very simple model.

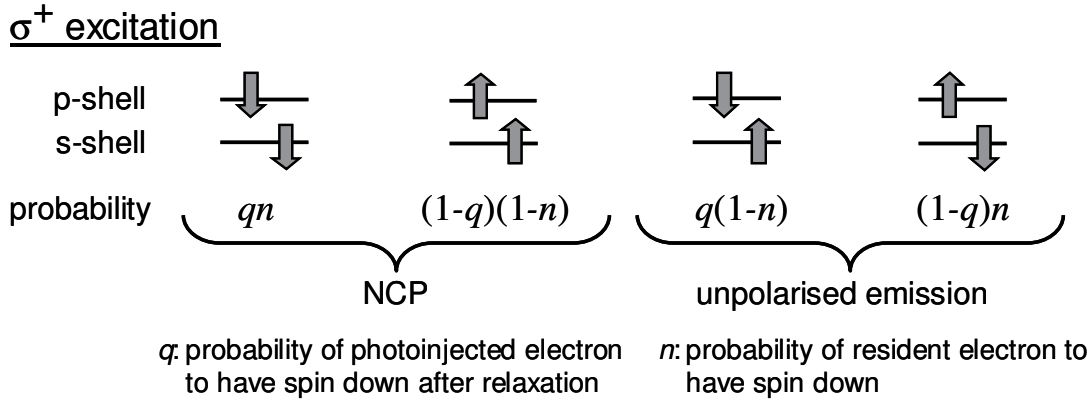

Figure 3.5: The four possible electron spin configurations of the electron-excited trion. q is the probability that the photoinjected electron keeps its spin $\downarrow$ during relaxation, n is the probability that the resident electron has spin $\downarrow$.

Again, we chose the example of σ^+ polarised excitation where an electron with spin $\downarrow$ and a hole with angular momentum $\Uparrow$ is created.

We express the degree of polarisation of the resident electron in terms of the probabilities of finding spin down photoinjected and resident electrons in a quantum dot. Let the probability that the photoexcited electron keeps its spin $\downarrow$ during relaxing to the p-shell be q, and the probability of the resident electron having spin orientation $\downarrow$ be n. Correspondingly, $1-q$ and $1-n$ are the probabilities for $\uparrow$ photoexcited and resident electrons. The probability of the flip-flop process in the hot bright trion is f, the probability of a direct radiative decay is $(1-f)$. Figure 3.5 depicts the probabilities of the four different electron configurations to occur. From the eight possible hot trion spin configurations including the hole angular momentum degree of freedom we can work out, that the degree of circular polarisation of the photoluminescence is given by

$$\rho_c = f(1-n-q). \tag{3.2}$$

We rewrite equation 3.2 introducing the photoinjected and resident electron polarisations $Q = 1-2q$ and $N = 1-2n$:

$$\rho_c = \frac{f}{2}N + \frac{fQ}{2}. \tag{3.3}$$

A value of ± 1 of N indicates 100 % spin polarisation of the resident electrons in either direction and a value of 0 indicates no polarisation, corresponding to 50 % up and 50 % down resident electrons. This analogously applies to Q for the photoinjeced electrons. f is the probability for the electron-hole flip flop to occur.

Let us analyse the power dependence of the negative circular polarisation in terms of equation 3.3. In this expression only the resident electron spin memory

$N = \rho_e$ is power dependent. Thus, the power dependence of the negative circular polarisation is solely determined by the average spin memory N which is accumulated after several excitation cycles. The increase of negative circular polarisation with power directly reflects the increase of resident electron polarisation. The degree of polarisation of the photoluminescence is consequently a measure for the polarisation of the resident electron *before* the excitation. In particular, there exists a linear dependence between the polarisation of the photoluminescence and the spin polarisation $\rho_e = S_z/S$ of the resident electron.

In our studies of the electron-nuclear spin system in singly negatively charged quantum dots we exploit these properties of the negative circular polarisation effect: We optically *create* electron spin polarisation ρ_e and *read out* the resident electron spin polarisation by monitoring the degree of circular polarisation of the photoluminescence. All experiments presented in this work are based on the measurement of the circular polarisation of the photoluminescence after excitation with circularly polarised light.

3.3 Unpolarised Nuclear Spin System

3.3.1 The Nuclear Spin Fluctuation Field

Having discussed how the resident electron spin becomes optically oriented we now study the nuclear spin system in quantum dots and its effect on the resident electron spin polarisation. An electron inside a quantum dot is strongly localised compared to bulk semiconductors. In the quantum dot ground state, a single electron has a s-type wavefunction leading to a non-zero probability of the electron to be found at the site of *each* quantum dot nucleus. Thus, the spin-spin interaction between the electron spin and the nuclear spins is strongly enhanced as compared to bulk semiconductors. The electron spin interacts with the spins of the quantum dot nuclei via the hyperfine interaction. The interaction between an s-shell electron spin $\mathbf{S}$ and a single nuclear spin with spin $\mathbf{I}$ is given by the Fermi contact hyperfine Hamiltonian [15, 16, 90, 91]

$$\hat{H}'_{hf} = \frac{16\pi}{3}\frac{\mu_I}{I}\,\mu_B\,(\hat{\mathbf{I}}\cdot\hat{\mathbf{S}})\,|\psi(\mathbf{R}_i)|^2. \tag{3.4}$$

μ_B is the Bohr magneton, μ_I the nuclear magnetic moment, $|\psi(\mathbf{R}_i)|^2$ the probability density of the electron at the location of the i^{th} nucleus $\mathbf{R}_i$ and $\hat{\mathbf{S}}$, $\hat{\mathbf{I}}_i$ the spin operators of the electron spin and the nuclear spin. The electron wavefunction has an overlap with a few thousand to 10^6 nuclei, depending on the quantum dot type[5]. For the quantum dots studied here about 10^5 nuclei interact with the electron, which can be estimated if we consider a disk shaped geometry of the

[5] CdSe/ZnSe quantum dots contain a few thousand nuclei [92–94], some III-V semiconductor quantum dots may contain up to 10^6 nuclei, see e. g. [20]).

dots with a diameter of 20 nm and a height of 5 nm. In order to obtain the interaction of the electron spin with all nuclei in the extent of the electron wave function we thus have to sum equation 3.4 over all nuclei:

$$\hat{H}_{hf} = \frac{16\pi}{3}\,\mu_B \sum_i \frac{\mu_{I_i}}{I_i}(\hat{\mathbf{I}}_i \cdot \hat{\mathbf{S}})\,|\psi(\mathbf{R}_i)|^2. \tag{3.5}$$

We wish to express the action of the nuclear spins on the electron in terms of a magnetic field. We thus interpret the energy represented by the Hamiltonian 3.5 as an electron spin energy in an effective magnetic field $\mathbf{B}_N$,

$$E_Z = \mu_B g_e \mathbf{B}_N \mathbf{S}\,, \tag{3.6}$$

with the electron g factor g_e. Comparing 3.6 and 3.5 thus yields for the nuclear magnetic field acting on the electron

$$\mathbf{B}_N = \frac{16\pi}{3g_e} \sum_i \mu_{I_i} \frac{\mathbf{I}_i}{I}\,|\psi(\mathbf{R}_i)|^2\,. \tag{3.7}$$

The effective nuclear magnetic field $\mathbf{B}_N$ can thus be interpreted as the sum of the magnetic fields produced by the $\approx 10^5$ nuclei acting on the electron.

Without any external influence the nuclear spins are generally randomly polarised with every direction having the same probability. However, even in a completely unpolarised nuclear spin system the sum in equation 3.7 is not zero. When the nuclear spins are completely randomly polarised , in any given direction $\alpha = x, y, z$ the number of nuclei constituting the nuclear magnetic field parallel and antiparallel to this direction should be equal. However, due to statistical fluctuations, in reality one has for $\tilde{N}$ nuclear spins in each direction an error of $\sqrt{\tilde{N}}$. For a system of $N_L = 3\tilde{N}$ nuclear spins, the error thus is $\sqrt{N_L/3}$ along each axis. This results in an effective magnetic field $\delta\mathbf{B}_N$ [91]. The magnitude of this nuclear spin fluctuation (NSF) field can be estimated using the maximum nuclear magnetic field, corresponding to a nuclear spin system which is fully polarised in one direction. If we distribute the maximum magnetic field evenly among all N_L nuclear spins[6], a single nuclear spin on average produces a magnetic field $\beta_N = B_{N,max}/N_L$. With $\sqrt{N_L/3}$ nuclei contributing to $\delta B_{N,\alpha}$ we obtain

$$\delta B_{N,\alpha} = \sqrt{\frac{N_L}{3}}\beta_N = \frac{B_{N,max}}{\sqrt{3N_L}}\,. \tag{3.8}$$

We will later estimate[7] that $B_{N,max} \approx 8.3$ T. With this value and $N_L = 10^5$ we obtain $\delta B_{N,\alpha} \approx 15$ mT. Thus the inplane nuclear fluctuation field is $\delta B_{N,xy} \approx 20$ mT. The magnitude of the total nuclear fluctuation field is $\delta\mathbf{B}_N \approx 26$ mT.

[6] This is obviously a simplification as the quantum dots are composed out of three different nuclear species. However, we only aim at obtaining a rough estimate and justifying $\delta B_N \propto 1/\sqrt{N_L}$.

[7] See chapter 3.4

In a magnetic field of this magnitude an electron precesses with a revolution time of the order of 1 ns whereas the timescale of the precession of the nuclear spins in the hyperfine field of the electron is in the order of 1 μs. Therefore, the electron initially is exposed to a "snapshot" of the nuclear spin fluctuation field $\delta\mathbf{B}_N$ with the nuclear spin configuration remaining "frozen". We denote the *frozen* nuclear fluctuation field $\mathbf{B}_f$. The direction and magnitude of $\mathbf{B}_f$ vary randomly from quantum dot to quantum dot in the ensemble. Ensemble averages of expressions depending on B_f can be calculated using the distribution of the frozen fluctuation fields. For each direction $\alpha = x, y, z$ the distribution of $B_{f,\alpha}$ is given by a Gaussian probability density distribution function [17, 95]

$$W(B_{f,\alpha}) = \frac{1}{\sqrt{\pi}\Delta_{B_{f,\alpha}}} \exp\left(-\frac{B_{f,\alpha}^2}{\Delta_{B_{f,\alpha}}^2}\right), \tag{3.9}$$

where $\Delta_{B_{f,\alpha}}$ is the dispersion of the nuclear fluctuation field distribution.

The resident electron spin precesses about the frozen fluctuation field. The fact that the frozen fluctuation field in each quantum dot has a different direction lets the resident electrons in different quantum dots precess about different axis. This leads to a rapid decay of the ensemble average electron spin orientation on a timescale of a few nanoseconds corresponding to the precession period of the electron spin about $\mathbf{B}_f$. Note that this is also true for a single dot when the polarisation is measured as an average over many excitation cycles [17].

3.3.2 Spin Precession

In this work, we often will have to deal with the action of magnetic fields on the spin of the resident electron. We generally analyse this action by using the picture of spin precession about the magnetic field. In this section we wish to briefly discuss this concept and define several quantities which will be used later.

In our experiments, the resident electron spin is always initialised parallel to the z axis. We thus have to deal with the precession of an initial spin $\mathbf{S}_0 = (0, 0, S_0)$. Further always measure the z projection of the resident electron spin. We can therefore confine ourselves to consider S_z. The time evolution of the z projection of a spin $\mathbf{S}_0$ precessing in an oblique magnetic field $\mathbf{B} = (B_x, B_y, B_z)$ is given by

$$S_z(t) = S_0\left(\frac{B_z^2}{B^2} + \frac{B_x^2 B_y^2}{B^2}\cos\omega t\right). \tag{3.10}$$

$\omega = \mu_B|g_e|B/\hbar$ is the Larmor precession frequency of the electron spin in the magnetic field B with the Bohr magneton μ_B and the electron g factor g_e. Figure 3.6 illustrates the behaviour of $S_z(t)$. S_z/S_0 is shown as a function of time in units of the precession period $T_p = 2\pi/\omega$ for different directions of the magnetic field indicated by the angle θ between $\mathbf{B}$ and the z axis. In a purely transverse magnetic field ($\theta = 90°$) $\mathbf{S}_0$ precesses in the z-y-plane. S_z thus changes sinusoidally between $+S_0$ and $-S_0$.

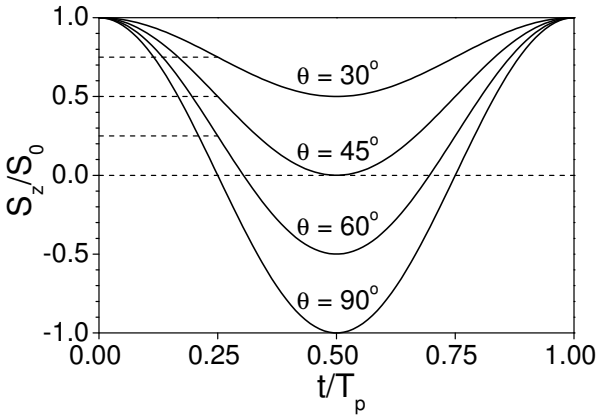

Figure 3.6: Time evolution of S_z of a precessing spin for different angles θ between the z axis and the direction of the field about which the spin precesses. x axis in units of the precession period T_p. The dashed lines show the respective time averages.

Obviously in quantum dots the resident electron spin is not allowed to precess for an infinitely long time. The spins either relax or become reoriented along the z axis by a new excitation of the quantum dot. In order to determine which S_z of a precessing spin we actually measure, we thus have to distinguish two regimes:

Regime (i): the time the spin is given to precess is short compared to T_p. Then, the precession is terminated well *before* the spin has completed one revolution. The measured S_z will be that at the point of time the precession is stopped. This is illustrated in figure 3.7 (a). The grey arrows correspond to the position of the spin at certain points of time in the course of the precession and the z projections at that times.

Regime (ii): the time the spin is given to precess by the spin relaxation time or the time interval between two initialisations of the spin is long compared to the precession period T_p of the spin. In this case the spin performs several revolutions before the precession is terminated. As the electron spins do not precess coherently after non-resonant excitation we see a *time average* of the precessing spin. In figure 3.7 (b) regime (ii) is depicted. The measured spin polarisation corresponds to the z projection of the time averaged electron spin $\mathbf{S}_{av}$.

Let us first consider regime (i) and define a quantity which will occur again later in this work. There exists a characteristic life time $T_2^\star$ of the system with

$$1/T_2^\star = 1/\tau_r + 1/\tau_s \,, \tag{3.11}$$

where τ_s be the spin relaxation time and τ_r the reinitialisation time of the spin. Let us further assume that the spin precesses in a purely transverse magnetic field $B_x\mathbf{e}_x$. The precession period T_p is proportional to $1/B_x$. Thus, the higher B_x the faster the precession and the further the spin will have precessed when the precession is stopped after $t \approx T_2^\star$. The magnitude of S_z at that time will be the one observed. It is hence determined by a competition between the strength of the magnetic field governing the precession period T_p and $T_2^\star$ determining when

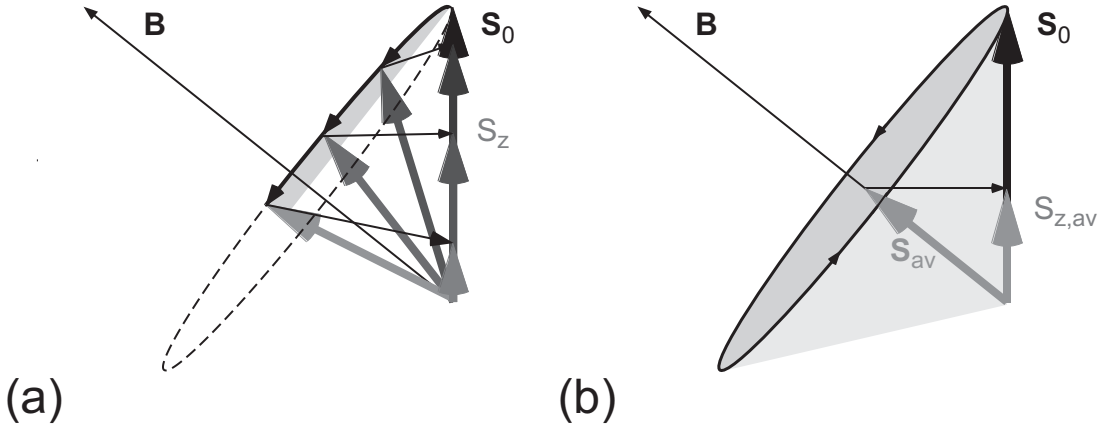

Figure 3.7: (a) Regime (i): Precession of an electron spin $\mathbf{S}_0$ about the total magnetic field $\mathbf{B}$. The time span the spin is allowed to precess before it is reinitialised or decays determines the z projection S_z left at that point of time. The grey arrows show the position of the spin at different points of time during its precession and the respective z projections. (b) Regime (ii): The spin performs several revolutions before it is reinitialised. Thus, the z projection of the time averaged spin $\mathbf{S}_{av}$, $S_{z,av}$, is observed.

the precession is terminated. Measuring the electron polarisation ρ_e as a function of the magnetic field B_x yields a Lorentz curve

$$\rho_e(B_x) = \frac{\rho_e(0)}{1 + (\frac{g_{e,x}\mu_B B_x}{\hbar} T_2^\star)^2} \,. \tag{3.12}$$

$g_{e,x}$ is the electron g factor in x direction. A measure for the depolarisation of a spin with characteristic life time $T_2^\star$ in a transverse magnetic field is the half width at half maximum $B_{1/2}$ of the Lorentz curve. From equation 3.12 it is found that

$$B_{1/2} = \frac{\hbar}{|g_{e,x}|\mu_B T_2^\star} \,. \tag{3.13}$$

Measuring a B_x dependence of the electron spin polarisation could thus in principle be used to determine $T_2^\star$ via $B_{1/2}$. That this is not true in general will become obvious later in this work.

In our experiments, however, the smallest magnetic field acting on the resident electron spins is defined by the nuclear frozen fluctuation field B_f which is of the order of tens of millitesla. This corresponds to precession periods in the range of at most several nanoseconds. We excite the sample with pulsed laser excitation. The lower limit for the time interval between two initialisations of the resident electron spin is thus given by the pulse separation of the laser pulses which is in our experiments 13.2 ns. The time the spin is allowed to precess is thus long compared to the precession period. We thus expect that in our experiments the

system is in regime (ii). We always observe the z projection of a *time average* of the precessing initial spin $\mathbf{S}_0$.

We inspect this situation further. The time average $\bar{S}_z$ of $S_z(t)$ in equation 3.10 is obviously given by

$$\bar{S}_z = S_0 \frac{B_z^2}{B^2} \,. \tag{3.14}$$

The time average $\mathbf{S}_{av}$ of a precessing spin is directed along the precession axis which is defined by the magnetic field $\mathbf{B}$ (see figure 3.7 (b)). Thus, $\bar{S}_z$ can also be expressed in terms of the angle θ between the magnetic field and the z axis according to

$$\bar{S}_z = S_0 \cos^2 \theta \,, \tag{3.15}$$

where θ is given in terms of the magnetic field as

$$\theta(\mathbf{B}) = \frac{\pi}{2} - \arctan\left(\frac{B_z^2}{\sqrt{B_x^2 + B_y^2}}\right) . \tag{3.16}$$

The value of $\bar{S}_z$ is thus only determined by the *direction* of the magnetic field and not by its magnitude as long as B is large enough to ensure that the precession period T_p is small compared to the time the spin is allowed to precess.

3.3.3 Action of the Frozen Fluctuation Field on the Resident Electron Spin Polarisation

In chapter 3.3.1 we have shown that in quantum dots is generally always acted upon by the frozen fluctuation field $\mathbf{B}_f$. In this section we wish to ascertain how the resident electron spin is influenced by B_f and how this is reflected in measurements of the resident electron spin polarisation.

In the absence of an external magnetic field, only the internal nuclear frozen fluctuation field acts on the electron spin. The direction and the magnitude of $\mathbf{B}_f$, however, is different in each dot of the ensemble. The ensemble average can be expressed by globally using an average magnetic field $B_{f,\alpha}$ for every direction $\alpha = x, y, z$. Let us recall what we have discussed in the previous section 3.3.2: in our experiments the time the electron spin is given to precess is $t \geq 13.2$ ns which is long compared to the precession period T_p in a magnetic field of tens of millitesla as it is given by B_f. We thus always measure a time averaged z projection of the precessing electron spin. The action of the frozen fluctuation field on the resident electron is therefore expressed by the equation

$$\bar{S}_z(\mathbf{B}_f) = S_0 \frac{B_{f,z}^2}{B_f^2} \,, \tag{3.17}$$

introduced in chapter 3.3.2 (3.14). In a completely randomly polarised nuclear spin system $B_{f,x} = B_{f,y} = B_{f,z}$. Inserting this in equation 3.17 yields

$$S_z(\mathbf{B}_f) = \frac{S_0}{3}\,. \tag{3.18}$$

For a randomly polarised nuclear spin system with all directions having the same probability the ensemble average electron spin polarisation thus quickly decays to about one third of its initial value [17, 18].

The angle theta between the average frozen fluctuation field $\mathbf{B}_f$ and the z axis is in this case

$$\begin{aligned} \theta(\mathbf{B}_f) = \quad \theta_m &= \frac{\pi}{2} - \arctan\left(\frac{B_{f,z}^2}{\sqrt{B_{f,x}^2 + B_{f,y}^2}}\right) \\ &= \frac{\pi}{2} - \arctan\frac{1}{\sqrt{3}} \\ &\mathrel{\widehat{=}} 54.7^\circ\,. \end{aligned} \tag{3.19}$$

θ_m is the "magic angle"[8] characteristic for a randomly polarised nuclear spin system.

The decay of the resident electron polarisation due to the *frozen* fluctuation field occurs on a timescale of several nanoseconds. The nuclear spin fluctuation fields $\delta\mathbf{B}_N$ in each quantum dot, however, evolve independently of one another on a time scale of microseconds. The precessing resident electrons follow $\delta\mathbf{B}_N$. When the electron spin is not reinitialised in intervals $\ll 1\ \mu$s, $\delta\mathbf{B}_N$ is not "frozen" anymore. The time evolution of the fluctuation field leads to the total decay of the electron spin polarisation on a microsecond timescale [17, 18].

The magnitude of B_f may be experimentally determined by measuring the dependence of the photoluminescence polarisation on a longitudinal external magnetic field $\mathbf{B} = B_z\mathbf{e}_z$ [95]. However, it is known that oriented electron spins transfer angular momentum to the nuclear spins. This leads to the build up of nuclear polarisation along the direction of the electron polarisation, in our case along the z axis, and consequently to an overbalance in favour of the nuclear magnetic field component along the z direction. For studying the electron polarisation in a *randomly* polarised nuclear spin system, the generation of nuclear spin polarisation thus has to be impeded. This is achieved by periodically switching the circular polarisation of the excitation between σ^+ and σ^- so that the net transfer of angular momentum into the system is zero. This prevents the accumulation of nuclear polarisation. The nuclear spin system of the quantum dots should consequently be randomly oriented under rapidly modulated excitation. Note that electron polarisation builds up on a timescale of hundreds of nanoseconds so that the microsecond modulation does not affect the accumulation of electron spin in the system.

[8] This term originates from the field of nuclear magnetic resonance.

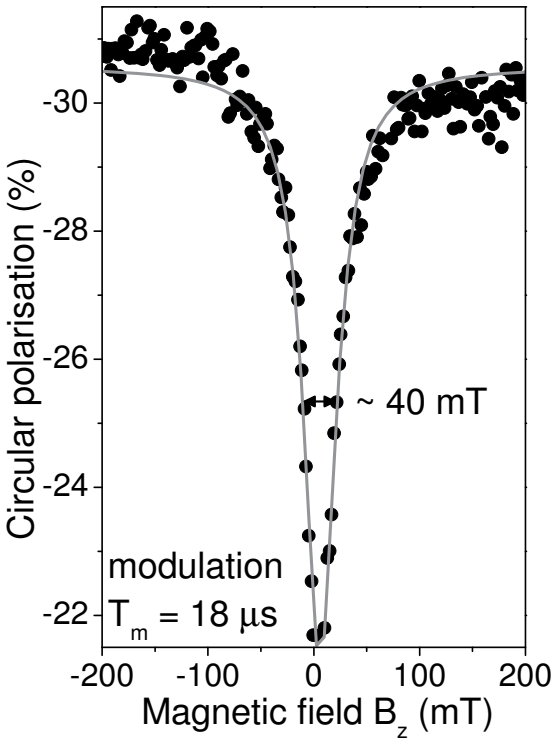

Figure 3.8: Dependence of the PL polarisation on a longitudinal magnetic field (circles), Lorentz fit (solid line). Modulation of the excitation polarisation between σ^+ and σ^- with period $T_m = 18$ μs impedes nuclear polarisation. At $B_z = 0$ mT the resident electrons are depolarised due to precession about the nuclear frozen fluctuation field. The external magnetic field gradually increases the field component in z direction which leads to a decrease of the angle θ. The electron polarisation becomes restored and saturates above $B_z > 90$ mT. The width of the dip then is a measure for the magnitude of the transverse frozen fluctuation field.

Figure 3.8 shows such a B_z dependence of the circular photoluminescence polarisation under excitation rapidly modulated between σ^+ and σ^- with period $T_m = 18$ μs. The resident electron spins are optically initialised as a consequence of the negative circular polarisation effect[9]. At $B_z = 0$ mT they only experience the frozen fluctuation field $\mathbf{B}_f$. The electron spins thus lose a large fraction of their initial spin polarisation because they precess about the frozen fluctuation field of the nuclei.

The vector diagrams figure 3.9 visualise what happens when the external magnetic field $\mathbf{B} = B_z \mathbf{e}_z$ is increased. The resident electrons in each quantum dot then experience a total field $\mathbf{B}_t = \mathbf{B} + \mathbf{B}_f$. Thus the z component of the total magnetic field experienced by the electrons grows constantly. This consequently leads to a decrease of the angle θ between the z axis and the precession axis defined by the total magnetic field. The z component of the precessing electron spin is restored with increasing B_z (see equations 3.17 and 3.19).

In figure 3.8, at external magnetic fields $B_z > 90$ mT the circular polarisation becomes saturated. There the external magnetic field is strong enough to fully overcome the frozen fluctuation field. The width of the dip is a measure for the magnitude of the in-plane component $B_{f,xy}$ of the frozen nuclear fluctuation field. In figure 3.8 the full width at half maximum of the dip is $B_{FWHM} \approx 40$ mT. This corresponds to an inplane frozen fluctuation field of $B_{f,xy} \approx 20$ mT which agrees with the estimate of $B_{f,xy} \approx 20$ mT given above and the theoretical estimates in [17, 91].

[9] c. f. chapter 3.2.

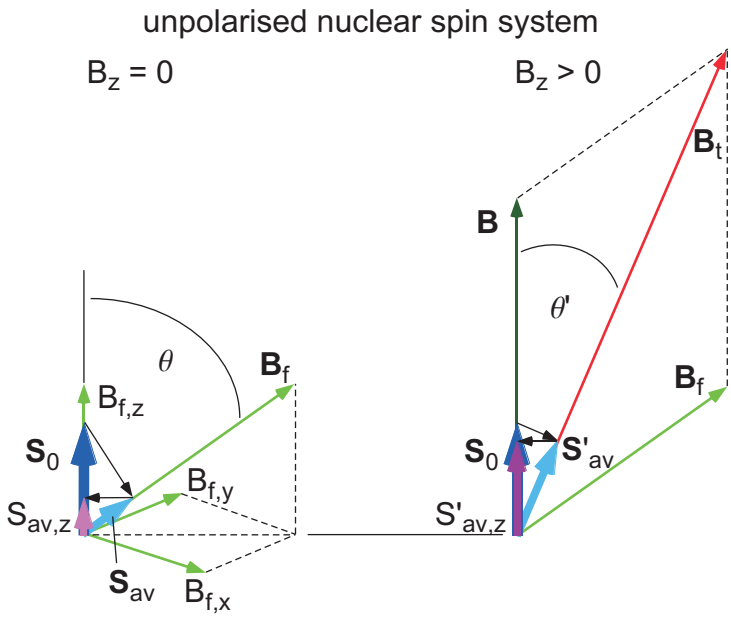

Figure 3.9: Vector diagram of the fields acting on the electron spin for an unpolarised nuclear spin system, initial spin $\mathbf{S}_0$, $\mathbf{S}_{av}$ time average of the precessing $\mathbf{S}_0$. At $B_z = 0$ the electron spin is largely depolarised. If an external field $= B_z \mathbf{e}_z$ is applied, the angle between the total field $\mathbf{B}_t = \mathbf{B}_f + \mathbf{B}$ and the z axis, θ', decreases compared to θ for $B_z = 0$. The projection of the precessing electron spin onto the z axis, $S'_{av,z}$, increases compared to $S_{av,z}$.

We observe in figure 3.8, though, that the ratio between the maximum polarisation at high B_z and the minimum polarisation at $B_z = 0$ is not one third as expected for randomly polarised nuclear spins according to equations 3.17 and 3.18. It was indeed shown that the amplitude and the width of the dip obtained for measuring the B_z dependence of the polarisation also depend on the excitation density [95]. The authors attribute this behaviour to the fact that even when the net spin transfer into the system is zero as it is the case when the excitation helicity is quickly modulated, an imbalance between the components of the frozen fluctuation field may occur due to optical pumping. This leads to a decrease of the transverse components of $\mathbf{B}_f$ and an increase of its longitudinal component. Therefore, the resident electron may have a polarisation which is greater than one third of the maximum polarisation for strong pumping also at $B_z = 0$. There could also exist a circular polarisation offset in figure 3.8 violating the proportionality between circular polarisation and electron polarisation.

3.4 The Overhauser Effect

The illumination of a semiconductor with circularly polarised light constantly injects angular momentum into the system. This leads to the optical orientation of electron spins along the excitation axis. In our case this orientation is accomplished by the negative circular polarisation effect as we have shown in the chapter 3.2. Optical orientation of the resident electrons may also result in a polarisation of the nuclei. The electrons transfer their spin to the nuclei via electron-nuclear spin flip-flops which are mediated by the hyperfine interaction [8, 11, 19–21]. This phenomenon is known as Overhauser effect[10] [96]. For quantum dots, it was shown that nuclear polarisation obtained in this way can lead to an effective nuclear magnetic field of the order Tesla [19, 22, 23]. We also call this nuclear magnetic field "Overhauser field". In most of these experiments the nuclear magnetic field was measured via the energy shift of the electron Zeeman levels caused by the nuclear field of the polarised nuclear spins, the Overhauser shift.

In contrast to the polarisation of nuclei solely by a large static magnetic field at millikelvin temperatures, the *optical* orientation of nuclear spins is referred to as "dynamic nuclear polarisation".

The Overhauser field has a dramatic influence on the electron spin polarisation. As we will see, it can e. g. depress the depolarisation of the electron spins by the frozen fluctuation field. It is therefore important to know how strong the Overhauser field can possibly become and which factors affect the generation of nuclear polarisation. In this section we at first approach the Overhauser field theoretically. Particularly, we focus on the question how the environment of the nuclear spins made up of their neighbour nuclei, the electron spin and external magnetic fields influence the ability of the nuclear spin system to become polarised.

The main interaction *depolarising* the nuclei is the dipole-dipole interaction between a nuclear spin and the nuclear spins in its vicinity. It is expressed by the Hamiltonian [90]

$$\mathcal{H}_{dd} = \frac{\mu_N^2}{2} \sum_{i \neq j} \frac{g_i g_j}{\mathbf{r}_{i,j}^3} \left(\mathbf{I}_i \mathbf{I}_j - 3 \frac{(\mathbf{I}_i \mathbf{r}_{i,j})(\mathbf{I}_j \mathbf{r}_{i,j})}{\mathbf{r}_{i,j}^2} \right) . \tag{3.20}$$

μ_N is the nuclear magneton and $\mathbf{r}_{i,j}$ is the vector between a nucleus i and the nuclei j interacting with it. The strength of the dipole-dipole interaction may be represented by an effective magnetic field exerted on a nuclear spin by its neighbouring spins, the dipole-dipole field or local field B_L [15, 16, 97, 98]. The magnitude of B_L has been calculated for GaAs [15] to be ≈ 0.15 mT. In a magnetic field of this magnitude the Larmor precession period of a nuclear spin

[10] The polarisation of nuclear spins via the hyperfine interaction with electron spins was first shown for metals by A. W. Overhauser in 1953.

is of the order of 10^{-4} seconds. This timescale defines the relaxation time T_2 of the nuclear polarisation.

The time to fully polarise the nuclear system via angular momentum transfer from oriented electrons is of the order of 10^{-2} to 10^{-1} seconds[11] [99], up to three orders of magnitudes slower than it takes to depolarise the nuclear spins via the dipole-dipole interaction. It thus looks like that a magnetic field $B \gg B_L$ is needed to suppress the dipole-dipole depolarisation in order to obtain nuclear spin polarisation. We will see, however, that the nuclear spins can also be polarised at magnetic fields $B \gtrsim B_L$.

Due to the dipole-dipole field, if we study nuclear polarisation in an external magnetic field, we have to distinguish two regimes of fields allowing nuclear polarisation to occur, $B \gg B_L$ where the depolarising influence of B_L is suppressed, and second $B \approx B_L$.

If $B \gg B_L$ the dipole-dipole interaction between the nuclei can be neglected. The nuclei are thus decoupled from one another and the interaction of each of them with the electron may be calculated separately ([16], chapter 2, [13]). The average nuclear spin $\langle I \rangle$ for a nuclear species with spin I in the presence of an average electron spin S in a magnetic field $\mathbf{B}||\mathbf{S}$ is generally calculated in terms of the Brillouin function $\mathfrak{B}_I$ [90, 100, 101]

$$\mathfrak{B}_I(x) = \frac{2I+1}{2I} \coth\left(\frac{2I+1}{2I}x\right) - \frac{1}{2I}\coth\left(\frac{1}{2I}x\right) . \tag{3.21}$$

Originally, the Brillouin function has been defined in connection with the calculation of the magnetisation of an ideal paramagnet as a function of applied magnetic field. Under optical orientation conditions [16, chapter 2.9.5]

$$x \approx I \ln\left(\frac{1+2S}{1-2S}\right) . \tag{3.22}$$

The average nuclear spin I as a function of the average electron spin S is then given by

$$\langle I \rangle = I\, \mathfrak{B}_I(x) , \tag{3.23}$$

where $0 < \mathfrak{B}_I(x) < 1$ expresses the degree of nuclear polarisation ρ_n.

Often, the Brillouin function is approximated by the first term of its expansion in powers of S,

$$\mathfrak{B}_I^{(1)} = \frac{4}{3}(I+1)S . \tag{3.24}$$

Obviously this approximation is only valid when S is small. In this approximation the average nuclear spin reads

$$\langle I \rangle \approx \frac{4}{3} I(I+1)S . \tag{3.25}$$

[11] We will address the accumulation dynamics of nuclear polarisation in chapter 7.3.

We will now generalise this expression to the situation where the magnetic field $\mathbf{B}$ is not parallel to $\mathbf{S}$. In that case only the component of the electron spin parallel to the field, $\mathbf{S}\cdot\mathbf{B}/B$, contributes to the polarisation of the nuclei. On the other hand, under stationary conditions, the nuclear polarisation will be directed along the external field, $\langle\mathbf{I}\rangle = \langle I\rangle\mathbf{B}/B$ ([16], chapter 2.9.5). If we include these demands, we obtain the vector generalisation of equation 3.25 by replacing

$$S \longrightarrow \frac{\langle\mathbf{S}\rangle\cdot\mathbf{B}}{B^2}\mathbf{B}\,, \tag{3.26}$$

which yields the average nuclear spin

$$\langle\mathbf{I}\rangle = \frac{4}{3}I(I+1)\frac{\langle\mathbf{S}\rangle\cdot\mathbf{B}}{B^2}\mathbf{B} \tag{3.27}$$

for an arbitrary orientation of the magnetic field with respect to the electron spin.

Let us now investigate the case where the condition $B \gg B_L$ is no longer satisfied. If the nuclei are exposed to a magnetic field of magnitude *comparable to the dipole-dipole field*, B_L can no longer be neglected. One would expect that in this case the build up of nuclear polarisation is hindered as the depolarisation time T_2, given by the dipole-dipole interaction, is much shorter than the time the nuclear spins need to become polarised by oriented electrons. It is thus surprising that even in such small fields nuclear polarisation may occur. It was in fact shown that significant nuclear polarisation builds up at small external fields in the millitesla range and even at zero external magnetic field [23, 25, 102].

The key to this is the concept of nuclear spin temperature. The nuclear spins are well isolated from the lattice because the spin-lattice relaxation time T_1 is orders of magnitude greater than the relaxation time T_2 – it can be as long as days. The nuclear spin system, however, reaches thermodynamic equilibrium in the time $T_2 = 10^{-4}$ s. This equilibrium state can then be described by one single value, the nuclear spin temperature Θ.

The dipole-dipole interaction depolarises the nuclear spins much faster than the nuclear spin system would need to become polarised. As the dipole-dipole interaction does not conserve the total spin of the nuclear spin system, the polarisation in zero magnetic field is thus zero. In a magnetic field, however, even when it is small, angular momentum transfer into the nuclear spin system changes its Zeeman energy. Due to energy conservation, the Zeeman energy becomes transformed into the energy of spin-spin interactions. This lowers the nuclear spin temperature and leads to a non-vanishing nuclear polarisation at $B \neq 0$. The energy transfer between the Zeeman part and the spin-spin part of the total energy works best when the Zeeman energy and the spin-spin energy are comparable. This is the case, however, when $B \approx B_L$. Thus, in small magnetic fields comparable to the nuclear dipole-dipole field the cooling of the nuclear spin system is even most efficient.

In a magnetic field, the nuclear spin temperature Θ gives rise to the polarisation of the nuclear spins with the nuclear polarisation $\rho_c \propto B/\Theta$. It relates the magnetic field to which the nuclei are exposed, to the average nuclear spin achievable in this field, via [16]

$$\langle \mathbf{I} \rangle = \frac{1}{3}(I+1)\mu_I \frac{\mathbf{B}}{\Theta}\,. \tag{3.28}$$

I is the nuclear spin and μ_I the nuclear magnetic moment.

Oriented electrons may lower the temperature of the nuclear spin system. When an average electron spin $\langle \mathbf{S} \rangle$ is present, the inverse spin temperature in a small magnetic field is given by [16]

$$\frac{1}{\Theta} = \beta = \frac{4I}{\mu_I} \frac{\langle \mathbf{S} \rangle \cdot \mathbf{B}}{B^2 + \tilde{B}_L^2}\,. \tag{3.29}$$

$\tilde{B}_L = \sqrt{\xi} B_L$ and ξ is a parameter measuring the relative relaxation rates of the spin-spin and Zeeman energies. For GaAs it has been calculated that $\xi = 2.2$ and $\tilde{B}_L = 0.2$ mT [15]. In our measurements we only have access to $\tilde{B}_L$, and for this reason we focus on this quantity only.

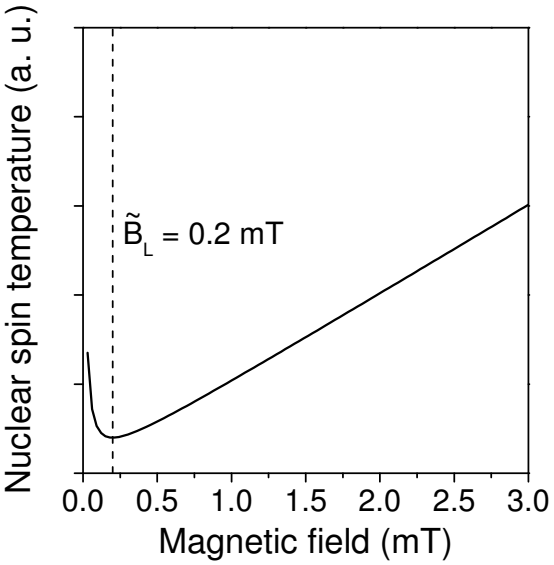

Figure 3.10: The nuclear spin temperature Θ as a function of a magnetic field B. The minimum of Θ is located at $B = \tilde{B}_L = 0.22$.

As explained above, the spin cooling is most efficient when $B \approx \tilde{B}_L$ which is illustrated by figure 3.10. The figure shows the nuclear spin temperature Θ as a function of a millitesla magnetic field B with $\tilde{B}_L = 0.2$ mT. Note the minimum at $B_{eff} = \tilde{B}_L$.

Inserting the expression for $1/\Theta$, equation 3.29, in equation 3.28 finally yields the average nuclear spin in a magnetic field $B \approx B_L$ [15, 103, 104],

$$\langle \mathbf{I} \rangle = \frac{4}{3} I(I+1) \frac{\langle \mathbf{S} \rangle \cdot \mathbf{B}}{B^2 + \tilde{B}_L^2} \mathbf{B}\,. \tag{3.30}$$

This equation is the generalisation of equation 3.27 to small magnetic fields ([16], chapter 2.11).

According to equation 3.30 the nuclear polarisation is zero in the absence of a magnetic field. It was shown, however, that the nuclei may also be polarised if no external field is applied [25, 102]. The reason for this is, that the magnetic moment of an oriented electron results in an effective electron magnetic field, the Knight field[12] $\mathbf{B}_e$ [105]. The Knight field is of the order of millitesla [15, 102] and thus allows nuclear polarisation to build up also in the case of zero external field. $\mathbf{B}_e$ is antiparallel to the electron spin and given by

$$\mathbf{B}_e = \Gamma 2b_e(0)\langle\mathbf{S}\rangle = 2b_e\langle\mathbf{S}\rangle, \tag{3.31}$$

if we assume that all the relevant nuclei are exposed to the same average static electronic field[13]. $b_e(0)$ is the maximum Knight field for a specific nuclear species at the site of the electron and $\Gamma < 1$ a factor taking into account that the real electronic field is smaller than the maximum field [15]. Consequently, b_e is the maximum electronic field in fact achievable for $S = 1/2$. We will determine the Knight field for the sample studied here in chapter 5.3.

In order to fully describe the nuclear polarisation with equation 3.30 we hence have to take the Knight field into account. We do this by replacing $\mathbf{B}$ in equation 3.30 by the sum of the externally applied magnetic field $\mathbf{B}$ and the internal Knight field, $\mathbf{B} \longrightarrow \tilde{\mathbf{B}} = \mathbf{B} + 2b_e\langle\mathbf{S}\rangle$. The average nuclear spin is then finally given by

$$\langle\mathbf{I}\rangle = \frac{4}{3}I(I+1)\underbrace{\frac{\mathbf{B}\cdot\langle\mathbf{S}\rangle + 2b_e\langle\mathbf{S}\rangle^2}{(\mathbf{B}+2b_e\langle\mathbf{S}\rangle)^2 + \tilde{B}_L^2}\,(\mathbf{B}+2b_e\langle\mathbf{S}\rangle)}_{:=\mathbf{S}_B}\,. \tag{3.32}$$

We define the abbreviation $\mathbf{S}_B$ for the part above the bracket in equation 3.32. Formally, equation 3.32 is then obtained from equation 3.25 by replacing S by the "effective electron spin" $\mathbf{S}_B$.

Finally, we use equation 3.32 in order to calculate the Overhauser field $\mathbf{B}_N(\mathbf{B})$ produced by polarised nuclei. If there are different nuclear species involved, the total Overhauser field is obtained by summing their contributions. With the nuclear polarisation of the i^{th} nuclear species, $\mathbf{I}_i/I_i$, the total Overhauser field reads

$$\begin{aligned}
\mathbf{B}_N(\mathbf{B}) &= f\sum_i b_{N,i}\,\frac{\langle\mathbf{I}_i\rangle}{I_i} \\
&= T\,(\mathbf{B}+2b_e\langle\mathbf{S}\rangle) \\
\text{with}\quad K &= \frac{4}{3}f\sum_i\left((I_i+1)b_{N,i}\right)\frac{\mathbf{B}\cdot\langle\mathbf{S}\rangle + 2b_e\langle\mathbf{S}\rangle^2}{(\mathbf{B}+2b_e\langle\mathbf{S}\rangle)^2+\tilde{B}_L^2}\,.
\end{aligned} \tag{3.33}$$

[12] The Knight field is named after Walter David Knight who first discovered the electronic field via a nuclear magnetic resonance shift in 1949.

[13] This is a strong simplification, of course. Let us consider b_e a suitable average of $\Gamma b_e(0)$.

The index i denotes the particular nuclear species, indium, gallium and arsenic in our case and $b_{N,i}$ is the field of the i^{th} nuclear species for the case of 100 % nuclear polarisation. The phenomenological leakage factor $f \leq 1$ accounts for losses of nuclear spin polarisation.

Two important features of the Overhauser field in the presence of an external magnetic field are contained in equation 3.33. (i) The nuclear magnetic field is parallel or antiparallel to the total magnetic field the nuclear spins are exposed to, namely the sum of the external field and the Knight field. (ii) K represents an amplification factor for the external field. The external field thus serves as a pointer defining the direction of $\mathbf{B}_N$ whereas the nuclear magnetic field acts as amplification of the external field. As in millitesla external fields B_N can be as large as Tesla under optical orientation, an amplification of a factor 100 to 1000 can occur.

For $In_{0.5}Ga_{0.5}As$ quantum dots it was estimated that [15, 25, 106]

$$\begin{aligned} b_{N,In_{50\%}} &\approx -4.3 \text{ T} \\ b_{N,Ga_{50\%}} &\approx -1.26 \text{ T} \\ b_{N,As} &\approx -2.76 \text{ T}\,. \end{aligned} \tag{3.34}$$

With these values we obtain a maximum nuclear field of $B_{N,max} = \sum_i b_{N,i} = -8.3$ T. This value was calculated and has not been experimentally verified so far. However, Overhauser fields of several Tesla have been already measured [22, 23].

3.5 Electron Spin Polarisation in the Overhauser Field

3.5.1 Theoretical Background

We have learned that on the one hand the Overhauser field achievable by angular momentum transfer from oriented electrons is strongly influenced by the average spin of the electron. On the other hand, the electron spin in turn precesses about the Overhauser field. Additionally, the electron-nuclear spin system is sensitive to even small external magnetic fields.

We thus have to cope with a system where its two constituents, the electron spin and the collectivity of nuclear spins inside the extent of the electron envelope wave function, are highly codependent. We know that nuclear polarisation is generated in the studied quantum dots. In our experiments we measure the electron spin polarisation via the negative circular polarisation of the photoluminescence under various conditions, particularly under the influence of longitudinal and transverse external magnetic fields. In doing so, we use the electron polarisation as a detector for the state of the nuclear spin system. It is therefore important to obtain an idea of how nuclear polarisation and the external magnetic field together influence the

electron spin polarisation. In this section we will discuss a theoretical model of the electron-nuclear steady state including the effects of externally applied magnetic fields. The considerations made here will not include the influence of the frozen fluctuation field $\mathbf{B}_f$. They will nevertheless provide important information for the interpretation of our experimental results.

The steady state electron spin $\langle \mathbf{S} \rangle$ precessing about the Overhauser field which in turn depends on $\langle \mathbf{S} \rangle$ may be expressed by the equation [15, 16]

$$\begin{aligned} B_{1/2}\,(\mathbf{S} - \mathbf{S}_0) &= \mathbf{A} \times \mathbf{S}, \\ \text{with} \quad \mathbf{A} &= \mathbf{B} + \mathbf{B}_N\,. \end{aligned} \tag{3.35}$$

$\mathbf{A}$ is the total field acting on the electron composed out of the external field $\mathbf{B}$ and the Overhauser field $\mathbf{B}_N$, $\mathbf{S}_0$ is the initial electron spin at $\mathbf{A} = 0$ and $B_{1/2}$ is the magnetic field characteristic for the depolarisation of an electron spin with a specific spin lifetime $T_2^\star$ by precession. The parameter $B_{1/2}$ was discussed in detail in chapter 3.3.2.

Let us further analyse equation 3.35 by replacing $\mathbf{B}_N$ by the expression for the Overhauser field derived in the previous section[14], equation 3.33,

$$\mathbf{B}_N = \frac{4}{3} f b_N{}' \frac{(\langle \mathbf{S} \rangle \cdot \mathbf{B} + 2b_e \langle \mathbf{S} \rangle^2)}{\tilde{B}^2 + \tilde{B}_L^2} (\mathbf{B} + 2b_e \langle \mathbf{S} \rangle = K\,(\mathbf{B} + 2b_e \langle \mathbf{S} \rangle\,. \tag{3.36}$$

$2b_e\langle \mathbf{S} \rangle$ is the Knight field, f a leakage factor and $b'_N = \sum_i b_{N,i}(I_i + 1)$. Inserting equation 3.36 in equation 3.35 yields

$$\begin{aligned} B_{1/2}\,(\mathbf{S} - \mathbf{S}_0) &= (\mathbf{B} + K(\mathbf{B} + 2b_e \langle \mathbf{S} \rangle)) \times \mathbf{S} \\ &= (1 + K)\,(\mathbf{B} \times \langle \mathbf{S} \rangle)\,. \end{aligned} \tag{3.37}$$

We see that only the Overhauser field component in the direction of the external field causes the electron to precess. This is because the Knight field is parallel to $\langle \mathbf{S} \rangle$ and the electron spin does not precess about its own axis. The consequence is that the precession axis for the electron spin is *exclusively* defined by the external field. This is an important property of the electron-nuclear spin system: The electron spins are acted upon by a magnetic field whose direction is determined by the external field but whose magnitude is predominantly governed by the Overhauser field. K represents the amplification factor by which the Overhauser field multiplies the external field. Very small external fields in the range of millitesla are hence able to guide the Overhauser field, for the electron spin, however, they appear to be amplified by up to a factor > 1000.

[14] For a comprehensive explanation of the nuclear field refer to section 3.4. Remember that in the derivation of this expression a linear approximation was used which gives only a satisfying accuracy for small I and $\langle S \rangle$. One has to investigate in each case if the approximation is valid. c. f. chapter 5.4 where we discuss a way to avoid the approximation. However, equation 3.35 will only be analytically solvable for S_z if we use the approximated expression.

We wish to solve equation 3.37 for S_z as this is the quantity we can access experimentally. Multiplying equation 3.37 by $\langle \mathbf{S} \rangle$ and $\mathbf{B}$ respectively shows that

$$\langle \mathbf{S} \rangle \cdot \langle \mathbf{S} \rangle = \langle \mathbf{S} \rangle \cdot \mathbf{S}_0 \tag{3.38}$$

$$\langle \mathbf{S} \rangle \cdot \mathbf{B} = \mathbf{S}_0 \cdot \mathbf{B} \,. \tag{3.39}$$

Squaring both sides of equation 3.37 and using these identities as well as the fact that $\mathbf{S}_0 = (0, 0, S_0)$ we end up with

$$\langle S_z \rangle = S_0 \frac{B_{1/2}^2 + B_z^2 (1+K)^2}{B_{1/2}^2 + B^2 (1+K)^2} \tag{3.40}$$

$$\text{and} \quad K = \frac{4}{3} b'_N f S_0 \frac{B_z + 2b_e \langle S_z \rangle}{(B^2 + 4b_e B_z S_0 + 4b_e^2 S_0 \langle S_z \rangle) + \tilde{B}_L^2} \,. \tag{3.41}$$

This leads to a third degree equation for $\langle S_z \rangle$. Solving it yields $S_z(\mathbf{B})$, the average z component of the electron spin as a function of an external field $\mathbf{B}$ considering the nuclear magnetic field. The solutions are unique if $B_{1/2}$ is not too small compared to the nuclear magnetic field.

In order to obtain a better understanding of the behaviour of the electron spin polarisation let us plot $\langle \mathbf{S} \rangle(\mathbf{B})$ for the case that a purely longitudinal external magnetic field $B_z \mathbf{e}_z$ is swept but with additionally a constant transverse magnetic field $B_x \mathbf{e}_x$ applied. A calculated example curve with $B_x = 2$ mT and $B_{1/2} \approx 226$ mT is shown in figure 3.11. The value chosen for $B_{1/2}$ corresponds to $T_2^\star = 100$ ps.

$\langle \mathbf{S} \rangle(\mathbf{B})$ exhibits a pronounced W-like shape. The local maximum in the middle of the "W" corresponds to the external magnetic field where the Knight field $B_e = 2b_e \langle S_z \rangle$ is compensated by B_z. This can be seen by inserting $B_z = -2b_e \langle S_z \rangle$ in equation 3.40. We see that at this point $K = 0$. The effective longitudinal field on the nuclei is zero and hence no Overhauser field can be generated. It follows

$$\langle S_z \rangle(-B_e) = S_0 \frac{B_{1/2}^2 + B_z^2}{B_{1/2}^2 + B^2} \,. \tag{3.42}$$

If $B_{1/2} \gg B$ we have $\langle S_z \rangle \approx S_0$ in the compensation point and consequently $B_e \approx 2b_e S_0$. The position of the two minima of the graph are determined by B_x. They shift to higher values of B_z with increasing B_x.

The dependence of $\langle S_z \rangle$ on small magnetic fields apparently exhibits a peculiar shape which could be exploited to measure the magnitude of e. g. the Knight field. Studying the electron polarisation as a function of millitesla external fields seems to be a promising approach to obtain a deeper understanding of the electron-nuclear spin system. We will come back to this idea later in chapter 5.3.

However, we have to keep in mind that the situation in our experiments may differ from what we have discussed so far in this section. Firstly, we assume

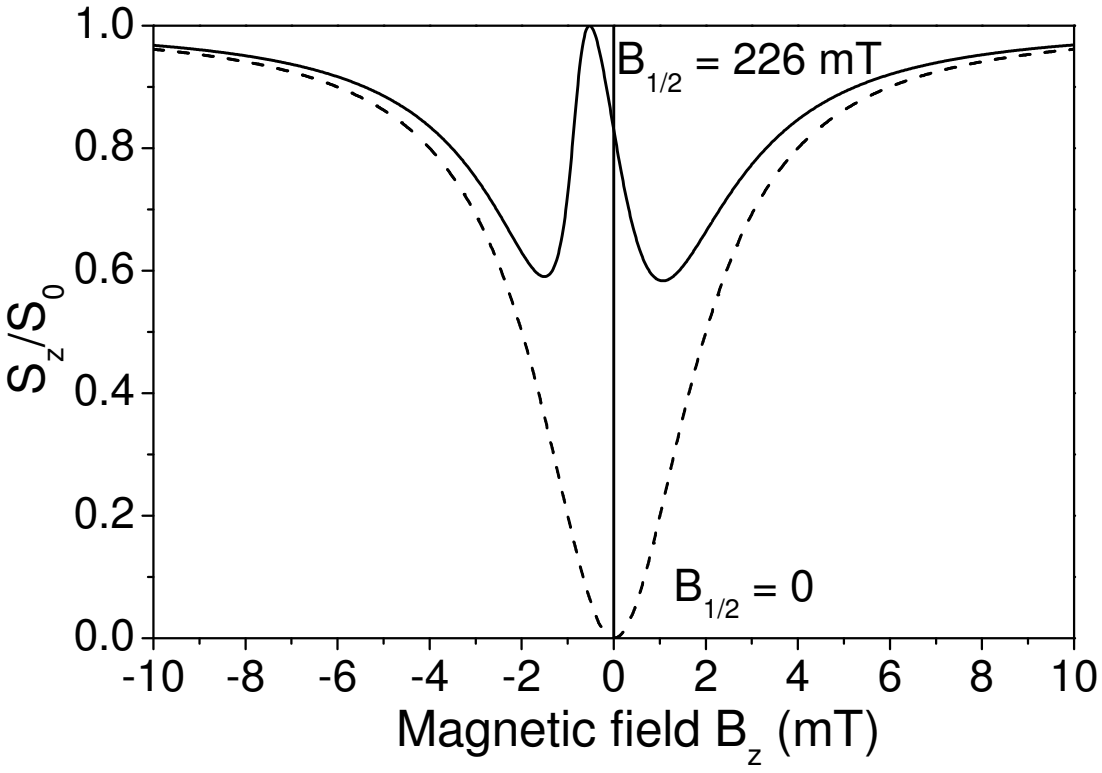

Figure 3.11: solid: W-shaped behaviour of S_z as a function of a longitudinal magnetic field B_z with a constant transverse magnetic field B_x applied. The maximum in the middle corresponds to the point where the Knight field is compensated by B_z. $B_{1/2} = 226.4$ mT ($T_2^\star = 100$ ps). dashed: Limiting case $B_{1/2} = 0$. For $B_{1/2} = 0$ the polarisation is only dependent on the direction of the magnetic field and not on its magnitude. $b_N = 1$ T, $I = 3/2$, $b_e = -1.72$ mT, $\tilde{B}_L = 0.22$.

that in our experiments we always observe the z projection of a time averaged precessing spin. In this limit $B_{1/2} \longrightarrow 0$ and the equation for S_z reduces to the one we have found in chapter 3.3.2 (equation 3.14),

$$\langle S_z \rangle(\mathbf{B}) = S_0 \frac{B_z^2}{B^2}.$$

The curve corresponding to this limit is shown in figure 3.11 (dashed). $\langle S_z \rangle$ then only depends on the direction of the external field but no longer the magnitude of the Overhauser field.

Second, we always have to take B_f into account. As soon as the Overhauser field becomes comparable to B_f, the electron spin polarisation starts to be governed by the frozen fluctuation field.

Nevertheless, we will see that we can use the influence of small magnetic fields in order to investigate the nuclear spin system. This will be discussed in detail in the experimental chapters 5.2 and 5.3.

3.5.2 The Overhauser Field vs. the Nuclear Frozen Fluctuation Field

We have seen that the resident electron spins are generally exposed to the frozen fluctuation field if the nuclear spins are randomly polarised but that spin oriented electrons can polarise the nuclear spins. We now show that the nuclear spins become polarised under optical orientation in our quantum dot ensemble and how the nuclear polarisation alters the behaviour of the electron spin polarisation which is otherwise dominated by the random spin fluctuations of the nuclear spin system.

As we have discussed in section 3.3.3, the frozen fluctuation field $\mathbf{B}_f$ generally causes a rapid partial depolarisation of the resident electron spin. This leads to a significant lowering of the circular photoluminescence polarisation compared to when e. g. an external magnetic field restores the electron spin polarisation. If, however, nuclear polarisation builds up in a specific direction as described in the previous sections 3.4 and 3.5.1, the situation is different. In the absence of transverse external magnetic fields, the quantisation axis of the electron-nuclear spin system is solely defined by the electron spin and thus indirectly by the optical axis. Resident electrons are continuously polarised along the z axis transferring their angular momentum to nuclear spins. They become polarised and consequently produce an Overhauser field B_N also parallel to $\mathbf{e}_z$.

Strong optical pumping thus causes an increase of the z component of the total nuclear magnetic field $B_{N,z} + B_{f,z}$. The Overhauser field along the z axis can become considerably larger than the in-plane components of the frozen fluctuation field:

$$B_N \gg B_{f,x/y}.$$

The imbalance of the nuclear field components decreases the angle between the total average nuclear field experienced by the resident electrons and the z axis. The sketch in figure 3.13 illustrates this: the angle θ' under optical orientation conditions is smaller than the "magic angle" $\theta_m = 54.7°$ characteristic for a completely randomly oriented nuclear spin system.

Precession of the electron spin $\mathbf{S}_0$ about this field (equation 3.15) thus conserves a greater fraction of the z projection $S_z = S_0 \cos^2(\theta)$ of the initially injected spin $\mathbf{S}_0$ compared to the case of random nuclear polarisation.

Let us study how the generation of nuclear polarisation affects the circular polarisation of the photoluminescence. This is demonstrated in figure 3.12. The figure shows two graphs displaying the dependence of the photoluminescence polarisation on a longitudinal external magnetic field with magnitude $-200\ \mathrm{mT} < B_z < +200\ \mathrm{mT}$. One graph was obtained modulating the excitation between σ^+ and σ^- with a modulation period of $T_m = 18\ \mu\mathrm{s}$ (full circles) exactly as was done to demonstrate the influence of the frozen fluctuation field (figure 3.8). The read out of the polarisation was always timed to the σ^+ cycle of the excitation.

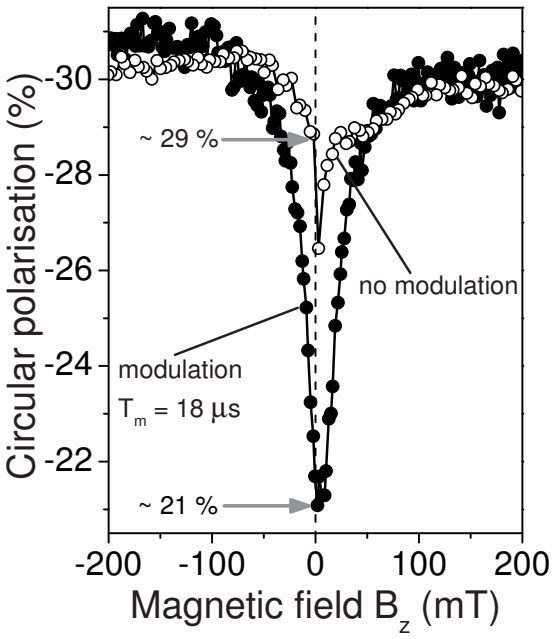

Figure 3.12: Dependence of the PL polarisation on an externally applied magnetic field in z direction. σ^+/σ^- modulated excitation with modulation period $T_m = 18$ μs (full circles), unmodulated excitation with σ^+ only (open circles). Without modulation nuclear polarisation in z direction builds up and the influence of the transverse NSF components $B_{f,x/y}$ is reduced. This leads to a significantly higher electron polarisation also at $B_z = 0$. For fast modulation (full circles) no significant nuclear polarisation can build up and at $B_z = 0$ the frozen fluctuation field leads to depolarisation of the ensemble average S_z.

The other graph corresponds to unmodulated, i. e. continuous excitation with the excitation helicity being σ^+ throughout (open circles). The sharp dip around $B_z = 0$ with the graph for unmodulated excitation is due to the rise of B_N in millitesla external fields. We are not considering this feature for the moment and focus on the broader dip only, to which the narrow one is superimposed.

Both graphs display a minimum at $B_z \approx 0$ mT and level off at about the same polarisation of $\approx 31\%$ for external fields > 100 mT. The graph obtained for modulated excitation shows only 21 % polarisation at $B_z = 0$ as compared to 29 % for the unmodulated case (indicated by arrows).

With modulated excitation the net angular momentum transfer into the system is zero impeding the generation of nuclear polarisation. At $B_z = 0$ the resident electrons are only exposed to the frozen fluctuation field $\mathbf{B}_f$. They become partially depolarised by precession about $\mathbf{B}_f$ (see chapter 3.3.3). Only when the external field dominates over the fluctuation field, $B_z > B_f$, the electron spin polarisation along the z axis is restored, as is reflected by the rise of the polarisation with externally applied magnetic field in figure 3.12.

We now compare this to the case where a nuclear field is allowed to accumulate. Continuous, unmodulated excitation causes optical orientation of the nuclear spins even at $B_z = 0$ and a nuclear field B_N in z direction builds up. This nuclear field plays exactly the same role as an external field in increasing the projection of the electron spin onto the z axis. The difference between the case of an unpolarised and a polarised nuclear spin system is schematically illustrated by the vector diagrams in figure 3.13. The angle θ' between the resultant field onto the electron, given by $\mathbf{B}_f + \mathbf{B}_N$, and the z axis becomes smaller. B_N dominates over B_f and the polarisation reaches ≈ 29 % at $B_z = 0$. This demon-

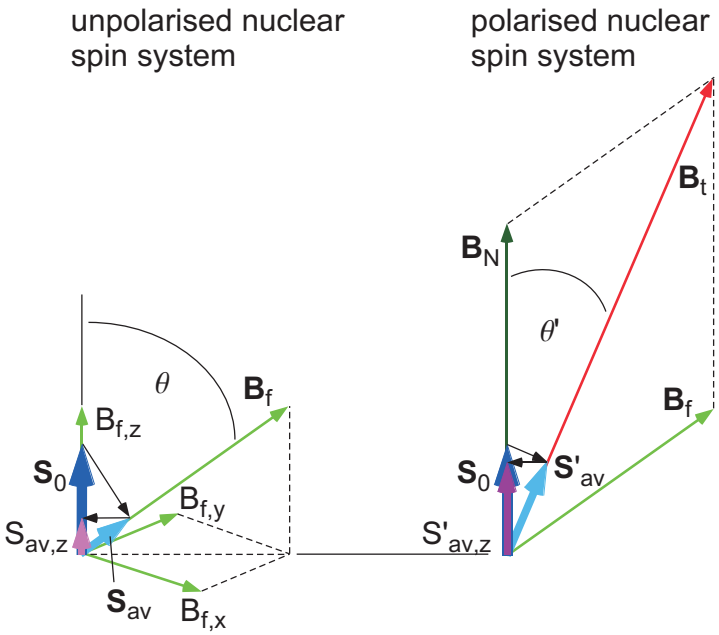

Figure 3.13: Vector diagram of the fields acting on the electron spin for a unpolarised and a polarised nuclear spin system, initial spin $\mathbf{S}_0$, $\mathbf{S}_{av}$ time average of the precessing $\mathbf{S}_0$. If a nuclear field B_N along the z axis is built up, the angle between the total field $\mathbf{B}_t = \mathbf{B}_f + \mathbf{B}_N$ and the z axis, θ', decreases compared to θ for randomly polarised nuclear spins. The projection of the precessing electron spin onto the z axis, $S'_{av,z}$, increases compared to $S_{av,z}$.

strates that for a significant fraction of the quantum dots, a substantial nuclear polarisation with $B_N \gtrsim B_f$ must occur at zero external magnetic field[15]. When B_z is increased the condition $B_z + B_N \gg B_f$ is met by more and more quantum dots. We emphasise that in the ensemble there may be quantum dots with a very high nuclear and electron spin polarisation whereas some quantum dots may contain an unpolarised electron-nuclear spin system leading to the average circular polarisation of the photoluminescence of 30 ± 2 % measured at $B_z = 0$ in the sample under study.

The fact that the electron polarisation reacts in the way described in this section to the state of the nuclear spin system makes it a sensitive tool for detecting the ensemble averaged nuclear polarisation via the photoluminescence polarisation. Particularly, the circular polarisation of the photoluminescence may serve as indication that a nuclear polarisation in z direction is really generated in the quantum dots.

[15] We will provide further evidence for nuclear polarisation in the quantum dots under study in chapter 5.2.

3.6 Summary

As we have seen, the behaviour of the electron-nuclear spin system is governed by the balance between the optical orientation of the electron spin, the electron mediated orientation of the nuclear spins and the various magnetic fields acting on the electron and the nuclei. In order to obtain a complete picture of the codependencies in the electron-nuclear spin system we thus wish to recapitulate what we have discussed in this chapter.

We have to distinguish different regimes concerning the strength of the external field $\mathbf{B}$, the frozen nuclear fluctuation field $\mathbf{B}_f$ and the Overhauser field $\mathbf{B}_N$. Table 3.1 gives an overview of the order of magnitude of the magnetic fields involved. Figure 3.14 schematically depicts the actions on the electron spin and on the nuclear spin for each regime. The letters in brackets itemising the following explanations refer to figure 3.14.

No nuclear polarisation

If only little or no nuclear polarisation is allowed to build up the Overhauser field can be neglected. If we want to obstruct the generation of nuclear polarisation in our experiments, the sample is generally excited with light whose circular polarisation is rapidly alternating between σ^+ and σ^-. The time averaged flux of angular momentum into the system is then zero.

(a) $B_f \gg B$**:** When the external magnetic field is negligibly small compared to the nuclear frozen fluctuation field, the injected electron spin $\mathbf{S}_0 = (0, 0, S_0)$ exclusively precesses about $\mathbf{B}_f$. Averaged over the ensemble, the angle between $\mathbf{B}_f$ and $\mathbf{e}_z$ is then given by the "magic angle" $\theta_m = 54.7°$. This leads to a rapid partial decrease of the z projection of $\mathbf{S}_0$.

(b) $B \gg B_f$**:** When the external magnetic field is considerably larger than the frozen fluctuation field, the electron spin predominantly precesses about $\mathbf{B}$. If $\mathbf{B}||\mathbf{e}_z$, θ decreases compared to θ_m, S_z and the circular PL polarisation increase. θ becomes zero in the limit $B_f/B \longrightarrow 0$. In this limiting case S_z is fully retained, $S_z = S_0$.

Table 3.1: Magnitudes of the magnetic fields involved in the electron-nuclear spin system.

nuclear dipole-dipole field	$\tilde{B}_L$	< 1 mT
Knight field	B_e	< 1 mT
nuclear frozen fluctuation field	B_f	tens of mT
Overhauser field	B_N	tens of mT – several Tesla

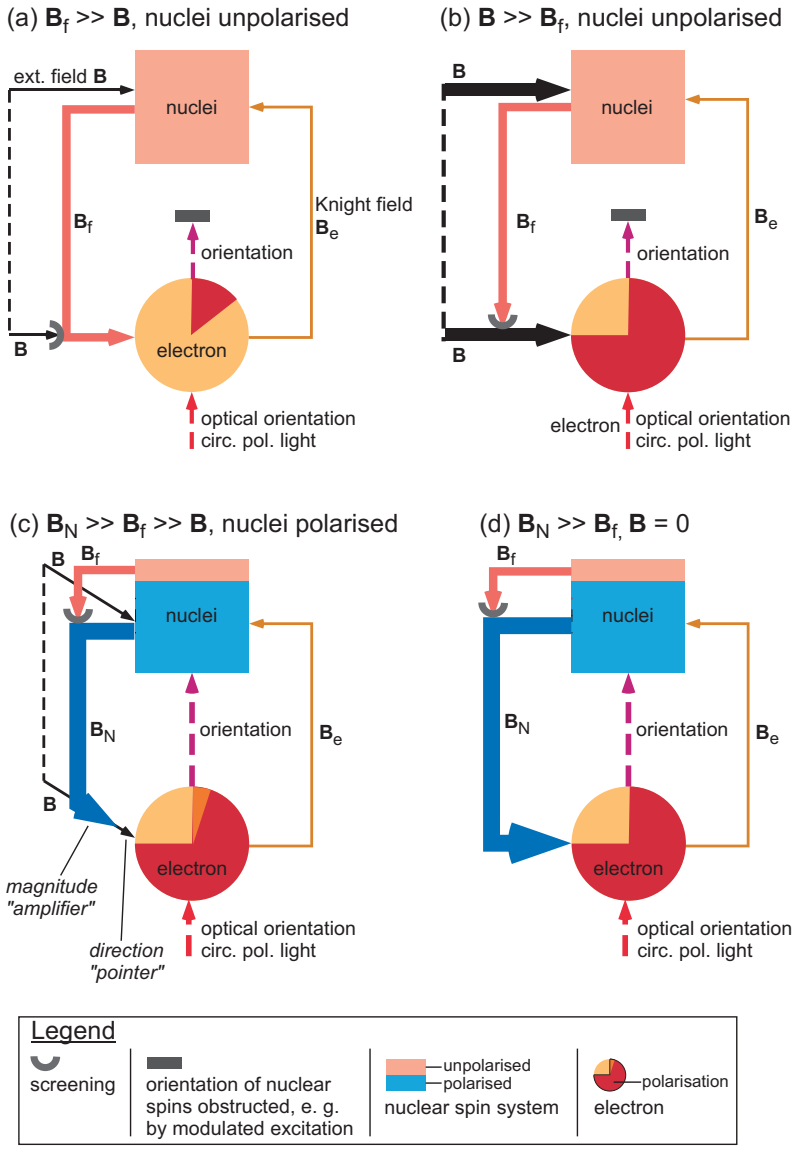

Figure 3.14: Illustration of the interplay between the external magnetic field $\mathbf{B}$, the nuclear frozen fluctuation field $\mathbf{B}_f$, the Overhauser field $\mathbf{B}_N$ and the Knight field $\mathbf{B}_e$ for different regimes. Explanation on page 69. (a) The electron spin is exclusively acted upon by the frozen fluctuation field, the small external field does not play a role as it is screened by $\mathbf{B}_f$. $\mathbf{B}_f$ depolarises the electron spin. (b) Unpolarised nuclear spin system, $\mathbf{B} > \mathbf{B}_f$. The electron predominantly experiences the external field which overcomes $\mathbf{B}_f$. An external magnetic field in z direction supports electron spin polarisation. (c) Polarised nuclear spin system, large Overhauser field $\mathbf{B}_N \gg \mathbf{B}_f \gg \mathbf{B}$. B_N overcomes the residual fluctuation field. The direction of B_N is governed by $\mathbf{B}$. (d) $\mathbf{B} = 0$, the nuclear spins become polarised in the Knight field of the electron. The large Overhauser field along $\mathbf{e}_z$ supports polarisation of the electron spin.

Nuclear spins polarised

As we have learned, the nuclear spin system can be polarised via optically oriented electrons. The polarisation of the nuclear spins is most efficient at magnetic fields $B_{eff} \gtrsim \tilde{B}_L$, where $\mathbf{B}_{eff}$ is the sum of the Knight field and the external field. The nuclear polarisation is accompanied by a large Overhauser field easily exceeding B_f. Concerning the external field we distinguish different situations again.

(c) $B_N \gg B_f \gg B$, oblique external field: The z components of the Knight field and the external field enable nuclear polarisation to be generated. A large Overhauser field builds up which is considerably larger than B_f. The direction of the Overhauser field, however, is determined by the external field: $\mathbf{B}_N$ becomes oriented parallel (or antiparallel) to the external field as soon as $B \gg \tilde{B}_L$ (when $B < \tilde{B}_L$ the external field is screened by $\tilde{B}_L$). Thus, even millitesla external fields can realign the Overhauser field which may be in the order of Tesla. In this way, the external field acts as a "pointer", the Overhauser field as an "amplifier". Depending on the direction of $\mathbf{B}_N$ electron polarisation becomes supported (greater longitudinal component) or destroyed (greater transverse component).

(d) $B = 0$: If $B = 0$, the nuclear spins only experience the Knight field B_e. They may become polarised with the help of B_e. The large Overhauser field is predominantly aligned in z direction and therefore supports electron spin polarisation. The oriented electron in turn stabilises the nuclear spin system.

4 The Experimental Setup

4.1 Polarisation Sensitive Photoluminescence

The experiments presented in this thesis are based on measuring the polarisation of the quantum dot resident electron spin via the circular polarisation of the quantum dot photoluminescence[1]. The experimental conditions described in this chapter represent the standard settings used in most of the discussed measurements. An overview of the most important settings is given in table 4.1. Whenever these conditions were modified it will be stated explicitly in the respective chapter.

Sample mounting, temperature control, optical alignment The sample was placed in an optical bath cryostat filled with liquid helium. By pumping on the helium volume, the helium was cooled further below the λ-point T_λ where helium becomes superfluid. For ^{4}He, $T_\lambda = 2,1768$ K is reached at a pressure of 5036 Pa. Below T_λ the heat conductivity of helium goes to infinity enabling a particularly efficient cooling of the sample. By constantly pumping, the sample was kept in superfluid helium at a temperature of $1.85 < T < 2$ K if not stated otherwise. The temperature could be monitored via the voltage over a resistor which was placed inside the cryostat next to the sample. Measurements at temperatures $T > 5$ K could be performed by keeping the sample in cold helium gas.

In order to control the alignment, the laser spot position on the sample and its size, an image of the sample could be generated on the chip of a charge coupled device (CCD) camera and viewed on a monitor.

Optical excitation The excitation was performed using a pulsed laser system. The mode locked titanium:sapphire laser had a pulse repetition rate of 75.6 MHz (pulse separation 13.2 ns) and a pulse duration of ≈ 1.5 ps. Time integrated laser powers of $0 < P < 50$ mW where used for excitation. A lens with a focal length of 10 cm was used to focus the laser on the sample. It is difficult, though, to exactly control the laser spot size. It may vary slightly for different experiments. We do therefore not indicate excitation *densities*.

[1] About the relationship of circular polarisation of the photoluminescence and the resident electron polarisation c. f. chapter 3.2.

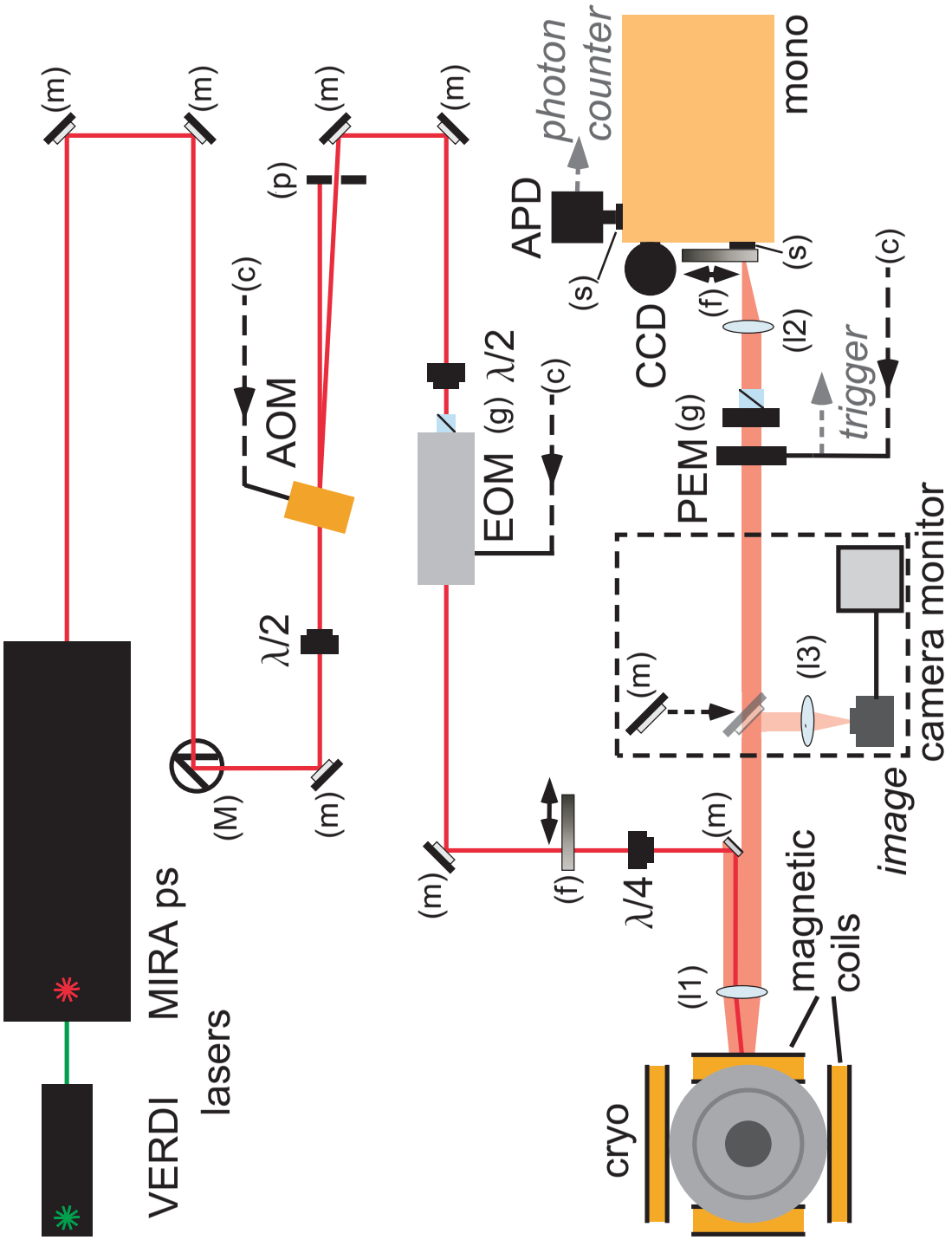
VERDI
MIRA ps
lasers
(M)
(m)
(p)
(c)
AOM
λ/2
(m)
(m)
(m)
(m)
(m)
(f)
λ/4
(m)
(l1)
magnetic
coils
cryo
(m)
(l3)
camera monitor
image
PEM (g)
(l2)
trigger
(c)
(f)
(s)
CCD
APD
(s)
photon
counter
mono
EOM (g) λ/2
(c)

Legend

MIRA	mode locked titanium:sapphire picosecond pulsed laser
VERDI	all solid-state 532 nm pump laser
(m)	mirrors
(M)	periscope
$\lambda/2$	$\lambda/2$ wave plate
AOM	acousto optical modulator
(c)	from controller
(p)	pin hole
(g)	Glan-Thompson prism
EOM	electro optical modulator
(f)	wedge filter
$\lambda/4$	$\lambda/4$ wave plate
(l1)	10 cm lens, focusing on sample, PL collection
cryo	optical bath cryostat, placed between magnetic coils
image	option to create an image of the sample on a CCD chip and view it on a monitor
PEM	photoelastic modulator, trigger to photon counter
(l2)	lens, focusing on monochromator entry slit
(s)	slit
CCD	InGaAs charge coupled device camera
mono	0.5 m monochromator
APD	silicon avalanche photo diode

In most experiments the excitation power was chosen with respect to the negative circular polarisation emitted from the sample. The negative circular polarisation effect is power dependent. It rises with power and eventually saturates[2]. The excitation power was thus generally set to a value where the maximum negative circular polarisation was obtained. In all other cases the excitation *power* will be indicated.

The photon energy of the excitation was set to 1.4595 eV (849.5 nm) corresponding to the low energy flank of the wetting layer. At this excitation energy the generation of negative circular polarisation proved to be most efficient. For the excitation circularly polarised light was used. The linearly polarised laser light was transformed into circularly polarised by use of a $\lambda/4$ wave plate at an angle of $\pm 45°$ to the polarisation axis of the laser.

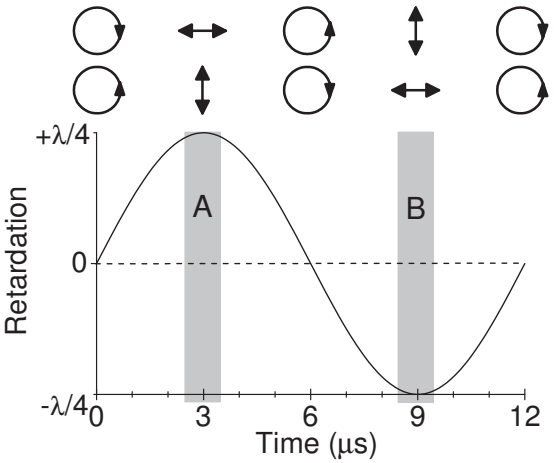

Figure 4.1: Retardation of the photoelastic modulator over time. Effect on incident circularly polarised light indicated above. Shaded areas: 1 μs wide count gates of the photon counter to alternately read out σ^+ and σ^- polarised photoluminescence.

Circular polarisation sensitive photoluminescence detection The photoluminescence was collected with the same lens used to focus the exciting beam on the sample. In front of the monochromator a photoelastic modulator (PEM) with a frequency of $f = 84$ kHz (period $\tau \approx 12$ μs) was placed. It was set to a maximum retardation of $\lambda/4$. The retardation of the PEM thus changes from zero over $+\lambda/4$ to $-\lambda/4$ and back to zero during one period T_{PEM} as shown in figure 4.1. Thus, at times $t_+ = 3 + n \cdot T_{PEM}$ μs the retardation is $+\lambda/4$ and at $t_- = 9 + n \cdot T_{PEM}$ μs it is $-\lambda/4$, with $1 \leq n < \infty$. σ^+ polarised light passing the PEM is consequently transformed into vertically linearly polarised light at times t_+ and into horizontally polarised light at times t_-. Analogously, the PEM transforms σ^- circularly polarised light into horizontally linearly polarised light at times t_+ and into vertically linearly polarised light at times t_-. Combining the PEM with a Glan-Thompson prism set to an angle of 0° made it thus possible to alternately detect σ^+ and σ^- polarised photoluminescence respectively: At times

[2] c. f. chapter 3.2.

Table 4.1: The settings used for the experiments presented in this thesis. Variations will be stated explicitly.

Temperature	$\lesssim 2$ K
Excitation energy	1.4595 eV (849.5 nm) – low energy flank of wl
Excitation power	saturation regime of NCP – ≈ 10 mW, 10 cm lens
Excitation polarisation	circular
Laser mode	picosecond pulses

t_+ initially σ^+ polarised light can pass the PEM-Glan-Thompson-prism system while initially σ^- polarised light is blocked. At t_- it is the other way round.

The photoluminescence was focused on the entry slit of a 0.5 m monochromator spectrally dispersing the light for wavelength selection. For alignment and optimisation the light was detected with an InGaAs charge coupled device (CCD) camera. The read out of the circular polarisation of the photoluminescence was performed using a silicon avalanche photodiode (APD) in combination with a two channel photon counter. The photon counter was triggered with the frequency of the PEM. Two read out gates A and B of width 1 μs were set in the photon counter visualised in figure 4.1 by the shaded areas. Gate A was timed to t_+ so that σ^+ polarised light was measured during A and gate B was timed to t_- in order to detect σ^- polarised light during B. The photon counter was controlled and the counts where read out by a personal computer. The circular polarisation of the photoluminescence was then determined by calculating $(n_A - n_B)/(n_A + n_B)$ where $n_{A(B)}$ is the number of counts during count gate A (B). The detection of σ^+ and σ^- polarised photoluminescence with a time-lag of ≈ 6 μs limited the influence of slow variations e. g. of the laser power. Alternatively, the PEM could be replaced by a $\lambda/4$ wave plate allowing the detection of σ^+ and σ^- photoluminescence by setting the wave plate to an angle of $\pm 45°$relative to the 0° position of the Glan-Thompson prism.

The intensity of the photoluminescence light on the CCD camera and the avalanche photodiode could be regulated with a wedge filter placed directly in front of the entry slit of the monochromator. Thereby, the overexposure of the detection devices could be avoided without having to change e. g. the slit width of the monochromator entry slit.

The center wave length of the monochromator was set to the maximum circular polarisation of the inhomogeneously broadened s-shell emission of the quantum dot ensemble. By then narrowing the slit width of the monochromator exit slit in front of the APD, a part of the spatially dispersed photoluminescence could be cut out for detection. In doing so, the sub ensemble of quantum dots emitting with the highest degree of circular polarisation could be chosen. Further, the inhomogeneities in size, composition and symmetry of the quantum dots actually measured were minimised thereby.

Magnetic field The cryostat was placed between three pairs of Helmholtz coils. They where used to compensate parasitic fields like the earth magnetic field in order to create a field free space with $B \leq 1$ μT at the site of the sample and to apply longitudinal (z direction) and transverse (x direction) magnetic fields up to 3 mT. Alternatively, a superconducting coil could be used inside the cryostat to apply a longitudinal field of ≤ 1.3 T. The current in the coils could be controlled via a personal computer allowing the synchronisation of the magnetic field and the read out of the photoluminescence in order to perform magnetic field dependent measurements.

4.2 Temporal Excitation-Detection Schemes

The simple photoluminescence setup was extended in order to realise various temporal excitation-detection schemes. The circular polarisation of the excitation could be modulated between σ^+ and σ^-, a dark time could be introduced and the point of time of the read out could be controlled. Thereby, various problems could be addressed, particularly time dependent measurements could be performed.

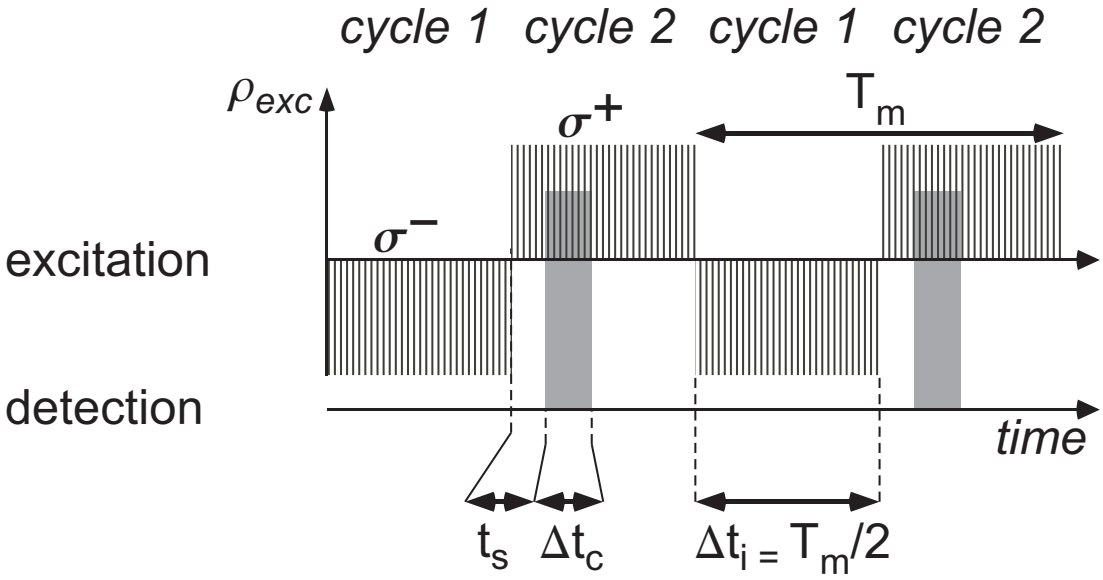

Figure 4.2: Excitation modulated between σ^+ and σ^- with period T_m, pulse train duration $\Delta t_i = T_m/2$. Detection (grey areas) always during *cycle 2*. Start of detection t_s after beginning of *cycle 2* can be varied as well as duration of read out gate Δt_c.

Circular polarisation modulation The circular polarisation of the excitation could be modulated using an electro optical modulator (EOM) in combination with a $\lambda/4$ wave plate at an angle of $\pm 45°$ to the linear polarisation axis. The

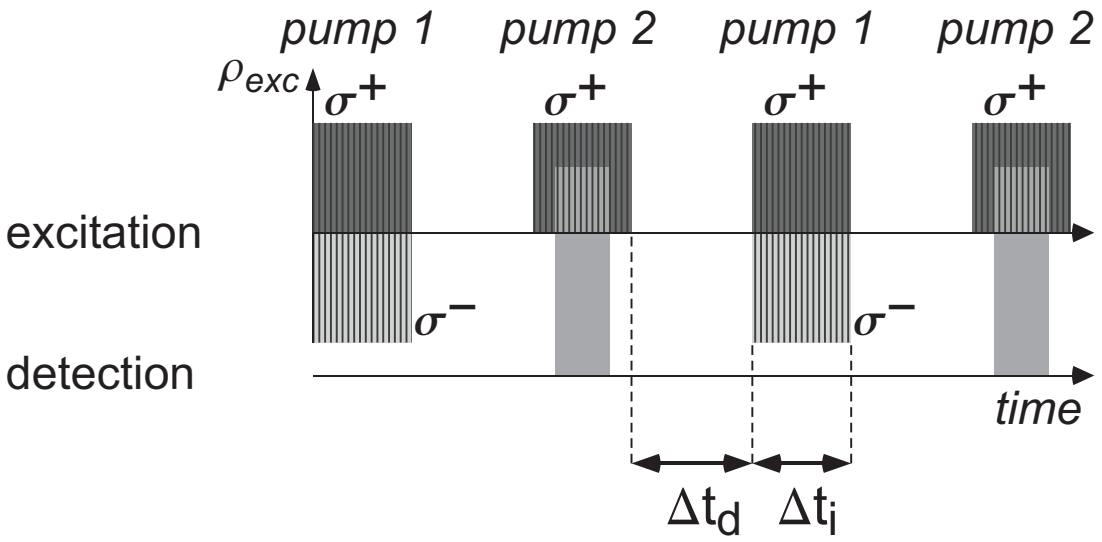

Figure 4.3: Excitation-detection scheme with darktime Δt_d between two excitation cycles *pump 1* and *pump 2* of duration Δt_i. *Pump 1* has either the same circular polarisation as *pump 2* ("co", dark grey) or opposite circular polarisation ("cross", light grey). Detection (grey areas) always during *pump 2*.

EOM flips the linear polarisation of the laser between vertical and horizontal with period T_m leading to alternately σ^+ and σ^- circularly polarised light after the $\lambda/4$ plate. A function generator was used to trigger the EOM. Like this, pulse trains of the 13.2 ns separated picosecond laser pulses with opposite circular polarisation could be produced. Figure 4.2 illustrates this scheme. The square function shaped pulse trains had a sharp rise of a few nanoseconds. Their duration $\Delta t_i = T_m/2$ could be chosen to be 10 μs $\lesssim \Delta t_i < 1$. Thus, two excitation cycles *cycle 1* and *cycle 2* with oppositely circularly polarised excitation were defined. The photoluminescence was always read out during *cycle 2*, i. e. always during the same excitation polarisation.

The time between the beginning of *cycle 2* and the start of the read out, t_s, could be controlled as well as the duration of the counting, Δt_c. Time resolved measurements could hence be realised for $\Delta t_c \ll T_m/2$. By measuring the circular polarisation of the photoluminescence in dependence on t_s. Like this the circular polarisation could be sampled in time in the course of *cycle 2*. In the analysis then generally the position of the center of the read out gate $t = t_s + \Delta t_c/2$ is given. By choosing a wider count gate, the circular polarisation was measured time integrated as a function of T_m.

Dark time measurements Additionally, an acousto optical modulator (AOM) was included into he setup. It could be activated in order to periodically switch the excitation on and off. Like this, a "dark time" $0 < \Delta t_d < 500$ ms could be

created between the two illumination cycles "*pump 1*" and "*pump 2*" of duration Δt_i. The corresponding scheme is depicted in figure 4.3. The width of Δt_i could be controlled individually from Δt_d. The circular polarisation of the excitation during Δt_i could again be controlled with the EOM so that either a "co-polarised" scheme with all pulse trains having the same photon helicity could be realised or a "cross-polarised" scheme where the helicity during *pump 1* was inverted with respect to *pump 2*. The detection of the photoluminescence polarisation was performed always during the same excitation cycle *pump 2* to keep the conditions during the read out constant. With this scheme the circular polarisation of the photoluminescence could be measured as a function of the dark time.

4.3 Definitions and Conventions

Coordinate system and axis The definition of the coordinate system underlying all experiments is shown in figure 4.4. The z axis is defined by the optical axis of the experimental setup. The samples were mounted so that the growth direction of the quantum dots was parallel to the optical axis with the sample plane lying in the x-y plane of the coordinate system. The direction of the incident exciting beam was defined the positive z direction. The photoluminescence was collected along the negative z direction.

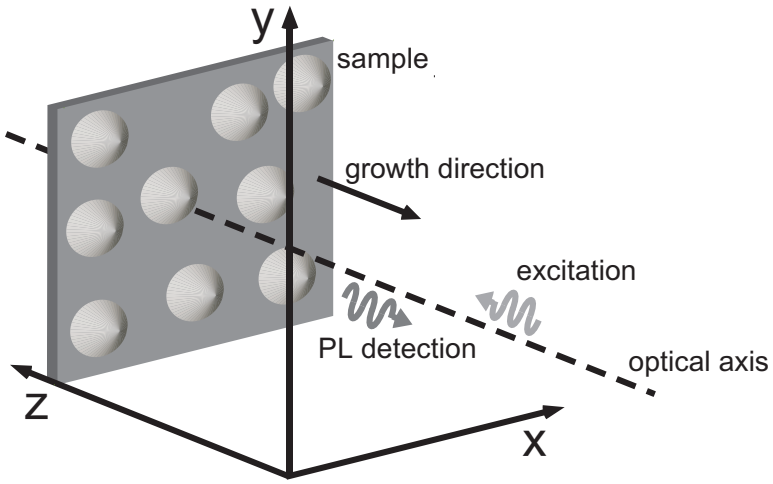

Figure 4.4: The coordinate system. $\mathbf{e}_z || \mathbf{k}$ of the exciting beam, the growth direction corresponds to the $-z$ direction, sample plane lies in the x-y-plane.

Circular polarisation Light of photons with positive helicity, i. e. the photon spin $\mathbf{s}$ being parallel to the $\mathbf{k}$-vector of the light, we call σ^+ polarised. Light where $\mathbf{s} \uparrow\downarrow \mathbf{k}$ we consequently call σ^- polarised. Looking towards the light source in $-\mathbf{k}$ direction, the electric field vector $\mathbf{E}$ at a fixed location rotates anticlockwise

Table 4.2: Overview of the definitions concerning circular polarisation. Rotation of the **E** field vector defined for the light wave propagating towards the observer.

Photon helicity		circular polarisation	rotation of **E**
$\mathbf{s} = +\hbar\,\mathbf{k}/k$	right-handed	σ^+	anti-clockwise
$\mathbf{s} = -\hbar\,\mathbf{k}/k$	left-handed	σ^-	clockwise

in the case of σ^+ polarised light ("left circular") and clockwise in the case of σ^- polarised light ("right circular"). These definitions are summarised in table 4.3.

In this work, almost all experiments are based on measuring the *degree* of circular polarisation of the photoluminescence as defined by equation 3.1. The circular polarisation is generally given in per cent (%) with a minus sign indicating that *negative circular polarisation* is measured, as explained in chapter 3.2. The minus sign should thus only be understood as a relative indication with respect to the circular polarisation of the excitation.

Magnetic fields An applied magnetic field $\mathbf{B} = B_z\mathbf{e}_z$ which is parallel to the optical axis and the growth direction of the quantum dots we call *longitudinal*. Alternatively such a geometry is called "*Faraday configuration*". Applied magnetic fields $\mathbf{B} = B_x\mathbf{e}_x$ and $\mathbf{B} = B_y\mathbf{e}_y$ lying in the sample plane we call *transverse*. This geometry with $\mathbf{B}\perp\mathbf{k}$ is also called "*Voigt configuration*".

5 Determination of the Internal Magnetic Fields Acting on the Nuclear Spins

5.1 Introduction

As we have shown in the chapter 3.5.1, the predominant factor governing the behaviour of the resident electron spin and the level of electron spin polarisation is the nuclear spin system. Unpolarised nuclear spins limit the level of electron spin polarisation by the action of the random nuclear fluctuation field whereas nuclear spins polarised along the excitation axis may enhance electron polarisation. The nuclear spin polarisation is in turn dependent on the electron spin. This makes the resident electron and the nuclear spins a highly codependent system. Although the state of this system is a result of the complicated mutual influence of the resident electron spin and the nuclear spins it is remarkable that it may be described by only a few quantities: the nuclear dipole-dipole field $\tilde{B}_L$, the Overhauser field $\mathbf{B}_N$ and the Knight field of the electron B_e. The Overhauser field may be calculated in theory if one knows the Knight field $\mathbf{B}_e = 2b_e\langle\mathbf{S}\rangle$ and the dipole-dipole field between the nuclear spins, $\tilde{B}_L$. Particularly at zero applied external field the relationship between B_e and $\tilde{B}_L$ is crucial concerning the degree of nuclear polarisation achievable. In turn, the knowledge of $\mathbf{B}_N(\mathbf{B})$ is necessary to explain the behaviour of the electron spin polarisation which, in our case, becomes manifest in the circular polarisation of the photoluminescence.

If one strives for a deeper understanding of the electron-nuclear spin system one thus has to determine the quantities governing the generation of nuclear polarisation, the Knight field and the nuclear dipole-dipole field. We know that every quantum dot sample is different. Particularly the composition of the dots can be poorly controlled and is often not exactly known. In order to obtain a *general* insight into the nature of the electron-nuclear spin system, it is therefore necessary to *specifically* measure these values at the *same sample*. We approach this goal by studying the influence of externally applied magnetic fields, both parallel and perpendicular to the helicity of the exciting photons. We use small magnetic fields in the range of several millitesla because they lead to a particularly rich behaviour of the polarisation allowing us to B_e and $\tilde{B}_L$ which are expected to lie in the sub millitesla range. The nuclear spins are very susceptible to millitesla

external fields whereas the electron spin reacts sensitively to the large nuclear magnetic field only. In this way the nuclear field acts as an amplifier for the external magnetic field and the photoluminescence polarisation (which reflects the electron spin polarisation) acts as a sensor for the state of the nuclear spin system. The indirect dependence of the polarisation on the external field at the same time provides access to the quantities we want to determine.

In the following sections we thus examine the evolution of the circular polarisation of the photoluminescence under the influence of transverse and longitudinal fields and show how these often surprising and complicated dependencies may be interpreted in order to extract the magnitude of the Knight field and the dipole-dipole field. In the last section we then assemble the pieces by calculating the maximum nuclear field. In the end we hope to complete the mosaic and provide a consistent picture of the coupled electron-nuclear spin system.

5.2 The Nuclear Dipole-Dipole Field

When spin oriented electrons are exposed to a magnetic field perpendicular to their spin orientation they start to precess about this field. For an electron spin, the projection onto the z axis will oscillate sinusoidally with time, until the electron spin is either reinitialised or it loses its phase information (spin coherence)[1]. Therefore, in a transverse magnetic field, the value of S_z is governed by the competition between the precession frequency of the electron spins and the time at which the spins are either reinitialised or decohere. S_z decreases the further they precess. In neutral quantum dots the precession is terminated by the radiative decay of the exciton or by spin relaxation. In our case of negatively charged quantum dots, the electrons do not precess before the radiative decay of the trion because the trion ground state contains two electrons with total spin zero. The precession only starts after recombination, when the resident electron is left behind in a well-defined spin state. The resident electron spin then has time to precess until it is reinitialised again. The cycle of spin initialisation, precession and reinitialisation is schematically illustrated in figure 5.1. In our case, the lower limit for the reinitialisation rate is given by the 13.2 ns pulse separation of the laser pulses.

The spin polarisation measured will be the value of S_z at the point where the precession is terminated. As the precession frequency is proportional to the magnitude of the field, in the same time interval the electron spin precesses further the higher the field, and thus loses increasingly more of its z component. Monitoring S_z via the photoluminescence polarisation on sweeping the transverse field yields a Lorentzian curve the width of which is inversely proportional to the spin lifetime of the electron $T_2^\star$ where $1/T_2^\star = 1/\tau_r + 1/\tau_s$. τ_r is the electron spin reinitialisation time and τ_s the spin relaxation time. With the electron g factor

[1] For a discussion of spin precession see also chapter 3.3.2.

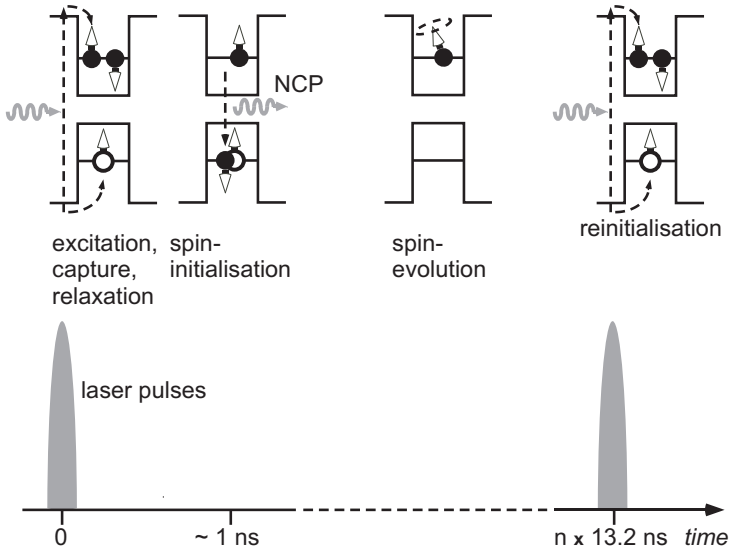

Figure 5.1: Excitation, spin initialisation, precession of the electron spin in external or nuclear magnetic fields, reinitialisation. $\approx$ 1 ns between electron-hole pair creation in the wetting layer and radiative decay of the trion, $\approx$ 12 ns to the next laser pulse. The lower limit for the time interval between two initialisations is given by the laser pulse separation of 13.2 ns.

in x direction, $g_{e,x}$, the Lorentz curve is then given by

$$\rho_c(B_x) = \frac{\rho_c(0)}{1 + (\frac{g_{e,x}\mu_B B_x}{\hbar} T_2^\star)^2} = \frac{\rho_c(0)}{1 + (\Omega T_2^\star)^2} \,. \tag{5.1}$$

This is known as Hanle effect[2] ([107] and e. g. [108]). From the width of the Hanle curve, the spin lifetime $T_2^\star$ could be extracted according to

$$T_2^\star = \frac{\hbar}{|g_{e,x}|\mu_B B_{1/2}} \,, \tag{5.2}$$

with the half width at half maximum $B_{1/2}$ of the Lorentz curve[3].

Figure 5.2 shows typical graphs for Hanle measurements obtained from the quantum dot ensemble under study in this thesis. A transverse magnetic field B_x was swept and the polarisation of the photoluminescence for each field value was recorded. The polarisation drops sharply from its maximum value at $B_x = 0$. The half width at half maximum of the peak is $\approx$ 0.2 mT. This width of the peak would thus correspond to a spin lifetime $T_2^\star$ of $\approx$ 57 ns according to equation 5.2 assuming $|g_{e,x}|$ in the x direction [109]. This reasoning is *not correct* in our case, however, as we will show in the following.

For that purpose, we now study Hanle curves obtained under modulated excitation where the excitation helicity was switched between σ^+ and σ^- with period T_m that is varied over a range between 1 ms and 100 ms. Figure 5.3 shows Hanle

[2]The effect is named after Wilhelm Hanle who first described it 1924 in his PhD thesis "Über magnetische Beeinflussung der Polarisation der Resonanz-Fluoreszenz von Quecksilber".

[3]We have discussed the quantity in detail in chapter 3.3.2.

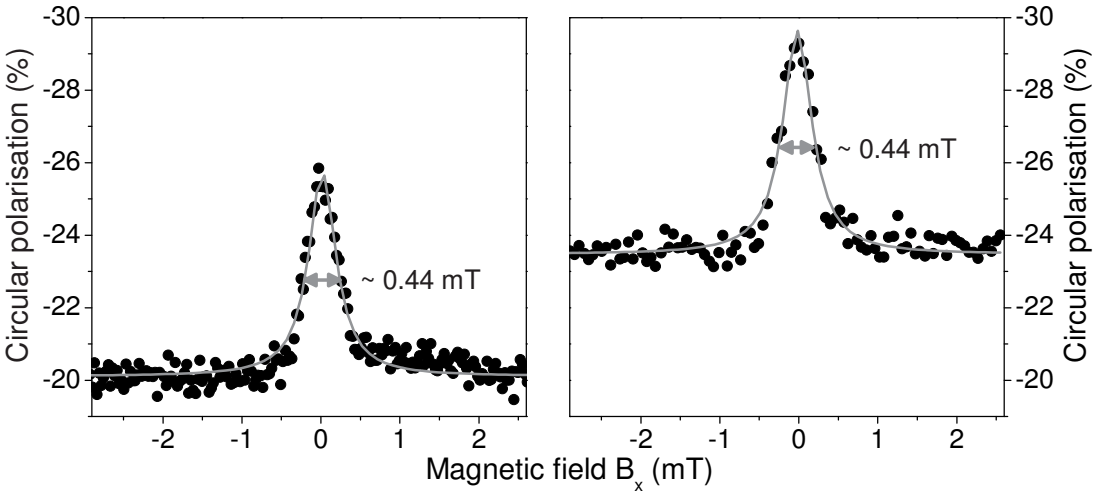

Figure 5.2: Typical curves obtained for Hanle measurements. Sweeping of a transverse magnetic field results in a depolarisation peak at $B_x = 0$. Irrespective the absolute amplitude of the peak, the peak width is always 0.44 ±0.02 mT. The width is given by twice the dipole-dipole field $\tilde{B}_L$.

curves for selected modulation periods $1 < T_m < 50$ ms where the read out of the polarisation was always performed during the σ^- cycle of the excitation, and for unmodulated excitation as reference. We observe that the amplitude of the peak at $B_x = 0$ decreases when the modulation period is decreased. The peak gradually disappears and may be almost completely switched off for modulation periods $T < 1$ ms. However, the dynamics of the electron spin takes place on a nanosecond timescale[4] which rules out an electronic origin as an explanation for the disappearance of the peak under modulated excitation.

Furthermore, the peak becomes broader for smaller T_m. Figure 5.4 (a) shows the width of the depolarisation peaks in dependence of T_m. In the traditional interpretation of the Hanle effect, however, the width of the Hanle curves is associated with the lifetime of the electron. In our experiments this is apparently not the case. A millisecond modulation should not affect the electron spin lifetime, which would lie at about 57 ns as calculated above for a FWHM of 0.4 mT of the Hanle peak.

Although transverse fields also lead to the depolarisation of polarised electron spins in the quantum dots under study, the situation obviously fundamentally differs from the one underlying the original Hanle effect. Particularly, the narrow peak appearing in Hanle measurements on our quantum dot sample can obviously not be used to calculate the relaxation time of the resident electron spin. Thus, care has to be taken when the width of the Hanle peak is used to determine the spin lifetime of the electron in quantum dots as has been suggested in the

[4]See chapter 7.2 where we discuss the accumulation dynamics of the electron polarisation.

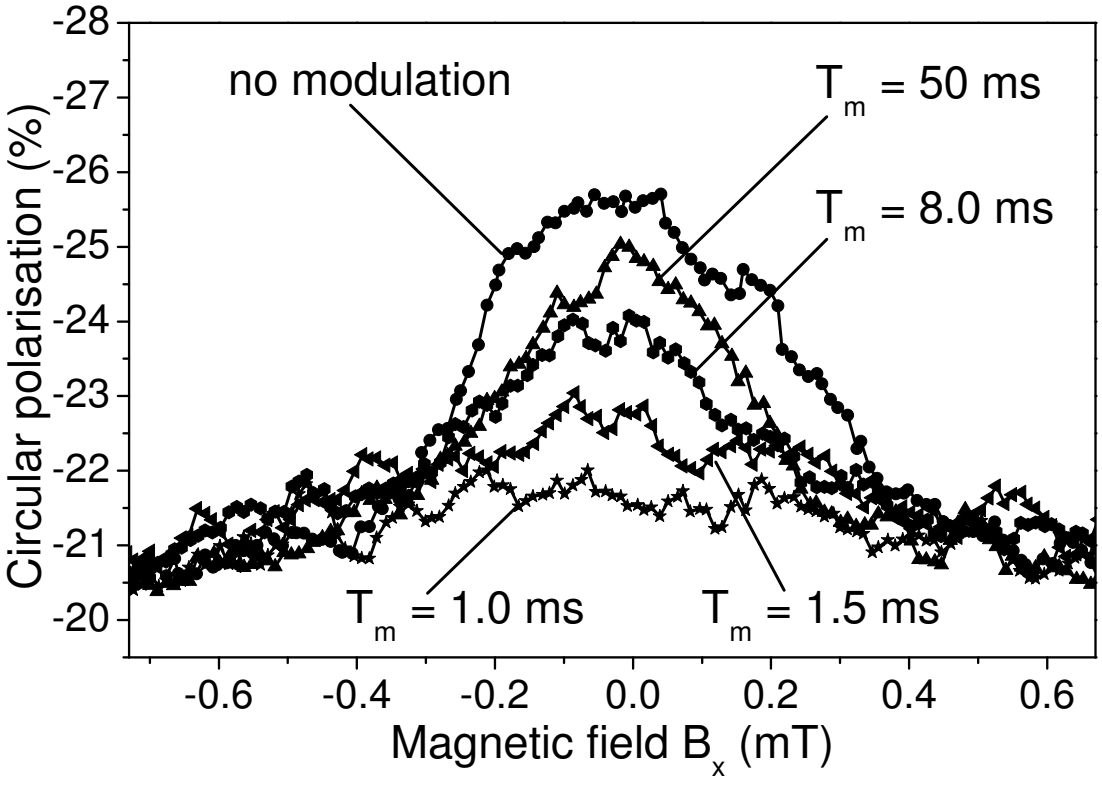

Figure 5.3: Hanle measurements for excitation modulated between σ^+ and σ^- circular polarisation with period T_m. The depolarisation peak almost vanishes for fast modulation.

literature [74, 108, 110].

The strong influence of the peak in our Hanle type measurements on the modulation, however, can be explained by the influence of the quantum dot nuclei. The accumulation of nuclear polarisation occurs on a timescale of tens of milliseconds [99]. In the modulated excitation scheme used here, however, the net spin transfer into the system is zero and neither excitation cycle gives the nuclear spins enough time to become maximally polarised. The spin orientation of the resident electron is generally influenced by the Overhauser field the magnitude and direction of which is in turn strongly dependent on external magnetic fields [15, 16]. Particularly in the region of small external fields this results in a behaviour of the electron spin that is predominantly governed by the nuclear field.

As we have discussed earlier, nuclear polarisation is generated at $B_x = 0$ due to the Knight field of the electron. This results in a nuclear field parallel to the z axis which adds to the background field caused by the nuclear spin fluctuations leading to a significant increase of the electron spin projection on the z axis compared to the case of an unpolarised nuclear spin system.

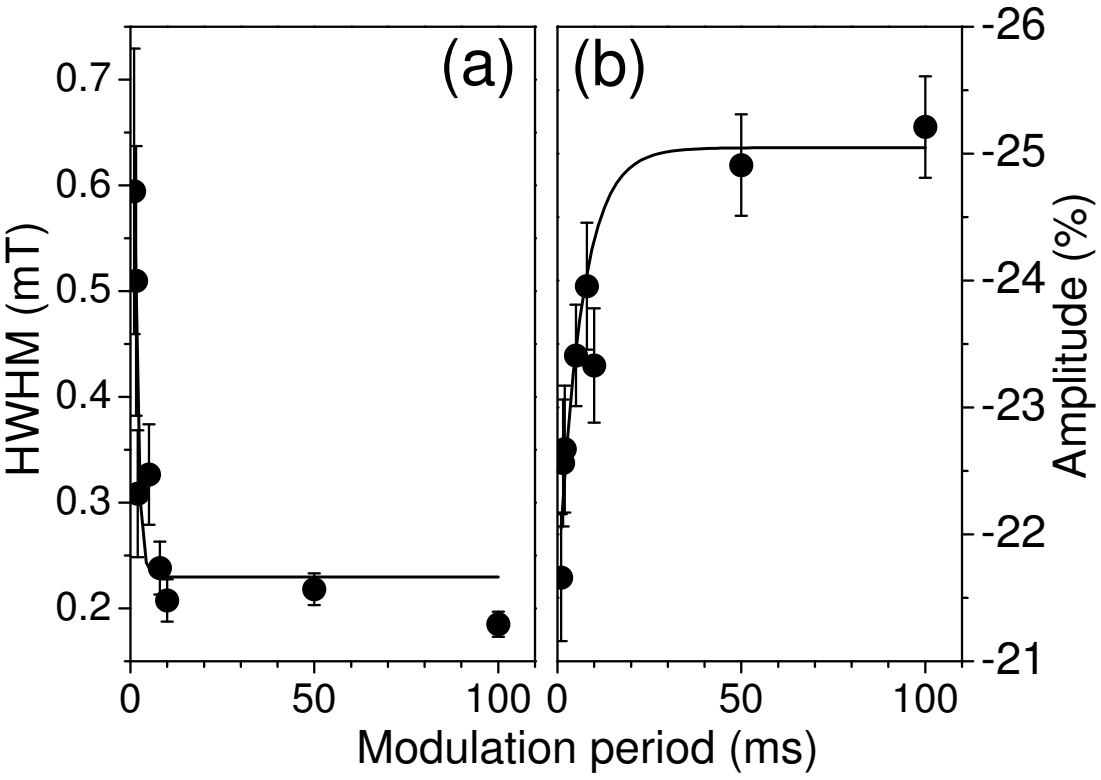

Figure 5.4: (a) Half width at half maximum of the depolarisation peak and (b) maximum of the peak, each in dependence of T_m. The peak becomes broadened by the random nuclear fluctuation field for smaller T_m but saturates at $2\tilde{B}_L$ for long T_m when the maximum nuclear polarisation may be generated. The amplitude saturates above $T_m \approx 40$ ms which marks the time the nuclear system needs to become maximally polarised.

In a transverse external magnetic field, the nuclear field becomes realigned along the external field. The electrons precess about the nuclear magnetic field component parallel to the external field. The component parallel to the Knight field does not lead to precession of $\mathbf{S}$ as $\mathbf{B}_e||\mathbf{S}$ (c. f. chapter 3.5.1). The electron spin thus experiences a purely transverse field where the external field is amplified by the x component of the nuclear magnetic field.

The precession period of an electron spin in a magnetic field of 10 mT is about[5] 14 ns. The Overhauser field, however, considerably exceeds the frozen fluctuation field which has a magnitude of ≈ 30 mT. A magnetic field of this strength would be enough, though, to cause several revolutions of the electron spin during the ≥ 13 ns time span between two optical orientation events which is defined by the repetition rate of the laser. This would lead to a complete depolarisation of the electron spin. What we observe is that the depolarisation peak under the

[5]Assuming an electron g factor of 0.5.

influence of a transverse magnetic field has a constant width of about 0.4 mT. It does not immediately drop down to zero as soon as a transverse field is applied. We attribute this behaviour to the presence of the dipole-dipole field $\tilde{B}_L$. As long as $\tilde{B}_L$ screens the external field, the nuclear spins do not become reoriented, but when the external field begins to exceed the dipole-dipole field, it is experienced by the nuclei. Only then the nuclear spins become realigned. The large transverse component of the nuclear field which is then present depolarises the spin of the resident electron.

When the electron spin polarisation along the z axis becomes destroyed by the precession of the electron spin, the average z component of the Knight field is zero. This geometry with no magnetic field along the excitation axis and an externally applied transverse field does not allow nuclear polarisation to be generated anymore. The electron-nuclear spin system breaks down.

This explains why the polarisation remains on a relatively high level outside the depolarisation peak in figure 5.2. When no nuclear field is present, the resident electron spin is again exclusively exposed to the frozen fluctuation field $\mathbf{B}_f$. Under its influence, the electron spin is depolarised to a fraction of $\geq 1/3$ of the initial electron spin polarisation[6]. Additionally, B_f screens the external magnetic field as long as it is significantly smaller than the frozen fluctuation field. Only when the externally applied magnetic field surmounts B_f, the electron spin is depolarised further.

Hanle measurements have been used before to determine the spin relaxation time of the electron in quantum dots [74, 108, 110]. We emphasise again that this is generally not possible in quantum dots because the electron spin dynamics is strongly influenced by the Overhauser field and by the nuclear frozen fluctuation field. Therefore, the depolarisation of the electron spin in a transverse field is not caused by the competition between the external field and the relaxation or reinitialisation time of the electron but by the nuclear magnetic field. It acts as amplification of the external field but is itself dependent on the magnitude of the external field and on the electron spin. Particularly, there is no linear dependence between B_x and the total magnetic field in fact experienced by the electron. Even when nuclear polarisation is switched off by modulated excitation the frozen fluctuation field B_f is still present and shields external fields unless they considerably surmount B_f. At fields lower than several tens millitesla the nuclear magnetic field or the frozen fluctuation field will *always* dominate the spin dynamics.

Let us now return to the Hanle curves under σ^+/σ^- modulated excitation. Figure 5.4 (b) shows the absolute peak amplitude of the depolarisation peak in dependence of modulation periods between 1 ms and 100 ms. The amplitude increases with growing modulation period T_m and saturates for large T_m. An asymptotic growth fit reveals that the polarisation approaches its asymptotic

[6] c. f. chapter 3.3.3.

value for modulation periods of $T_m > 40$ ms which is hence the timescale the nuclear spin system at least needs to become polarised[7]. The periodical flipping of the excitation helicity with $T_m < 40$ ms thus limits the maximal nuclear polarisation achievable in either of the two excitation cycles. The less time the nuclei have to become polarised before their spins start to become inverted again during the next excitation cycle with the opposite photon helicity the less nuclear polarisation may be accumulated.

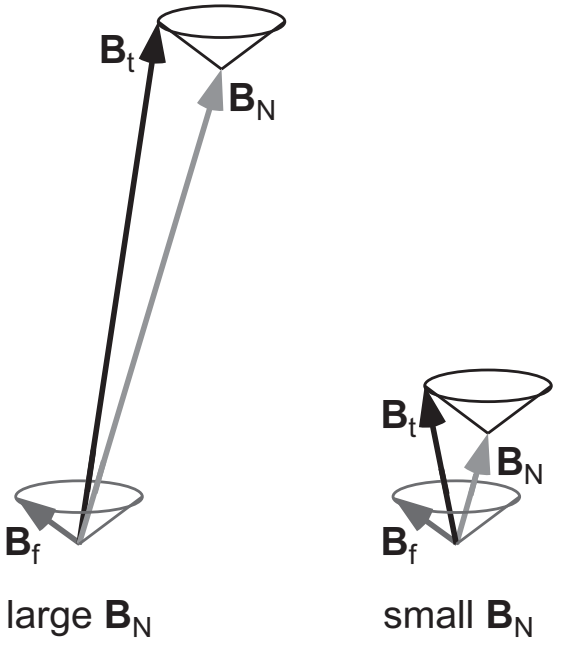

Figure 5.5: Total nuclear magnetic field $\mathbf{B}_t = \mathbf{B}_N + \mathbf{B}_f$, $\mathbf{B}_N$ Overhauser field, $\mathbf{B}_f$ frozen fluctuation field. At large B_N the relative deviation between $\mathbf{B}_N$ and $\mathbf{B}_t$ is small compared to small $\mathbf{B}_N$.

The smaller the nuclear field is, the more important becomes the influence of the frozen fluctuation field background of still unpolarised nuclear spins as schematically illustrated in figure 5.5. The width of the depolarisation peak becomes broader for shorter modulation period as shown in figure 5.4 (a) where the full width at half maximum of the Hanle peaks is plotted over the modulation time. This is due to the fact that it is washed out by the directional distribution of the random fluctuation field. The peak width, however, saturates for $T \geq 10$ ms at a value of ≈ 0.4 mT. In this regime the width is determined by the dipole-dipole field as discussed above. In order to obtain an estimate of the value of $\tilde{B}_L$ we therefore take the average value from several Hanle measurements. This evaluation yields an average peak width of 0.44 mT corresponding to $2\tilde{B}_L$. We thus obtain for the dipole-dipole field

$$\sqrt{\xi} B_L = \tilde{B}_L = 0.22 \pm 0.02 \text{ mT}. \tag{5.3}$$

Theoretical estimations for bulk GaAs yielded $\tilde{B}_L = 0.21$ mT, experimental data on GaAs gave $\tilde{B}_L = 0.25$ mT (both [15]) and recent experiments on self-assembled

[7] A further analysis of the polarisation dynamics will be provided in chapter 7.3.

(InGa)As quantum dots suggested that $\tilde{B}_L$ is of the order of 0.1 mT [99] which is all in good accordance with our result.

We conclude with a remark concerning the terms and conditions under which the width of the Hanle peak may serve as a measure for the dipole-dipole field. If the reinitialisation rate is high, e. g. for continuous wave excitation at high powers, the electron spin only precesses a small distance before it is reinitialised. A higher transverse magnetic field is thus needed to completely depolarise the electron spin. It may happen that already $B_x > \tilde{B}_L$ but still the nuclear magnetic field parallel to B_x is not strong enough to completely depolarise the electron spin. This can lead to a broadening of the depolarisation peak comparable to the original Hanle effect. In our experiments, however, we have a clear situation: we work with pulsed excitation providing a lower limit for the reinitialisation period of 13.2 ns, as mentioned before. Between the pulses the initialised resident electron spins precess in the transverse nuclear field and have enough time to become *completely* depolarised in a purely transverse magnetic field – but only when nuclear spins *experience* the transverse external field at all and become realigned to it. This, however, only happens when $B_x > \tilde{B}_L$.

5.3 The Knight Field of the Electron

As already discussed in chapter 3.4, there is a magnetic moment associated with the spin of the resident electron giving rise to a magnetic field, the Knight field [105]. The Knight field is antiparallel to the electron spin, $\mathbf{B}_e = 2b_e\langle\mathbf{S}\rangle$, and the direction of its z component is thus determined by the helicity of the exciting photons. The Knight field plays the key role in the electron-nuclear spin system in small external fields. In order to optically orient the nuclear spins in a quantum dot, the scalar product $\mathbf{S}\cdot\mathbf{B}_{eff}$ between the resident electron spin and the total magnetic field experienced by the nuclear spins must not vanish. This means that in fact in both the cases $\mathbf{B}_{eff} = 0$ and $\mathbf{S}\perp\mathbf{B}_{eff}$, optical orientation of the nuclear spins would not be allowed.

We know, however, that concerning the *external* magnetic field $\mathbf{B}$, in both cases, $\mathbf{B}||\mathbf{S}_0$ and $\mathbf{B}\perp\mathbf{S}_0$, the nuclear spins may nevertheless become polarised. However, the *effective* magnetic field acting on the nuclear spins $\mathbf{B}_{eff} = \mathbf{B}_e + \mathbf{B}$ is composed of the external field $\mathbf{B}$ and the Knight field of the electron $\mathbf{B}_e$. In the geometry where the external magnetic field is perpendicular to the excitation axis ("Voigt geometry") the Knight field provides the magnetic field parallel to the optical axis which is mandatory for nuclear polarisation to be generated. The same holds in the absence of any external magnetic fields. In this case the build up of nuclear polarisation is also only possible due to the presence of the Knight field [102][8].

[8] c. f. the theoretical considerations, chapter 3.4.

In order to determine the magnitude of the average Knight field, we make use of the fact that a magnetic field in z direction – either externally applied or provided by the internal Knight field – is indispensable to obtain nuclear polarisation. Studying the electron polarisation as a function of a longitudinal magnetic field of the same order of magnitude as the Knight field may reveal its strength. Again, the electron spin serves as a sensitive detector for the state of the nuclear spin system which in turn gives insight into the behaviour of the electron polarisation.

First, we exploit that at $B_{eff} = 0$ no nuclear polarisation can be generated. If a magnetic field B_z parallel to the optical axis is swept, there should be eventually a field value of the same magnitude but the opposite direction of the actual Knight field. In that point the Knight field is compensated and the effective field in z direction acting on the nuclei, $B_{eff} = B_e + B_z$, should be zero. No nuclear polarisation should be present which expectedly should lead to a decrease of the electron polarisation also.

Figure 5.6 shows such B_z dependencies of the photoluminescence polarisation for either excitation helicity where all parasitic transverse fields have been compensated. We actually observe a dip in the polarisation which is shifted away from $B_z = 0$. The direction of the Knight field is determined by the electron spin orientation which in turn is governed by the excitation helicity. The fact that the position of the dip is mirrored upon inversion of the exciting circular polarisation hence indicates that this dip arises as a result of the Knight field. The dip position marks the magnetic field value where the Knight field is compensated, i. e. $B_e = -B_z$. With no effective field in z direction the nuclear spins cannot become polarised and the nuclear spin system remains randomly oriented. The resident electron spins lose their initially injected spin by precession about the frozen fluctuation field[9].

As we see from figure 5.6, the reduction in negative circular polarisation due to cancellation of the Knight field is a barely visible effect. The dip is not as deep as it should be for a complete absence of any effective field in z direction. Changes in the negative circular polarisation occur only when the nuclear magnetic field B_N becomes comparable to B_f and the influence of B_f starts to dominate. For $B_N \gg B_f$, the electron sees an almost purely longitudinal magnetic field. Thus in order to observe a significant depolarising effect arising from Knight field cancellation, we would have to achieve a drop in B_N from hundreds of millitesla or even several Tesla to a few tens of millitesla.

The compensation of the Knight field can, however, by no means be perfect. As we know that the Knight field at a particular nucleus varies across the quantum dot[10], we will only ever achieve cancellation of this field for a particular sub-set of

[9] See chapter 3.3.3.

[10] The inhomogeneity of the Knight field is by the way necessary to obtain maximal nuclear polarisation as was shown in the theoretical work of Giedke in [111].

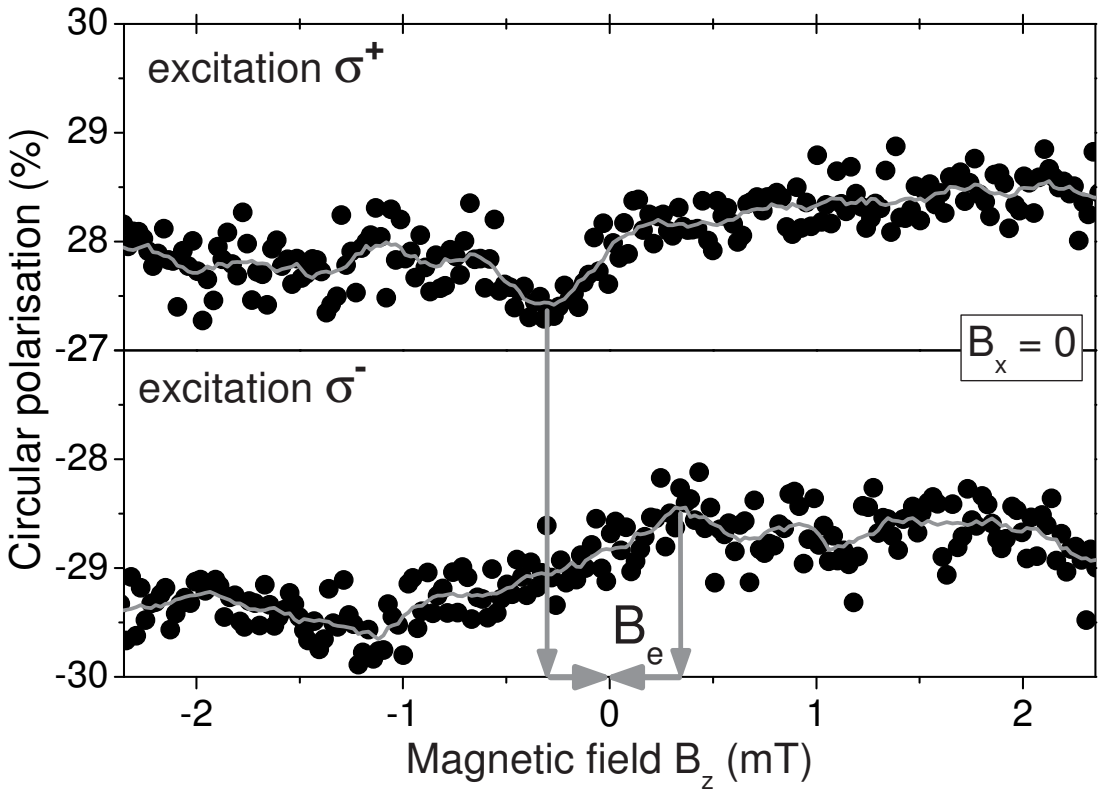

Figure 5.6: Dependence of the photoluminescence polarisation on a longitudinal magnetic field, excitation σ^+ (top) and σ^- (bottom). The dip is located at the magnetic field value where the Knight field is compensated and is consequently mirrored when the excitation helicity is inverted. The red arrows indicate magnitude and direction of the Knight field for either excitation polarisation. Note that here the signs of the circular polarisation indicate the different *electron* polarisations. The circular PL polarisation is always negative with respect to the excitation.

nuclei at any given field. Thus, we do not achieve the almost full depolarisation of the nuclei that we need in order to measure a visible effect.

We therefore additionally make use of the fact that $\mathbf{B} \perp \mathbf{S}$ impedes the build up of nuclear polarisation. We modify our experimental protocol to apply external magnetic fields both in the z *and* the x direction. As we have already observed in section 5.2, a transverse magnetic field B_x greater than ≈ 0.2 mT leads to significant depolarisation of the nuclei already when the Knight field is not compensated. Thus instead of being in a regime where most of the nuclei are polarised, we make use of the regime where at most a small nuclear field is generated that is of the order of B_f. We choose a suitable value of external field B_x, in order to decrease the value of B_N. Then, by applying a longitudinal field along z, the system is much more sensitive to the point where the Knight field is canceled. Even though the Knight field cannot be completely compensated in

the compensation point, B_e is weakened for all nuclei. Compared to the constant external field B_x the effective field B_{eff} experienced by the nuclei at $B_z \approx -B_e$ is small so that they are acted upon by an almost completely transverse magnetic field. At the compensation field value, we hence have the situation $B_{eff,z} \approx 0$ *and* $B_x \mathbf{e}_x \perp \mathbf{S}_0$. The field geometry at $B_z \approx -B_e$ thus largely impedes the build up of nuclear polarisation.

Let us now examine the behaviour of the negative circular polarisation values when performing the same sweep of the magnetic field B_z, as in figure 5.6, with the difference being this time that a constant transverse magnetic field B_x was applied to the system with values ranging from 0.57 to 2.27 mT. Figure 5.7 shows these B_z dependencies of the polarisation for the different applied B_x fields.

The B_z dependence now exhibits a distinct W-like shape that is mirrored on reversal of the excitation helicity. Each curve, however, displays a pronounced asymmetry about the $B_z = 0$ axis. In particular, at ± 0.5 mT, close to the value of Knight field compensation obtained in figure 5.6, a local maximum is observed for all curves (indicated by arrows in figure 5.7). For all B_x values taken, the negative circular polarisation at this maximum point is approximately ± 23 %. The negative circular polarisation then decreases in value, reaches a minimum and starts to increase again.

Let us first explain the local maximum in the middle of the "W". We propose that this maximum at ± 0.5 mT corresponds to the Knight field cancellation point. At this cancellation point, the nuclei feel no longitudinal field to counteract the nuclear dipole-dipole interaction. Additionally, due to the applied field perpendicular to the initial electron direction, optical orientation of nuclear spins is also inhibited for nuclei where the Knight field is only partially compensated. The nuclear system in this point is hence by approximation unpolarised. The value of the negative circular polarisation at that field is entirely governed by the fluctuation field B_f, which is always present in the system. The electron polarisation for compensated Knight field is therefore limited by the nuclear frozen fluctuation field B_f. Note, that the electron spin is not directly depolarised by the external transverse external field B_x. B_x merely hinders the build up of nuclear polarisation. It is, however, one order of magnitude smaller than B_f. We note that the value of 23 % does indeed correspond exactly to the negative circular polarisation value in the absence of nuclear polarisation, as shown in figure 5.2 at high B_x fields. As the B_z field is increased away from the compensation point, nuclear polarisation becomes allowed again. The negative circular polarisation value changes, first decreasing, and then increasing as a result of the effect of generation of a strong B_N field. Note that this method allows the Knight field to be determined much more easily. The local turning point in the negtive circular polarisation data is much clearer, and thus allows much better determination of the Knight field value than the method shown in figure 5.6 and in [102].

In order to numerically evaluate the magnitude of the Knight field we determine the position of the local maximum corresponding to the compensation point of

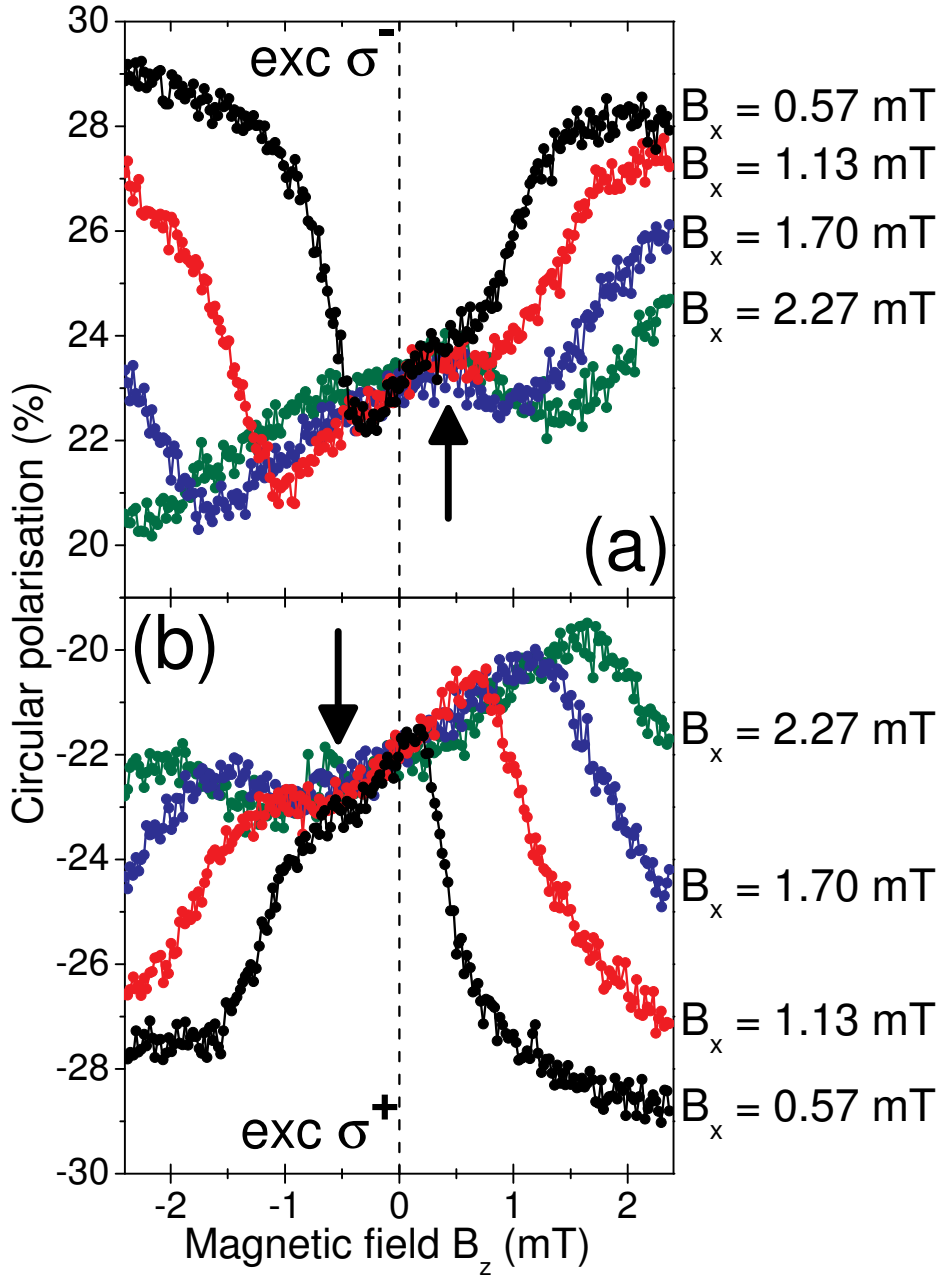

Figure 5.7: B_z dependence of the circular polarisation of the photoluminescence for different applied constant transverse fields B_x. (a) excitation σ^-, (b) excitation σ^+. The arrows indicate the magnetic field where the Knight field of the resident electron is compensated by the external field. There, nuclear polarisation is obstructed and the resident electrons solely experience the frozen fluctuation field. Excitation power is in the saturation regime of the negative circular polarisation. Note that here the signs of the circular polarisation indicate the different *electron* polarisations. The circular PL polarisation is always negative with respect to the excitation.

the Knight field. We find an average value of

$$|B_e| = 0.50 \pm 0.1 \text{ mT}. \tag{5.4}$$

This value is in good agreement with the result from single quantum dot spectroscopy where it was found that $B_e \approx 0.6$ mT [102].

Let us finally address the shape of the curves again in order to explain all their properties. It is on first sight surprising that the polarisation further decreases when $|B_z|$ is increased from the point where $B_{eff} = 0$ despite the fact that now an effective magnetic field in z direction is present. This effect, however, is understandable when we examine the total field acting on the resident electron spin. As soon as a magnetic field parallel to the excitation axis is present, $\mathbf{S} \cdot \mathbf{B}_{eff}$ is not zero anymore and nuclear spins are polarised by optical orientation via the spin oriented electrons. The direction of the nuclear field building up, however, is governed by the magnetic field the nuclear spins experience. The electron spins precess about the nuclear field component parallel to the external field[11] $\mathbf{B} = B_x\mathbf{e}_x + B_z\mathbf{e}_z$. The time average $\mathbf{S}_{av}$ of the precessing electron spin is parallel to the direction of the magnetic field. The angle between $\mathbf{S}_{av}$ and the z axis is thus determined by the direction of the external field. Between the Knight field compensation point and the two minima from which on the electron polarisation increases again magnitude *and* direction of the nuclear magnetic field change. More and more nuclear polarisation is generated with increasing B_z. B_N gradually starts to dominate over B_f. However, $B_{N,x} > B_{N,z}$ as long $B_x > B_z$ because B_N aligns along the external field. At the turning points where the electron polarisation increases again, $B_N \gg B_f$ is reached *and* B_z dominates over B_x so that the electron polarisation becomes restored. The two minima of the W shaped curves are thus predominantly determined by the constant transverse field B_x. This is confirmed by figure 5.7: they shift to higher B_z with increasing transverse field B_x.

Finally, we wish to add one more remark about the direction of the nuclear magnetic field. At the compensation point the electrons are only acted upon by the frozen fluctuation field. In this case the angle between the average electron spin $\langle \mathbf{S} \rangle$ and the z axis is given by the magic angle[12] of $\theta_m = 54.7°$. Between the compensation point and the minima the electron polarisation thus decreases *below* the value it takes for $B_N = 0$. The angle θ between the z axis and the Overhauser field can thus obviously be *increased* compared to θ_m when the nuclear field aligns along an external field with dominating B_x component. Thus, strikingly, the electron spin polarisation as well as the nuclear magnetic field direction can be regulated in a controlled way by the proper choice of an external magnetic field. This might give the possibility to deliberately manipulate *direction* and

[11] The Overhauser field also possesses a component parallel to the Knight field. However, $\mathbf{B}_e || \mathbf{S}$, the electron does not precess about itself. c. f. 3.5.1.

[12] c. f. 3.3.3.

magnitude of the nuclear magnetic field turning a quantum dot into a controllable "nuclear nano magnet".

5.4 The Nuclear Magnetic Field

Having determined the magnitude of the nuclear dipole-dipole field $\tilde{B}_L$ and the Knight field B_e we have made an important step towards understanding the behaviour of the electron-nuclear spin system in the studied sample. Now the goal is to quantify the maximal Overhauser field B_N possibly achievable. It is widely accepted that with an externally applied longitudinal magnetic field a significant nuclear polarisation can be generated. We want to focus on the case $B_z = 0$, however, and show that the Knight field of the polarised resident electron is enough to support a high degree of nuclear polarisation. We are even going to show later that the coupled electron-nuclear spin state exhibits spin lifetimes of hundreds of milliseconds which can only occur when a very large Overhauser field is present.

A lot of effort is being made nowadays in order to approach the limit of 100 % nuclear spin polarisation. It is therefore important to understand to what extend it is possible to polarise the nuclear spins in quantum dots depending on the magnitude of an external millitesla magnetic field and the electron spin polarisation present in the quantum dot. In this section we are therefore going to calculate the *maximum* nuclear magnetic field which may build up in the studied quantum dots using the equations derived in chapter 3.4 together with the experimentally determined B_e and $\tilde{B}_L$ fields.

In chapter 3.4 the equations for the nuclear polarisation and the nuclear field where derived using a linear approximation. We will have to check if this approximation is valid in our case. It will be found that this is not the case, which makes it necessary to find a way to avoid the linear approximation. With the newly derived equations we are then going to estimate the maximal nuclear magnetic field achievable in the studied quantum dots.

In the preceding sections 5.2 and 5.3 we have experimentally found that in the studied quantum dot ensemble the nuclear dipole-dipole field is $\tilde{B}_L \approx 0.22$ mT and that the average Knight field is $|B_e| = 2b_e\langle S_z\rangle \approx 0.5$ mT where b_e is the maximum Knight field achievable. The maximum circular polarisation obtained in the experiment presented in chapter 5.3 where the Knight field was determined was $\rho_c \approx 2\langle S_z\rangle = 0.29$. The magnitude of b_e is thus

$$b_e = \frac{B_e}{2\langle S_z\rangle} = \frac{B_e}{\rho_c} \approx 1.72 \text{ mT}. \tag{5.5}$$

These experimentally determined quantities will enter the equations in order to calculate B_N.

In chapter 3.4 we have found that the nuclear spin polarisation $\rho_{nuc} = \langle I \rangle / I$ of a nuclear species with spin I and the Overhauser field $\mathbf{B}_N$ under optical orientation and under the influence of the small external magnetic field $\mathbf{B}$ are given by

$$\frac{\langle \mathbf{I} \rangle}{I} = \frac{4}{3}(I+1)\mathbf{S}_B \tag{5.6}$$

$$\text{and} \quad \mathbf{B}_N(\mathbf{B}) = \frac{4}{3}\sum_i b_{N,i}(I_i+1)\mathbf{S}_B \tag{5.7}$$

$$\text{with} \quad \mathbf{S}_B = \frac{(B_z + 2b_e\langle S_z \rangle)S_0}{(B^2 + 4b_e S_0 B_z + 4b_e^2 S_0 S_z) + \tilde{B}_L^2}(\mathbf{B} + 2b_e\langle \mathbf{S} \rangle)\,. \tag{5.8}$$

where $b_{N,i}$ is the field of the i^{th} nuclear species for the case of 100 % nuclear polarisation. Let us quickly recall how these equations where constructed and particularly how the approximation mentioned above entered the derivation.

The general expression for the nuclear polarisation of a nuclear spin system exposed to an electron with average spin S is given by

$$\rho_n = \frac{\langle I \rangle}{I} = \mathfrak{B}_I(x(S))\,, \tag{5.9}$$

with the Brillouin function $\mathfrak{B}_I$ for the nuclear spin species with nuclear spin I. The vector generalisation of this expression to the case of a codependent electron-nuclear spin system under the influence of an external magnetic field was then obtained by only retaining the linear term of the expansion of $\mathfrak{B}_I$ in powers of S, $\mathfrak{B}_I^{(1)}$, and then replacing S by the "effective spin" $\mathbf{S}_B(\mathbf{B})$. It was already mentioned in chapter 3.4 that this is a good approximation if I and the average electron spin polarisation are small. However, we deal with indium having spin $I_{In} = 9/2$ and possibly high electron polarisations. We thus have to inspect if this approximation is still valid under the conditions present in our experiments.

Figure 5.8 shows the Brillouin functions $\mathfrak{B}_{1/2}$, $\mathfrak{B}_{3/2}$ and $\mathfrak{B}_{9/2}$ for nuclear spins $I = 9/2$, $I = 3/2$ and $I = 1/2$, as a function of the average electron spin polarisation $\rho_e = S_z/S$. Additionally, the respective linearisations $\mathfrak{B}_I^{(1)}$ of the Brillouin functions are shown. The shaded areas represent a deviation of up to 10 % from the respective Brillouin function. For $I = 1/2$, the linear approximation coincides with the function $\mathfrak{B}_{1/2}$ itsself. For $I = 3/2$ (gallium, arsenic) the approximation still deviates less than 10 % from the full Brillouin function $\mathfrak{B}_{3/2}$ if $\rho_e \leq 0.36$. For indium with $I = 9/2$, however, the error grows rapidly and becomes larger than 10 % already for $\rho_e \geq 0.13$. We see that the linear approximation is no longer valid for the combination of a large nuclear spin I with a large electron spin polarisation. Particularly, it is practically useless for indium.

Let us now investigate the situation in our sample. The effective spin $\mathbf{S}_B$ may be calculated using the parameters b_e and $\tilde{B}_L$ specific for the studied sample. At

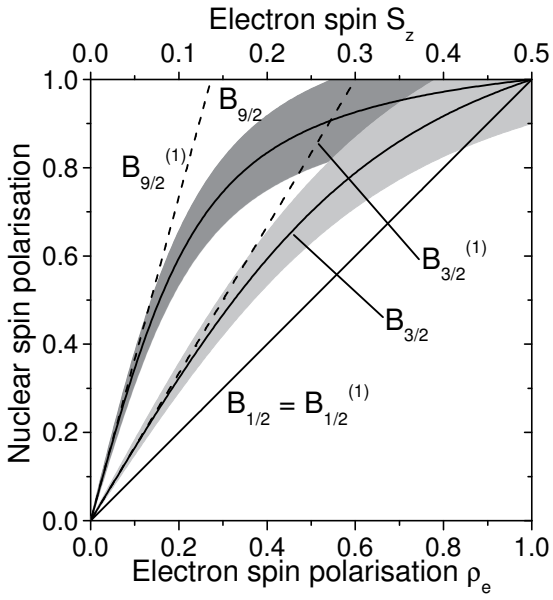

Figure 5.8: The nuclear polarisation $\langle I\rangle/I$ as a function of $S = S_z$ given by the Brillouin functions $\mathfrak{B}_I$ for the respective nuclear spin I (solid lines), the linear approximations $\mathfrak{B}_I^{(1)}$ given by the first term of the expansion of $\mathfrak{B}_I$ in S_z (dashed lines). For $I = 1/2$ all higher terms of the expansion of the Brillouin function vanish and the function coincides with the linear term of its expansion. The grey shaded areas illustrate the region with a deviation of up to 10 % from $\mathfrak{B}_I$.

zero external magnetic field the effective spin $\mathbf{S}_B$ reduces to

$$S_B = \frac{4b_e^2 S_z^2}{4b_e^2 S_z^2 + \tilde{B}_L^2} S_0 \tag{5.10}$$

$$= \frac{b_e^2 \rho_e^2}{b_e^2 \rho_e^2 + \tilde{B}_L^2} S_0 \,. \tag{5.11}$$

We calculate the value of S_B for the experimentally determined values of b_e and $\tilde{B}_L$. For $\rho_e = 1$ follows $S_B = 0.98 \cdot S_0$. It is obvious in this case that the linear approximation of the Brillouin function is not valid anymore neither for gallium and arsenic with $I = 3/2$ nor for indium with $I = 9/2$. Even for an average electron polarisation $\rho_e = 0.3$ which is typical for the experiments discussed in this thesis $S_B \approx 0.84 \cdot S_0$ and the linear approximation breaks down.

If we want to calculate the nuclear magnetic field we thus have to modify the equations. We aim at avoiding the approximation and keeping the full Brillouin function. To accomplish this, the vector generalisation from S to $\mathbf{S}_B$ is done by replacing S with $\mathbf{S}_B$ in *all orders* of the expansion of $\mathfrak{B}_I(x(S))$ in powers of S. In doing so we end up with the formal expression for the nuclear spin polarisation

$$\frac{\langle \mathbf{I}\rangle}{I} = \sum_{n=0}^{\infty} \frac{1}{n!} \frac{d^n \mathfrak{B}_I(x(S))}{dS^n}\bigg|_{S=0} (\mathbf{S}_B)^n \tag{5.12}$$

$$= \sum_{n=0}^{\infty} \left(\frac{1}{n!} \frac{d^n \mathfrak{B}_I(x(S))}{dS^n}\bigg|_{S=0} S_B^{\,n} \right) \frac{\mathbf{S}_B}{S_B} \tag{5.13}$$

$$= \mathfrak{B}_I(x(S_B)) \frac{\mathbf{S}_B}{S_B} \,, \tag{5.14}$$

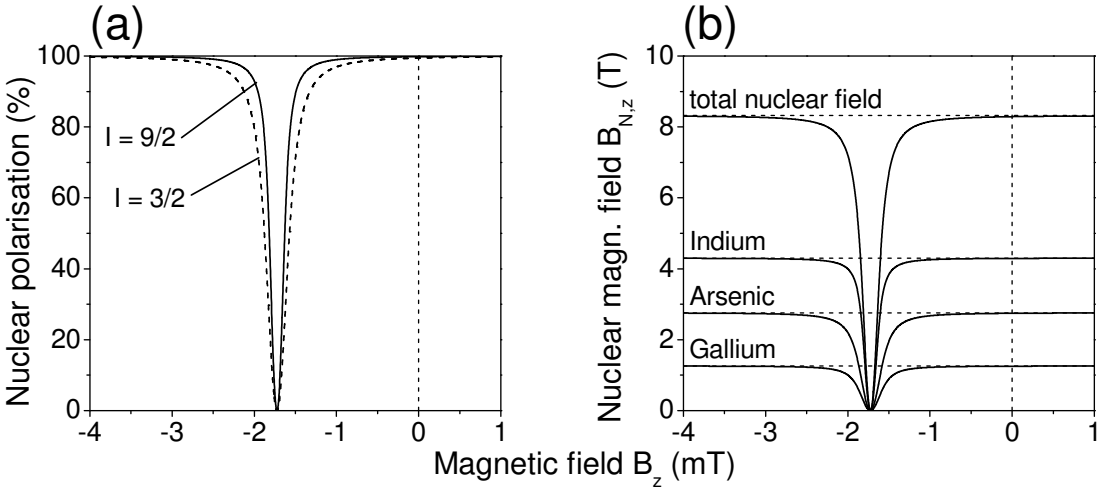

Figure 5.9: (a) The calculated nuclear polarisation as a function of a longitudinal external magnetic field, for nuclei with spin $I = 3/2$ (gallium, arsenic - dashed line) and $I = 9/2$ (indium - solid line), respectively. The minimum is shifted from zero by the magnitude of the maximal Knight field. (b) The nuclear fields of the different nuclear species and the total nuclear field, corresponding to the nuclear polarisations from (a). The dashed lines give the maximum value for 100 % nuclear polarisation of the respective nuclear species. The calculations were performed according to equations 5.14 and 5.15 using the measured values $b_e = 1.72$ mT and $\tilde{B}_L = 0.22$ mT, $S_z = S_0 = -1/2$.

with $S_B = |\mathbf{S}_B|$. $\mathbf{S}_B/S_B = \tilde{\mathbf{B}}/\tilde{B}$ is the unit vector along the sum of the external field and the Knight field, $\tilde{\mathbf{B}} = \mathbf{B} + \mathbf{B}_e$.

Generalising the *full* expression $\langle I \rangle / I = \mathfrak{B}_I(x(S))$ to the case of small magnetic fields[13] can thus be achieved by substituting S_B for the argument S in the Brillouin function with the direction of the nuclear polarisation determined by the factor $\mathbf{S}_B/S_B = \tilde{\mathbf{B}}/\tilde{B}$. Note that the expansion of $\mathfrak{B}_I(x(S))$ does only contain odd powers of S which allows to convert equation 5.12 into equation 5.13. The total nuclear field is then given by

$$B_N(\mathbf{B}) = f \sum_i b_{N,i}\, \mathfrak{B}_I(x(S_B)) \frac{\tilde{\mathbf{B}}}{\tilde{B}} \tag{5.15}$$

with the average leakage factor f.

With equations 5.14 and 5.15 at hand we can now calculate the nuclear polarisation and nuclear field. Let us first determine the maximum nuclear field achievable at $B_z = 0$. The nuclear field becomes maximal when the resident electron spin is fully polarised which may be the case in a fraction of the quantum dots of the ensemble. For $B_{N,z} \gg B_f$ we can assume $\langle S_z \rangle = S_0$. We thus set

[13] cp. with the derivation in chapter 3.4.

$\langle S_z \rangle = S_0 = -1/2$ and calculate $B_{N,z}(B_z)$. $\mathbf{S}_B$ then only has a component in z direction which is given by

$$S_{B,z} = \frac{(B_z + 2b_e S_0)^2}{(B_z + 2b_e S_0)^2 + \tilde{B}_L^2} S_0 \,. \tag{5.16}$$

Figure 5.9 (a) shows the nuclear polarisation calculated with equation 5.14 and 5.9 (b) the nuclear magnetic field calculated with equation 5.15 plotted vs. the longitudinal external magnetic field B_z. The leakage factor f was set to one so that the result should be understood as the maximum polarisation which could possibly be generated with the measured values of b_e and $\tilde{B}_L$. The curves are shifted away from $B_z = 0$ by the value of the Knight field being $b_e = 1.72$ mT for the fully polarised electron spins assumed for this calculation. The nuclear polarisation rapidly increases and becomes saturated already for an effective field $B_z + b_e \gtrsim 1$ mT. We extract from figure 5.9 the nuclear polarisation $\rho_n(0)$ and the magnitude of the nuclear magnetic field at $B_z = 0$. For $I = 3/2$ $\rho_n(0)$ is already as high as 99.5 %, for $I = 9/2$ even 99.8 %. This corresponds to a total nuclear magnetic field $B_{N,tot}(0) \approx 8.29$ T. 8.32 T is the nuclear magnetic field corresponding to 100 % polarisation of all three nuclear species. The maximum nuclear spin polarisation at $B = 0$ for the measured values of b_e and $\tilde{B}_L$ is hence almost 100 %. We conclude that there is a non-vanishing probability that a close to unity nuclear polarisation is at least met in a fraction of the quantum dots of the ensemble.

Obviously, not in all quantum dots can the resident electron spin become fully polarised. We therefore continue by studying the dependence of the nuclear polarisation on the average electron spin at zero external field. We set $\langle S_z \rangle = S_0$ as if an electron spin with polarisation $0 < \rho_e < 1$ was placed inside the quantum dot. The external magnetic field is kept fixed at $B_z = 0$.

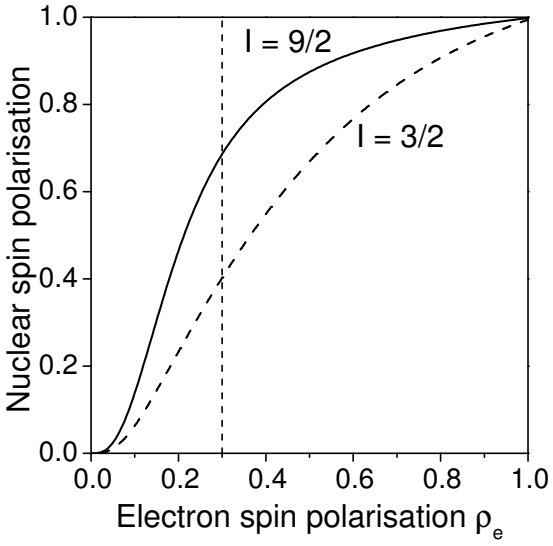

Figure 5.10: The nuclear magnetic field as a function of the electron spin polarisation, $B_N \langle S_z \rangle$ according to equation 5.14, for $I = 9/2$ (solid line), $I = 3/2$ (dashed line), $\langle S_z \rangle = S_0$. $B_z = 0$, $b_e = 1.72$ mT, $\tilde{B}_L = 0.22$ mT. Dashed line: $\rho_e = 0.3$, a value typical for the performed experiments.

Figure 5.10 shows this dependence for $I = 9/2$ (solid line) and $I = 3/2$ (dashed line). The vertical line indicates an electron polarisation of $\rho_e = 0.3$ typical for our experiments. The polarisation of the $I = 3/2$ nuclei gallium and arsenic at $\rho_e = 0.3$ is $\rho_{nuc} \approx 0.4$, the polarisation of indium at this electron polarisation is ≈ 69 %. These values correspond to a total nuclear field at $\rho_e = 0.3$ and $B = 0$ of still $B_N \approx 4.5$ T.

We conclude that in many quantum dots a nuclear magnetic field in the Tesla range could be generated at zero external magnetic field whereas the quantum dots with a highly polarised resident electron could house an almost fully polarised nuclear spin system with $B_N(0) > 8$ T. There surely will be losses of nuclear spin polarisation so that $f \neq 1$ but even then a nuclear magnetic field of the order of Tesla can be expected.

5.5 Summary

Let us now put all the findings of the previous studies together to obtain a comprehensive picture of the electron-nuclear spin system in quantum dots.

- The dynamics of the resident electron spin is always determined by the nuclear magnetic field. When the nuclear spin system is unpolarised the electron spin is depolarised by the frozen fluctuation field $B_f \approx 20$ mT.
- When the nuclear spins become polarised the electron spin is acted upon by the large Overhauser field $\mathbf{B}_N$. Considerable nuclear polarisation is already generated at zero external field in the studied quantum dots due to the Knight field of the electron.
- The Overhauser field can be directed by millitesla external fields.
- The average dipole-dipole field in the studied ensemble is $\tilde{B}_L \approx 0.22$ mT, the average Knight field $B_e \approx 0.5$ mT.
- The maximum Overhauser field possibly achievable according to the common equations at zero external field and with the measured values for B_e and $\tilde{B}_L$ is $B_N > 8$ T.

6 Power Dependence and Large External Magnetic Fields

In the experiments discussed so far the excitation density was always chosen to be in the saturation regime of the negative circular polarisation. Further, we focused on studies exploiting the influence of small external magnetic fields $B \leq 3$ mT. In this section we present experiments which on the one hand address the excitation power dependence of the electron-nuclear spin system. On the other hand we show measurements in larger longitudinal external magnetic fields $B_z \leq 1$ T. Both topics represent work in progress [112]. The final interpretation therefore requires further studies. Nevertheless, the experiments may still give important additional insights into the nuclear spin system in quantum dots.

Let us begin by studying the power dependence of the nuclear spin polarisation. For different excitation powers, we measure the dependence of the circular polarisation of the photoluminescence on a longitudinal magnetic field -130 mT $< B_z <$ 300 mT[1]. The obtained curves can be seen in figure 6.1.

We firstly want to focus on the basic properties of the curves. In figure 6.1 (a) it can be observed that the B_z dependence of the circular polarisation is dominated by two features, a sharp dip around $B_z = 0$ and a broad dip to which the narrow one seems to be superimposed. The position of the broad dip is shifted away from $B_z = 0$ while the position of the sharp dip is not influenced within the B_z resolution of the measurement. Furthermore, the broad one is mirrored at the $B_z = 0$ axis upon inversion of the circular polarisation of the excitation. This is a clear sign that the position of the broad dip is indirectly governed by the polarisation of the resident electron. This behaviour can be explained in terms of the nuclear magnetic field building up when nuclear spins become optically oriented via oriented electron spins. As we have seen, the nuclear magnetic field $B_N(B_z)$ sharply increases with the externally applied longitudinal magnetic field under optical orientation[2]. B_N reaches the maximum value achievable under the respective conditions within millitesla and then remains constant for higher external magnetic fields. Therefore, if the external magnetic field is swept, there is a point, where the external magnetic field is equal in magnitude but opposite in sign relative to the nuclear magnetic field. At this point, $B_z \approx -B_N$. The

[1] Note that the B_z resolution is $\Delta B_z \approx 2$ mT. Features as those discussed in the sections before in connection with experiments performed in magnetic fields $B \leq 3$ mT, e. g. the effects caused by the Knight field, cannot be resolved here.

[2] $B_N(B_z)$ for the parameters determined in sections 5.2 and 5.3 was calculated in section 5.4.

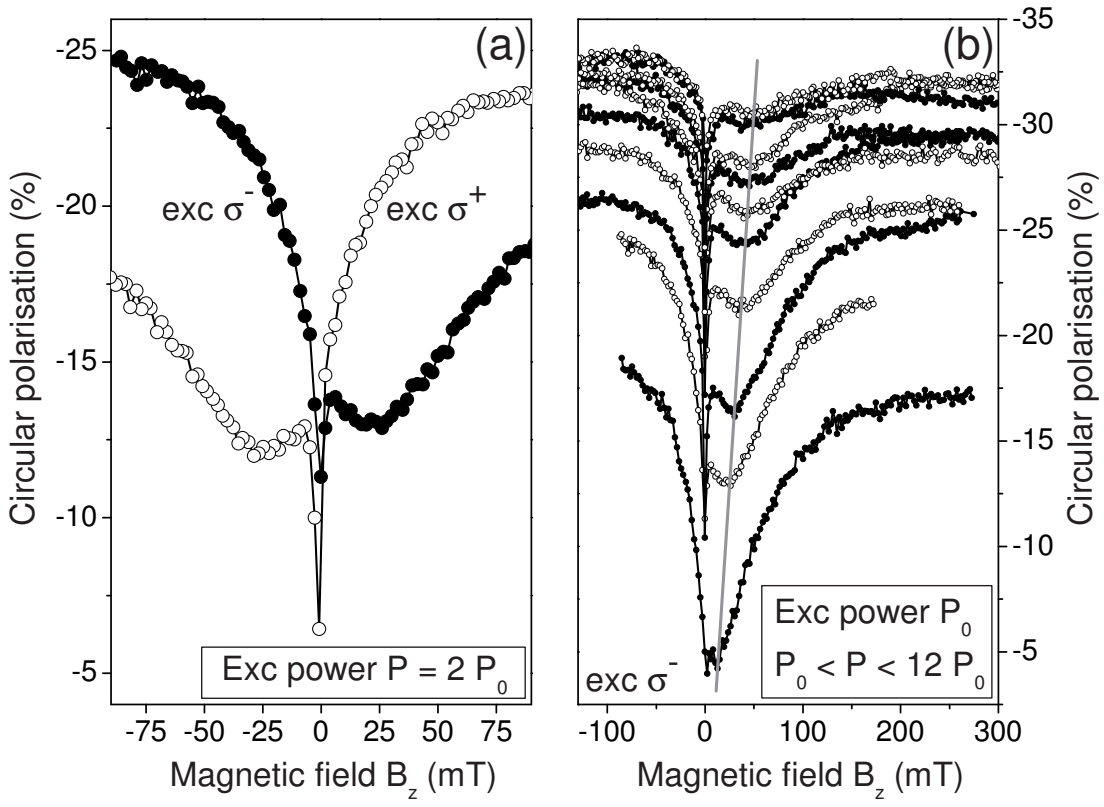

Figure 6.1: (a) Curves for $P = 2P_0$, excitation σ^+ (open circles) and σ^- (full circles). The dip is mirrored on inversion of the excitation helicity which provides evidence that it is caused by the Overhauser field. (b) Circular polarisation of the photoluminescence as a function of longitudinal magnetic field for different powers, $P_0 = 0.25$ mW. The minima of the curves correspond to the point $B_z = -B_N$. With higher excitation power the dip shifts to higher magnetic fields (indicated by the straight line). However, also the circular polarisation in the minima increases indicating that for higher powers the compensation of the Overhauser field by the external field is no longer perfect at all.

shift of the broad dip thus corresponds to the magnetic field value where the nuclear magnetic field in z direction is compensated. The position of the broad dip is shifted away from zero by the magnitude of the nuclear field. The resident electron is predominantly exposed to the depolarising transverse components of the frozen nuclear fluctuation field[3]. At this compensation field, the electron spin polarisation and with it the circular polarisation of the photoluminescence is thus minimal. We will use the position of the dip to measure the nuclear magnetic field. The sharp dip around $B_z = 0$ is probably caused by the B_z dependence of the nuclear polarisation in millitesla external fields.

How does now the shape and position of the curves are related to the excitation power? Figure 6.1 (b) shows B_z dependencies for various excitation densities varying over a range of one order of magnitude. Several observations can be made: The position of the dip shifts to higher magnetic fields for higher excitation power (indicated by the straight line in figure 6.1 (b)), the dips become broader and the circular polarisation at the point of the compensation increases. Further, the asymmetry of the dips increases for higher powers.

At high excitation densities, a higher rate of angular momentum transfer into the system is possible. The resident electron is reoriented more often and thus is able to perform more spin flips with nuclear spins aligning them. As expected, higher excitation densities allow a higher degree of nuclear polarisation to be generated, reflected by the position of the dips in figure 6.1 (b).

Figure 6.2 (a) shows the dip position plotted vs. the excitation power. One can see that the nuclear magnetic field monotonically increases with power and apparently levels off at $B_z \approx 50$ mT for the highest powers. This seems to contravene our conviction that the nuclear spins can become polarised to a high degree producing nuclear magnetic fields in the order of several Tesla[4]. However, we also observe that the width of the curves increases with growing excitation power. For the highest powers where the dip position saturates, the dip almost vanishes. The width is on the one hand governed by the transverse frozen fluctuation field B_{tv}, on the other hand, however, by the spread in magnitude of the longitudinal component $B_{N,z}$. B_{tv} is likely to be constant to a good approximation for small nuclear magnetic fields at low excitation densities and should rather decrease if the z component of the nuclear magnetic field increases at higher powers. Therefore, we conclude that for high excitation densities the distribution of $B_{N,z}$ in the ensemble increases. This is already a hint that there is a significant fraction of quantum dots containing a much higher nuclear field as is suggested by the maximum dip shift of $B_{N,z} \approx 50$ mT we observe. Studying the evolution of the circular polarisation ρ_c with power at the point $B_z = -B_{N,z}$ confirms this. At the compensation point for the lowest power $P_0 = 0.25$ mW $\rho_c \approx 4$ %, whereas it increases with power to $\rho_c \approx 30$ % for the highest powers – the same level

[3] c. f. 3.3.1.

[4] We calculated the nuclear magnetic field possibly achievable in section 5.4. c. f. also [25].

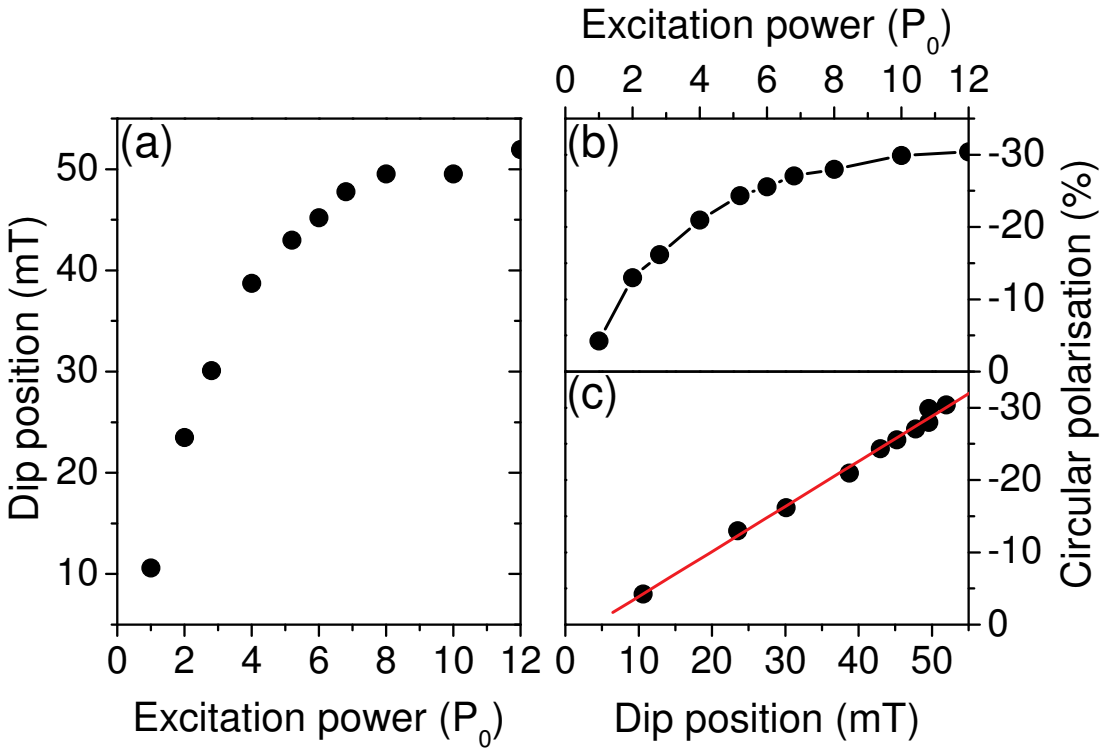

Figure 6.2: Position of the dip $B_z = -B_N$ from figure 6.1 vs. excitation power. B_N saturates at ≈ 50 mT. That this is not the highest nuclear magnetic field in the system, though, is seen in (b). (b) Circular polarisation in the compensation point vs. power. The circular polarisation also increases with power, evidencing that the compensation is not total: There have to exist higher Overhauser fields in the system. (c) Dip position vs. circular polarisation in the dip. There exists a linear correlation.

as achievable for $B_z = 0$. This shows that only for a fraction of the quantum dots the nuclear magnetic field can be compensated. Obviously, the quantum dots with a nuclear magnetic field which is much larger than the magnetic field range covered by the present experiment, $B_{N,z} \gg 100$ mT, cannot be observed in terms of the dip position or its width but only enter via the magnitude of the circular polarisation. If a large fraction of the quantum dots houses a highly polarised nuclear spin system, there is a general rise of the ensemble average circular photoluminescence polarisation. Interestingly, there is to a good approximation a linear dependence between the dip position and ρ_c at the nuclear field compensation point (figure 6.2 (c)).

After the considerations of the previous section, one might wonder how the B_z dependence of the circular polarisation continues for higher external magnetic fields. We therefore extend the magnetic field range to $B_z \leq 1$ T. Figure 6.3 shows B_z dependencies of the circular photoluminescence polarisation for three different excitation powers and for σ^+ polarised excitation (figure 6.3 (a)) and σ^-

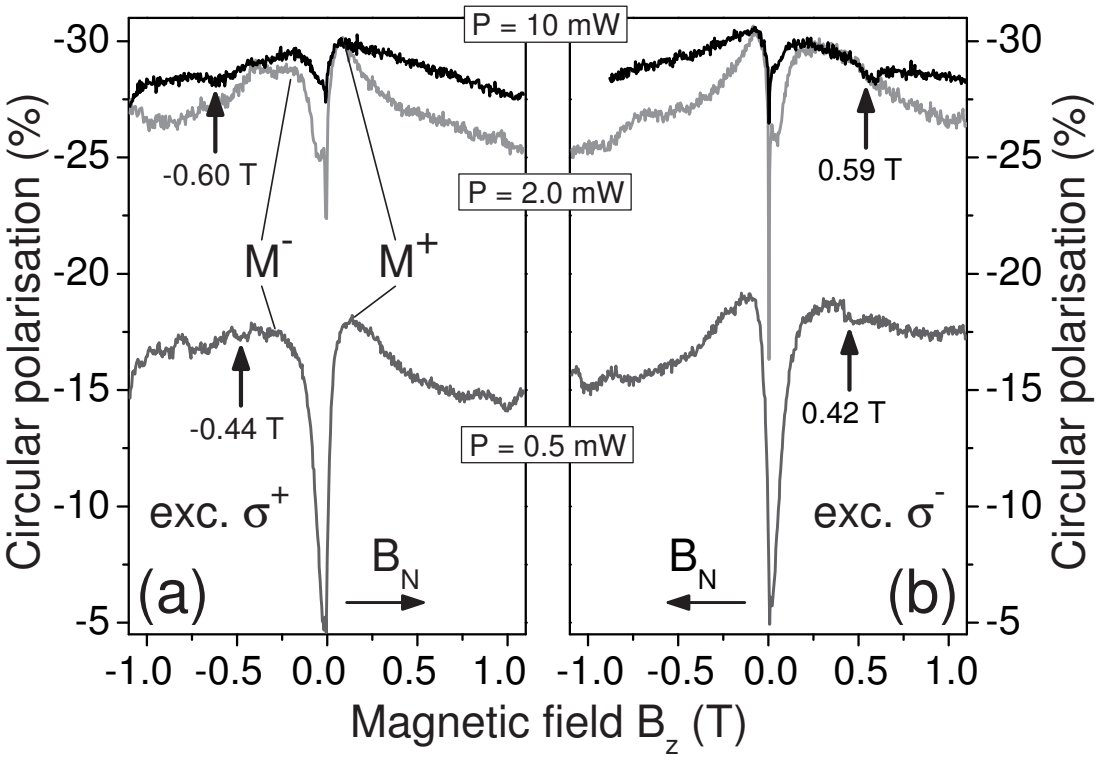

Figure 6.3: (a) Circular polarisation of the photoluminescence as a function of a longitudinal magnetic field B_z for different excitation powers, excitation σ^+ and (b) σ^-. The arrows indicate features which might occur due to the possible bistability of the nuclear polarisation – see text.

polarised excitation (figure 6.3 (b)). The highest power $P = 10$ mW corresponds to the saturation regime where the maximum negative circular polarisation is reached at $B_z = 0$ T. In the center we observe the dip again as we already know it from the power dependent measurements discussed above in this section. Again, the center of the dip is shifted to $B_z = -B_{N,z}$ where a part of the nuclear magnetic field is compensated by the external field. On the side to which the dip is shifted, thus $B_z \mathbf{e}_z \uparrow\downarrow \mathbf{B}_N$. In the figure, the direction of B_N is indicated with arrows. Besides this dip we additionally observe several noticeable features.

- The dip exhibits a pronounced asymmetry. On the side where $B_z \mathbf{e}_z \uparrow\uparrow \mathbf{B}_N$ the rise is much steeper than on the other side.
- The polarisation maxima at the base of the central dip (marked M^+ and M^- in figure 6.3) do not exhibit the same circular polarisation. On the side where $B_z \mathbf{e}_z \uparrow\downarrow \mathbf{B}_N$, the polarisation is smaller.
- From both, M^+ and M^-, the polarisation *decreases* again with further increase of $|B_z|$.

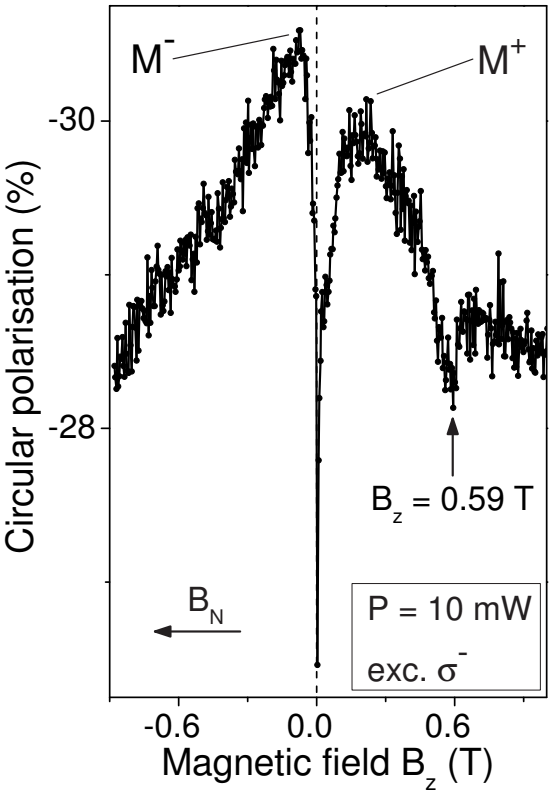

Figure 6.4: Circular polarisation as a function of longitudinal magnetic field B_z. Excitation power is in the saturation regime of the NCP, excitation σ^-. M^+, M^- maxima at $B_z > 0$ and $B_z < 0$ respectively. The direction of the Overhauser field B_N is indicated by the arrow.

- For the two lower powers, the circular polarisation seems to increase again for the highest fields $B_z \gtrsim 1$ T.

- Small, dip like features appear at $B_z \approx \pm 0.6$ T for $P = 10$ mW and at $B_z \approx \pm 0.4$ mT for $P = 0.5$ mW (marked with arrows in figure 6.3). They are not very pronounced. The fact that these dips appear for both excitation polarisations at the same $|B_z|$ but with opposite signs, however, suggests, that these feature are no artefacts.

As the experiments discussed here represent work in progress, the observations will not be fully explained. Let us nevertheless give some thoughts to each of the points mentioned above.

Let us at first address the general shape of the curves. We focus on the curve obtained for excitation power $P = 10$ mW where the saturation regime of the negative circular polarisation with respect to power was already reached. Further, we describe the measurement with σ^- excitation. The explanations apply analogously to the case of σ^+ excitation. For more clarity, the curve is plotted again in figure 6.4. The direction of the Overhauser field B_N is indicated by an arrow. At $B_z \approx 0$ we observe a sharp dip superimposed to the broader dip. As mentioned above in connection with the power dependent measurements, the sharp dip is probably caused by the rise of the Overhauser field in millitesla effective fields.

The broad dip is shifted by ≈ 40 mT towards positive magnetic fields due to the partial compensation of the Overhauser field as discussed before. B_N thus has a negative sign. We wish to point out again that there is no total compensation of B_N. Particularly, we have to keep in mind that we measure an ensemble. In different quantum dots the electron-nuclear spin system may be in significantly different states. This is surely the case in the B_N compensation point. While the nuclear magnetic field is well compensated for a part of the quantum dots, in others there has to exist an Overhauser field which is considerably larger. Otherwise it is not explicable why the circular polarisation in the compensation point is as high as ≈ -29 %. On the $-B_z$ flank of the dip, the circular polarisation steeply increases up to a maximum marked M^- in figure 6.4. The rise is sharp because the Overhauser field and the external field have the same direction and reinforce each other. At M^- the circular polarisation reaches its absolute maximum of $\rho_c = -30.6$ %. At this point, the frozen fluctuation field is overcome by $B_z + B_N$ in most of the quantum dots. On the $+B_z$ flank of the dip the increase of circular polarisation is slowed down because there $B_z \mathbf{e}_z \nparallel \mathbf{B}_N$. The fields counteract one another. At the maximum M^+ on the positive side the circular polarisation is $\rho_c = -30.1$ %, about 0.5 less than at M^-.

The direction of the Overhauser field is only determined by the electron spin orientation which in turn depends on the excitation helicity. B_N should thus not change its direction when the excitation is kept constant. It is therefore surprising that the circular polarisation *decreases* on *both* sides beyond the maxima M^+ and M^- to higher $|B_z|$. At least for the side where B_z and B_N are parallel this is not explainable in terms of the nuclear spin system. Even if B_N became zero, the large external field 0.1 T $< B_z <$ 1 T would suppress the frozen fluctuation field. However, the negative circular polarisation effect *itself* may be magnetic field dependent. The effect is based on electron-hole spin flip-flops mediated by the anisotropic exchange interaction[5]. For higher magnetic fields the electron spin splitting becomes greater than the anisotropic exchange coupling which may depress the spin flip-flops. The negative circular polarisation would then decrease with increasing magnetic field [64]. Nevertheless, the circular polarisation at $B_z = 1$ T is still high. What we see in figure 6.4 is thus maybe a combination of the magnetic fields B_z and B_N affecting the negative circular polarisation and the effect of the fields directly on the resident electron spin polarisation. It will thus be necessary to study the negative circular polarisation effect itself in more detail before the shape of the curves discussed in this section can be fully explained. Particularly, the negative circular polarisation as a function of B_z has to be determined by switching off the influence of nuclear polarisation.

Finally, we wish to briefly discuss the feature at $B_z \approx \pm 0.6$ T marked with an arrow in figure 6.4 and figure 6.3. As we have seen, this feature is mirrored at the $B_z = 0$ axis upon inversion of the excitation helicity. It thus appears on the side

[5] c. f. chapter 3.2.

where $B_z \mathbf{e}_z \uparrow\downarrow \mathbf{B}_N$. It is hence not likely that it is merely a measurement artefact. Moreover, a similar behaviour is observed with the curves measured at lower power where it appears at a lower B_z. At that point the circular polarisation increases by 0.5 percentage points within one B_z step of 3 mT – at an external field of 0.6 T! This jump in circular polarisation could occur due to an abrupt increase in nuclear polarisation.

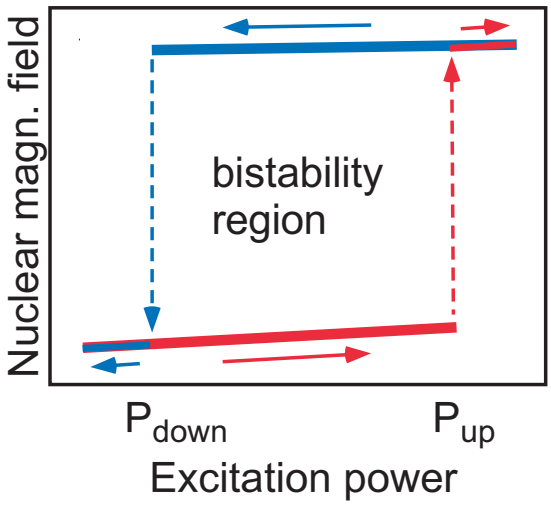

Figure 6.5: Sketch of the phenomenon of bistability. Overhauser field as a function of excitation power. When ramping the excitation power (dark) at a fixed external magnetic field there exists a power P_{up} where the nuclear magnetic field exhibits a step like increase. When decreasing the power again, a step like decrease is observed which occurs at a power $P_{down} < P_{up}$, though. In the region $P_{down} < P < P_{up}$ there exists a bistable regime of the nuclear polarisation.

Recently, a phenomenon was reported appearing in power dependent measurements in Tesla magnetic fields which might explain this step like behaviour: bistability of nuclear spin polarisation [22, 113–115]. When quantum dots were exposed to a constant longitudinal magnetic field 1 T $< B_z <$ 3 T under optical orientation conditions and the excitation power increased, at a certain power P_{up} a threshold-like abrupt increase of the nuclear magnetic field was observed in the case where the nuclear field was aligned antiparallel to B_z. When the power was decreased again, a step-like decrease of the nuclear field occurred – but at a power $P_{down} < P_{up}$. Thus, two significantly different nuclear spin configurations exist for the same magnetic field and excitation power ("bistability"). See the sketch figure 6.5 for a better understanding of the bistability effect. In our experiments, we vary the magnetic field at fixed excitation power. Such a step like change of the Overhauser field might thus also happen in our experiments due to the possible bistability regime of the nuclear spin system. The complete clarification of this feature of the curves requires further studies, though.

7 The Accumulation Dynamics of Nuclear and Electron Spin Polarisation

7.1 Introduction

In chapter 5 we have studied in detail the steady state of the electron-nuclear spin system. We have learned how it develops under optical orientation due to the codependence between electron and nuclear polarisation. In this chapter, we wish to focus on the accumulation dynamics and study how long nuclear and electron spins need in order to become maximally polarised. A first glimpse on this topic was already given in chapter 5.2. There, Hanle curves were studied with the circular polarisation of the excitation switched periodically between σ^+ and σ^-. This excitation scheme will also be the basis of the measurements presented in this chapter.

7.2 Build Up of Electron Spin Polarisation under Optical Orientation

As we have seen in section 3.2, it takes several excitation events in order to fully establish the emission of negative circular polarisation from negatively charged quantum dots. A quantum dot whose resident electron has already been oriented by the negative circular polarisation effect has a greater probability to emit negative circular polarisation after the following excitation cycle than quantum dots containing previously unpolarised resident electrons. In this way, the degree of polarisation of the resident electron becomes accumulated until the maximum fraction of quantum dots is populated with a polarised resident electron. Coevally, the photoluminescence reaches the maximum degree of negative circular polarisation after the respective number of excitations.

In order to study how long the build up of resident electron polarisation takes, we examine the circular polarisation of the photoluminescence under alternating excitation with σ^+ and σ^- polarised light as illustrated in figure 7.1. The excitation was periodically flipped between the two excitation helicities with period T_m. Electron spin polarisation is accumulated during illumination with one he-

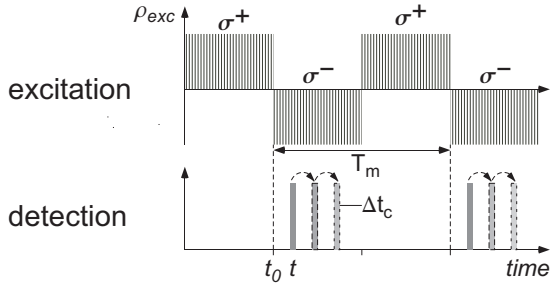

Figure 7.1: Excitation-detection scheme: The excitation is periodically switched between σ^+ and σ^- with period $T_m = 100$ μs forming pulse trains of either helicity. The photoluminescence was read out during a count gate (grey) of width $\Delta t_c = 200$ ns. The read out was performed at different times before and after the flipping of the excitation helicity allowing direct time sampling of the PL polarisation.

licity between $-T_m/2 < t < 0$. When the excitation helicity is flipped at $t = 0$, the resident electron spin polarisation begins to become reversed. The negative circular polarisation of the photoluminescence was recorded during a narrow read out gate. This read out gate was placed at different times t before and after the switching of the excitation helicity. In doing so, the resident electron's polarisation was sampled during its reversal. The modulation period was $T_m = 100$ μs, the count gate had a width of $\Delta t_c = 200$ ns. The excitation power was chosen so that the negative circular polarisation obtained for continuous excitation was just saturated[1]. No external magnetic field was applied. The result of this measurement is shown in figure 7.2 (a).

Time zero corresponds to the point where the excitation helicity switches from σ^+ to σ^-. Before $t = 0$ the polarisation has reached its maximum value of 22 % during the σ^+ excitation cycle. This is the polarisation level that can be achieved for the 100 μs modulation period used here. Under this rapidly alternating excitation no significant nuclear polarisation is generated. This is in accordance with a Hanle curve which has been taken for comparison, figure 7.2 (b). The maximum polarisation of the photoluminescence for modulated excitation in figure 7.2 (a) approximately corresponds to the polarisation level outside the Hanle peak where the nuclear polarisation has been destroyed[2]. The resident electron is thus only exposed to the frozen fluctuation field $\mathbf{B}_f$. A polarisation of the photoluminescence *below* the level which is allowed by the frozen fluctuation field can only occur due to the fact that the electron polarisation inside the quantum dots has not yet been accumulated to the maximum value achievable under the given excitation conditions.

After the polarisation of the excitation has flipped at time $t = 0$, the spins of the resident electrons are gradually repolarised in the opposite direction due to the inverted excitation helicity. This process is reflected by the decrease in the circular polarisation of the photoluminescence. At $t \approx 190$ ns the circular

[1] See figure 3.4
[2] See chapter 5.2

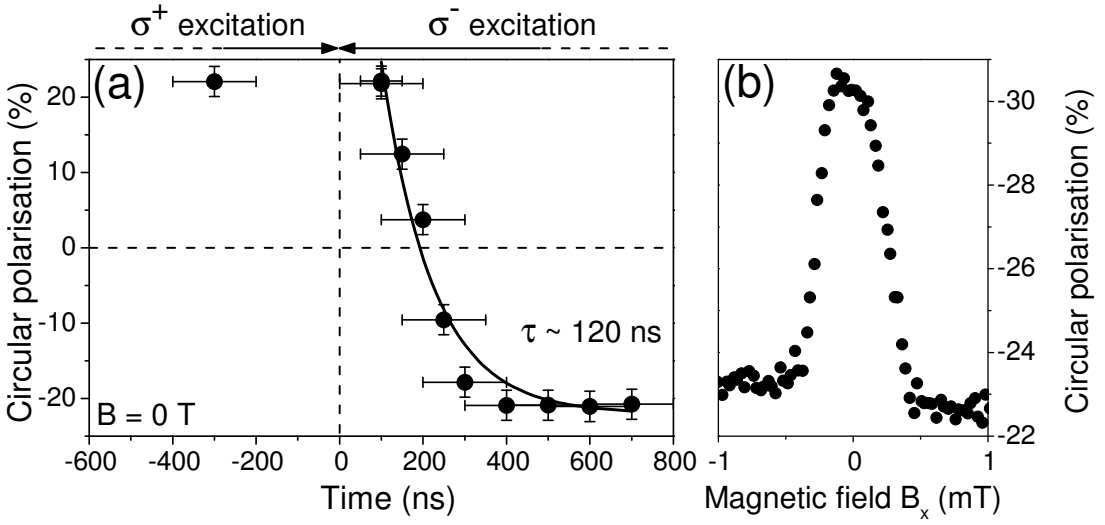

Figure 7.2: (a) The polarisation of the PL measured at different times before and after the excitation helicity switched from σ^+ to σ^- at $t = 0$. Solid line: Exponential fit to the data, time constant $\tau \approx 120$ ns. The polarisation becomes completely repolarised from S_z to $-S_z$ after $t > 500$ ns. Here, the positive sign of the circular polarisation for $t < 0$ indicates the direction of the *electron spins*. The circular polarisation of the photoluminescence is negative with respect to the excitation at all times. (b) Hanle curve, continuous excitation. Outside the Hanle peak nuclear polarisation is absent, the circular polarisation level there is ≈ 23 % – exactly like it is the case in (a) where nuclear polarisation is hindered by the rapidly modulated excitation.

polarisation passes the zero polarisation level where an equal number of quantum dots contain a resident electron with $+S_z$ as with $-S_z$. Then, the polarisation increases again with inverted sign. At $t > 500$ ns the polarisation is ≈ -21 % and has almost reached $|\rho_c| = 22$ % corresponding to the level shortly before the excitation polarisation has flipped. This reflects the average resident electron spin projection on the z axis achievable under the exclusive influence of the nuclear fluctuation field. An exponential fit to the data yields a time constant of the repolarisation of $\tau \approx 120$ ns. Note, that the circular polarisation is *negative* with respect to the *excitation* in both cycles, before and after $t = 0$. The positive sign for the circular polarisation in the cycle $t < 0$ indicates that the actual orientation of the electron spins is opposite relative to the cycle $t > 0$.

We thus maintain that under the general conditions of an unpolarised nuclear spin system and the excitation power being in the saturation region of the negative circular polarisation for continuous, unmodulated excitation, the resident electron spin polarisation is built up on a timescale of 100 ns. Particularly, the electron spins are completely repolarised from one polarisation direction to the opposite one after 500 ns or correspondingly after $n \gtrsim 38$ laser pulses. It takes an

accordingly shorter time to reach maximum polarisation starting with an unpolarised electron spin system. Note also, that a nuclear field along the z direction very likely leads to a decrease of the accumulation time for the electron spins as the optically oriented electrons then initially keep a greater part of their S_z.

7.3 Build Up of Nuclear Spin Polarisation

We have already briefly addressed the accumulation dynamics of nuclear polarisation in chapter 5.2. There, Hanle curves were studied which had been measured using an excitation scheme where the excitation helicity was periodically switched between σ^+ and σ^-. In this chapter, we will exploit this scheme further in order to obtain quantitative results concerning the dynamics of nuclear spin polarisation.

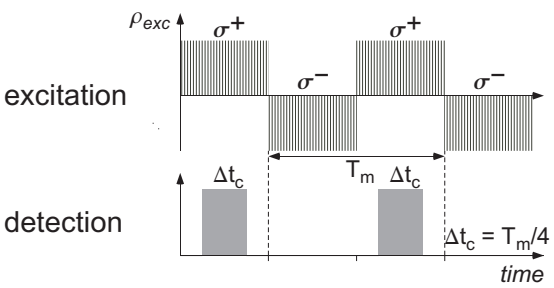

Figure 7.3: Excitation-detection scheme: The excitation is periodically switched between σ^+ and σ^- with period $T_m = 2\Delta t_i$ forming pulse trains of either helicity. The photoluminescence was read out during a count gate (grey) of width $\Delta t_c = \Delta t_i/2$ starting at $t = \Delta t_i/4$ after the switching of the excitation helicity.

The excitation scheme is shown in figure 7.3. We excite the sample with laser pulse trains of opposite polarisation with the width of the pulse trains being $T_m/2 = \Delta t_i$. The circular polarisation of these pulse trains is thus switched between σ^+ and σ^- with period T_m. The read out of the photoluminescence was always performed during the same excitation cycle concerning the polarity, e. g. only during the σ^+ excitation pulse train. The count gates started $\Delta t_i/4$ after the switching of the excitation helicity and had a width of $\Delta t_i/2$. The excitation power was set to the regime where the negative circular polarisation is in saturation for unmodulated excitation.

Figure 7.4 (a) shows the circular polarisation of the photoluminescence for different modulation periods T_m (open circles, labeled σ^{+-}) and – for comparison – the polarisation for continuous excitation with one polarisation (full circles, labeled σ^{++}). The circular polarisation of σ^{+-} increases with increasing modulation period T_m and eventually saturates at the value of the data points for σ^{+-} excitation. Figure 7.4 (b) shows the difference between the polarisation obtained for unmodulated excitation and modulated excitation for each modulation period T_m. The difference decreases to zero for high T_m where the polarisation for unmodulated excitation reaches the value for continuous excitation, in this case ≈ 32.5 %. The saturation of the photoluminescence polarisation corresponds to

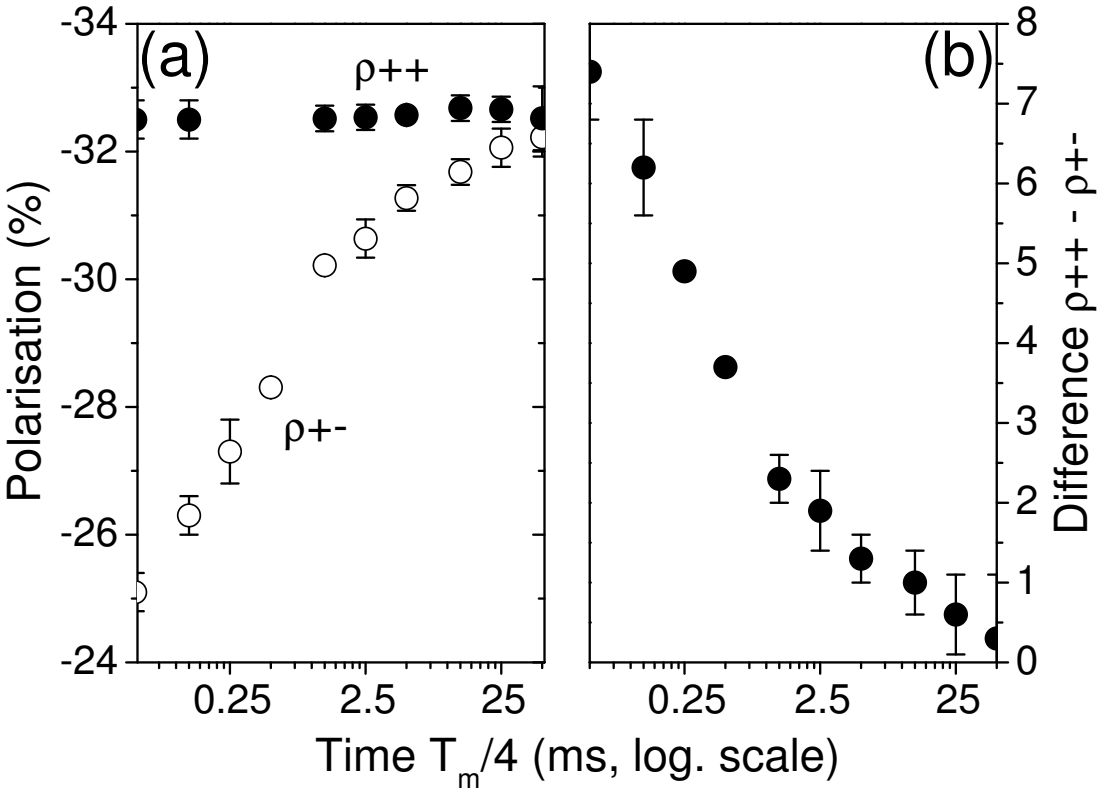

Figure 7.4: (a) Circular polarisation of the PL for unmodulated excitation with σ^+ polarised light (full circles, ρ^{++}) – and for excitation modulated between σ^+ and σ^- with period T_m according to figure 7.3 (open circles, ρ^{+-}). The PL level becomes saturated for $T_m/4 \gtrsim 50$ ms. (b) Difference $\rho^{++} - \rho^{+-}$. Excitation density in the saturation regime of the NCP.

the situation where $B_{N,z}$ considerably outvalues the transverse frozen fluctuation field B_{tv}. The time where the saturation regime is reached consequently is the time this nuclear field needs to build up.

For modulated excitation, the time averaged net transfer of angular momentum into the system is zero. During each excitation pulse train the nuclear spins become polarised in the direction defined by the excitation helicity. After the switching the electron spins are optically oriented in the opposite direction and hence start to flip the nuclear spins. At fixed excitation power, the maximum nuclear polarisation achievable during illumination with a specific circular polarisation in either of the two cycles is only defined by the duration of the pulse trains. We have learned in chapter 7.2 that the electron spins need at most a few hundred nanoseconds to become maximally polarised. Therefore, the rise of photoluminescence polarisation with T_m of the order of milliseconds is exclusively caused by the accumulation of nuclear spin polarisation.

The excitation-detection scheme used here gives a time averaged electron po-

larisation integrated over half an excitation cycle from $\Delta t_i/4$ to $3\Delta t_i/4$ after the switching of the excitation helicity. The proper time scale to analyse this experiment is therefore $\Delta t_i/2 = T_m/4$. The time where the difference between ρ^{++} and ρ^{+-} circular polarisation vanishes corresponds to the timescale the nuclear spins at least need to become polarised. We read off that this time is ≈ 50 ms.

We should additionally emphasise that the rise of photoluminescence polarisation with T_m does not obey an exponential growth law. Indeed, the nuclear polarisation might follow an exponential-asymptotic growth. The electron polarisation, however, which we can only observe, does not depend linearly on the nuclear field.

The time where the degree of circular polarisation saturates is a lower limit for the accumulation time of the nuclear magnetic field. *Maximally* polarising the nuclear spins may take longer. The saturation of the circular polarisation occurs as soon as $B_{N,z} \gg B_{tv}$ is achieved. The accumulation process may continue without having further effect on the electron polarisation and with it on the polarisation of the photoluminescence.

We hence maintain that the nuclear spin systems needs at least 50 ms to become polarised to the degree achievable under the given conditions: pulsed excitation and excitation power in the saturation regime of the negative circular polarisation.

With the measurement described above we gain only indirect access to the nuclear spin dynamics. Now we present a measurement scheme which allows the direct observation of the nuclear field's evolution with time. In order to directly study the change of the nuclear field with time we have used the excitation-detection scheme illustrated in figure 7.1 again. The excitation was switched periodically between σ^+ and σ^-. This time the period was chosen to be $T_m = 4$ ms in order to allow some nuclear polarisation to be generated. The photoluminescence polarisation was read out during a count gate with duration $\Delta t_c = 200$ μs which was positioned at different times t after the switching of the excitation polarisation at $t = 0$. At each time t a B_z dependence of the circular polarisation $\rho_c(B_z)$ was recorded with -130 mT $\leq B_z \leq 130$ mT [112]. Although the circular polarisation of the photoluminescence is of course still only an indirect measure for the nuclear spin system, information about the actual strength and direction of the nuclear field are encoded in the shape of the $\rho_c(B_z)$ curves.

Figure 7.5 shows such curves for ten different times 106 μs $\leq t \leq$ 1800 μs where the times given correspond to the position of the center of the 200 μs wide count gate. Thus the whole σ^- excitation cycle after the inversion of the excitation helicity from σ^+ to σ^- is sampled. Each curve displays a sharp dip around $B_z = 0$ caused by the build up of nuclear polarisation in millitesla magnetic fields. The curves may be viewed as broad Lorentz shaped dips with the sharp dip superimposed to the Lorentzian. For the analysis of the nuclear field dynamics though, the important feature is the position of the Lorentz curve's minimum. This point marks the magnetic field value where the external field compensates most of the

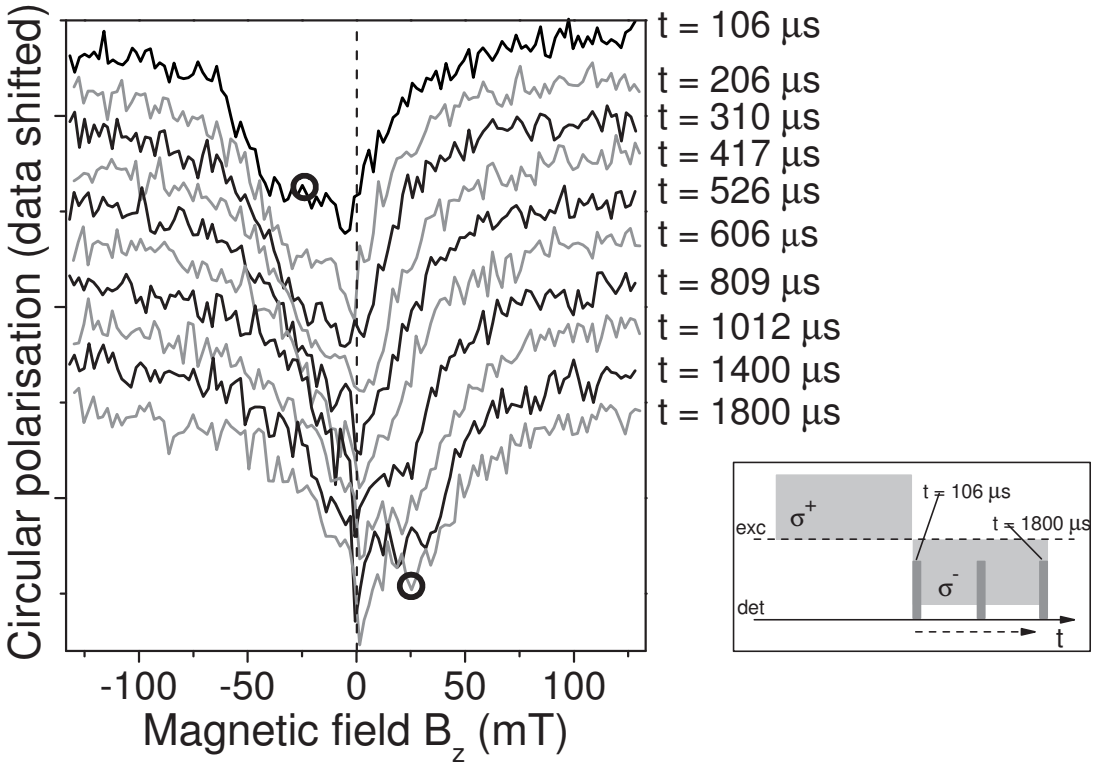

Figure 7.5: B_z dependencies of the circular polarisation of the photoluminescence. σ^+/σ^- modulated excitation with period $T_m = 4$ ms, curves recorded at a point of time t after the switching of the excitation helicity from σ^+ to σ^- (excitation-detection scheme figure 7.1 and the sketch on the right). The point where the longitudinal nuclear field is compensated by the external magnetic field B_z (indicated by black circles) shifts from $B_z < 0$ at small t to $B_z > 0$ at t approaching $T_m/2$. Thus, direct monitoring of the nuclear field dynamics is achieved. Excitation power in the saturation regime of the NCP.

nuclear field in z direction, $B_z \approx -B_{N,z}$. The electron is then predominantly exposed to the transverse components of the nuclear fluctuation field. The electron spin precesses in this transverse field and the circular polarisation of the photoluminescence in this point is minimal. The position of the compensation point thus is a direct measure for the magnitude *and* the direction of the nuclear field in z direction. We expect that shortly after $t = 0$ the nuclear field is still oriented according to the previous excitation helicity. Then the nuclear spins become gradually repolarised, and at the end of the cycle for $t \approx T_m/2$ the nuclear field should be maximally restored in the opposite direction. Indeed, we observe that for early times after t_0 the dip is located at negative values of B_z corresponding to $B_{N,z} > 0$ whereas it has shifted to positive B_z for times close to $T_m/2$ (in figure 7.5 indicated by a black circle for $t = 106$ μs and $t = 1800$ μs).

In order to determine the value of $B_{N,z}$ for each t we fit the curves with the

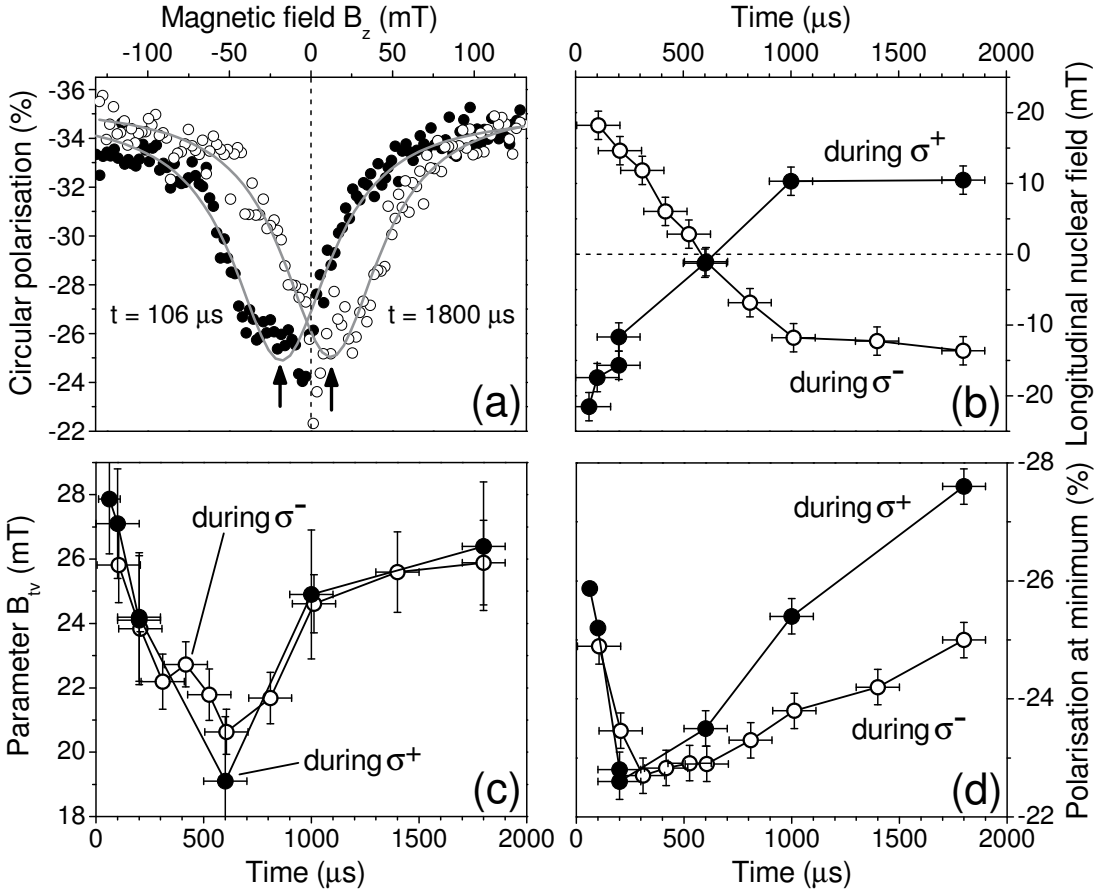

Figure 7.6: Data from time resolved B_z dependencies under σ^+/σ^- modulated excitation with $T_m = 4$ ms (c. f. figure 7.5, excitation scheme figure 7.1, explanation see text). Excitation power in the saturation regime of the NCP. (a) Two example curves for $t \ll T_m/2$ (full circles) and $t \approx T_m/2$ (open circles). Fits according to equation 7.1. (b) Longitudinal nuclear field $B_{N,z}$ obtained from the fit with function 7.1 as a function of the time after the switching of the excitation helicity, recorded during σ^+ cycle of the excitation (full) and the σ^- cycle (open). (c) Magnitude of parameter B_{tv}, determined by fit with function 7.1. (d) Circular polarisation at the point $B_z = -B_{N,z}$ (indicated by arrows in ((a)).

function

$$\rho_c(B_z) = \rho_a \frac{(B_z + B_{N,z})^2}{(B_z + B_{N,z})^2 + 2B_{tv}^2} + \rho_m. \tag{7.1}$$

Here ρ_m is the polarisation value at $B_z = -B_{N,z}$, ρ_a the amplitude of the dip, $B_{tv} = B_{f,x} = B_{f,y}$ the transverse components of the nuclear frozen fluctuation field and $B_{N,z}$ the longitudinal nuclear field. Note that $B_{N,z}$ generally also depends on B_z. It rises, however, on a millitesla field range so that we can neglect this dependence. $\rho_c(B_z)$ describes the z projection of the time average of a precessing spin[3]. Figure 7.6 (a) shows one B_z dependence from the beginning (full circles) and one from the end of the σ^- excitation period (open circles) as well as the corresponding fits (grey lines). The arrows indicate the shift of the dips corresponding to the parameter $B_{N,z}$ in equation 7.1. In figure 7.6 (b) the parameter $B_{N,z}$ of the fitted curves is plotted versus the time after the switching of the excitation, for detection during the σ^- period of the excitation (open circles) and σ^+ excitation (full circles).

We observe that for detection during the σ^+ cycle shortly after $t = 0$ $B_{N,z}$ is still positive, then decreases in magnitude, passes zero at $t \approx 600$ μs and saturates towards the end of the cycle. This behaviour can be explained in terms of the repolarisation of the nuclear spins after the inversion of the exciting polarisation at $t = 0$.

At $t = 0$ the nuclear field still has approximately the value accumulated during the previous excitation period with σ^- polarised light, $B_{N,z} > 0$. Then the nuclear spins become reoriented and the absolute value of the nuclear field decreases, eventually passes zero at $t \approx 600$ μs and increases again until it eventually becomes saturated. For detection during the σ^+ period this evolution is inverted as expected. Now, at early times $t < 600$ μs $B_{N,z}$ is negative. At $t \approx 600$ μs $B_{N,z}$ crosses zero again. It is positive at the end of the cycle. This dependence on the excitation helicity provides another strong confirmation of the interpretation of the dip position in terms of the longitudinal nuclear field. The saturation of the nuclear spin polarisation is reached after ≈ 1 ms. This is considerably faster than the time of 50 ms we have determined from the experiment presented in figure 7.4. We have to recall though that in the present experiment the degree of nuclear polarisation achievable is restricted by the relatively fast excitation polarisation modulation used here.

Figure 7.6 (c) shows the fit parameter B_{tv} of equation 7.1 as a function of time. B_{tv} is proportional to the width of the curves. We associated this parameter with the transverse, i. e. in-plane, component of the nuclear frozen fluctuation field. We observe that this parameter is maximal at the beginning of the excitation cycle and at its end with the maximal value being $B_{tv} \approx 27$ mT. B_{tv} has a clear minimum around $t \approx 600$ μs – exactly where the longitudinal component

[3]See chapter 3.3.2. $\rho_c(B_z)$ was derived from equation 3.15. See also the discussion on page 50.

of the nuclear magnetic field $B_{N,z}$ is approximately zero. This clearly contradicts the expectations. In the case of relatively weak nuclear polarisation as it is the case for the modulated excitation with $T_m = 4$ ms used here the transverse components of $\mathbf{B}_f$ should be approximately constant. Rather should B_{tv} *decrease* for increasing $B_{N,z}$ because nuclear spins gain longitudinal component at the cost of their transverse components. In no case, however, is the transverse nuclear field expected to grow with increasing longitudinal field. It is therefore likely that it is not justified to exclusively relate the width of the dips of figure 7.5 to the transverse nuclear fluctuation field. The distribution of $B_{N,z}$ could also play a role. While the distribution parameter for the transverse nuclear field component might not change very much in dependence of t during the reversal of the nuclear polarisation, the distribution of the longitudinal nuclear field component could depend on t. When the longitudinal nuclear magnetic field is maximal at the beginning and at the end of the excitation cycles, also its spread is wider, where $B_{N,z} \approx 0$ the distribution is also minimal. The width of the dips in figure 7.5 is then caused by both the longitudinal and the transverse distribution parameter. When the longitudinal field distribution is large, at each magnetic field value the nuclear magnetic field is only compensated for a subensemble leading to a broadening of the dip. This explains the fact that the width is minimal at the point where the longitudinal nuclear magnetic field has its zero crossing. In order to affirm this explanation for the dip width we investigate the circular polarisation in the points where the longitudinal nuclear field should be compensated. Figure 7.6 (b) shows the circular polarisation at the minima of the Lorentzian fit curves, i. e. at the compensation point, in dependence of t. We observe that the circular polarisation has a minimum in the time region where $B_{N,z}$ has its zero-crossing. This supports the conclusion that the distribution of the longitudinal nuclear field component is minimal there: Due to a narrow field distribution, the compensation at that point is better than at times where the field distribution is broader. There, a larger longitudinal component remains uncompensated and leads to a higher circular polarisation of the ensemble photoluminescence. The width of the Lorentzian in the zero-crossing region of $B_{N,z}$ would then come closest to the more or less constant transverse nuclear magnetic field $B_{tv} \approx 20$ mT.

Various factors complicate the mathematical analysis of the nuclear field dynamics in the experiment presented here. The sample consists of three nuclear species which most likely exhibit a different dynamics and sub-ensembles of quantum dots might behave differently. Therefore, we have confined ourselves to phenomenologically analyse the dynamics of the nuclear spin polarisation accumulation. Nevertheless, combining time dependence and magnetic field dependence can become a helpful tool to directly study the behaviour of the nuclear spin system with time.

Finally, we add a somewhat speculative consideration. We inspect the curves from figure 7.5 more closely. It seems that on the Lorentz shaped broad polarisation curves there are – besides the narrow dip near $B_z = 0$ – superimposed at

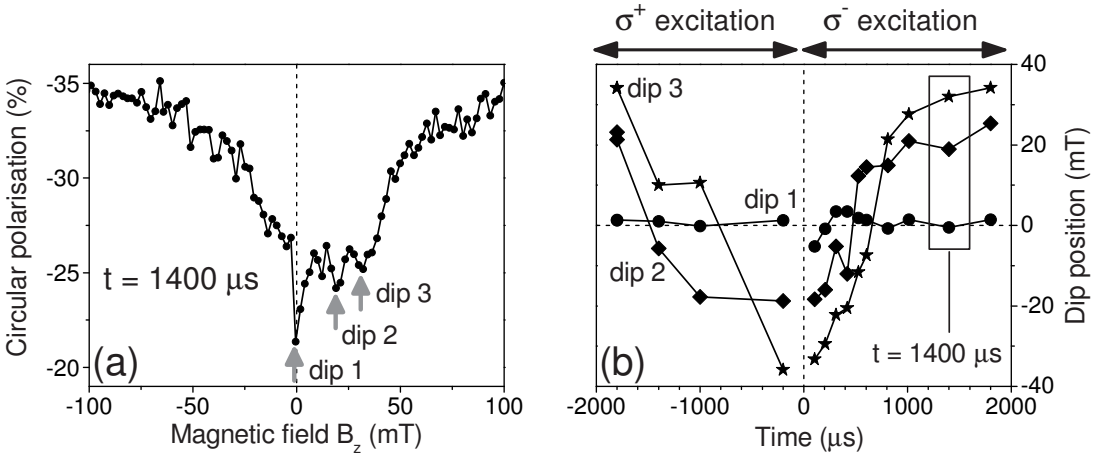

Figure 7.7: (a) A B_z dependence taken at $t = 1400$ μs after the flipping of the excitation helicity. The arrows indicate dips superimposed on the broad Lorentzian – colours corresponding to the respective data in (b). The dip at $B_z = 0$ is probably due to increase of B_N at millitesla magnetic fields. (b) The position of the three dips from (a) vs. the time t after the switch of the excitation helicity at which the B_z dependence has been taken. The magnitude of the dip position at the beginning of the cycle corresponds to that at the end. This is confirmed by measurements at $t < 0$. Thus there is a continuous connection.

least two more resonances with the external magnetic field as can be seen more clearly in figure 7.7 (b). The figure shows the B_z-curve at $t = 1400$ μs as an example. The dips are indicated by arrows. These dips can be observed more or less clearly for all times t. In figure 7.7 (b) the magnetic field position of the dips is plotted versus the time t at which the respective B_z dependence was recorded. The dip position B_z at $t \approx 0$ is equal to $-B_z$ at $t \approx T/2 = 2000$ μs as expected. This behaviour is confirmed by measurements performed at negative times where the excitation helicity is opposite to the one at $t > 0$. It seems that several resonances of the external field with the longitudinal nuclear magnetic field occur. The dip near $B_z = 0$ is probably caused by the dependence of the nuclear magnetic field on millitesla scale external fields[4].

[4] c. f. chapters 3.4 and 5.4.

8 Long Spin Lifetimes and the Nuclear Spin Polaron

8.1 The Nuclear Spin Polaron

In quantum dots the main mechanism depolarising the resident electron spin is the interaction with the nuclear spin system. When the nuclear spins are completely randomly polarised the precession of the resident electron about the frozen fluctuation field $B_f \approx 25$ mT leads to the partial loss of the electron spin polarisation on a nanosecond timescale and to a total depolarisation after at most a microsecond due to the fluctuation of B_f. The spins of the quantum dot nuclei thus represent an obstacle for keeping spin polarised electrons in quantum dots for a preferably long time, e. g. in order to use the stored electron spins for quantum information applications. We have also seen that the depolarising effect of the nuclear fluctuation field can be overcome by externally applying a magnetic field $B \gtrsim 100$ mT which considerably outvalues the nuclear fluctuation field. Indeed it was shown that an electron spin lifetime of $T_1 > 20$ ms can be obtained, in an external magnetic field of $B = 4$ T [116]. Little is on the other hand known about the electron spin relaxation in zero magnetic field in dependence on the state of the nuclear spin system. That the nuclear spin system does not only act destructively on the electron spin polarisation has already been shown in this work. We have shown that nuclear polarisation is generated via optical orientation if we constantly inject angular momentum in our quantum dots by illumination with circularly polarised light. If nuclear polarisation parallel to the z axis is generated in this way, the nuclear magnetic field accompanying the polarised nuclear spins causes a significant increase of the average resident electron spin also at $B = 0$.

We measure the electron spin polarisation via the negative circular polarisation of the photoluminescence. In our experiments we excite the sample with a pulsed laser system with the pulses being separated by 13.2 ns. Thus, the time between two excitation events corresponds at least to the time between two laser pulses. The degree of negative circular polarisation achievable at fixed excitation density and zero magnetic field is determined by the degree of polarisation *memory* outliving the time between the initialisations of the resident electron spin in the respective quantum dot[1]. If no nuclear polarisation is present, a large part of the

[1]See the sketch figure 5.1 for the excitation cycle of a quantum dot with initialisation, evolution

electron polarisation is already lost within nanoseconds between the excitations. The fact that we see a drastic increase in negative circular polarisation if the nuclear spins become polarised thus implicates that the resident electron spin memory increases from a few nanoseconds to at least tens of nanoseconds in the case of a partially polarised nuclear spin system. This gives already a sign that the electron spin memory could be increased also at $B = 0$ by properly preparing the nuclear spin system.

In chapter 5.4 we have estimated that under ideal conditions a nuclear polarisation close to unity might be generated in a fraction of the quantum dots in the studied ensemble. In such quantum dots the strongly polarised nuclear spin ensemble possibly stabilises the electron spin much more than it might has been expected. When discussing the electron spin relaxation in quantum dots at small magnetic fields it is therefore essential to take the influence of the nuclear spin system into account. It is thus important to study the resident electron spin lifetime in dependence on the state of the nuclear spin entirety.

In this chapter we are therefore going to study the persistence of the electron-nuclear spin polarisation memory after the excitation has been switched off. In order to achieve this we develop an excitation-detection scheme including a variable dark time between the excitation cycles which allows to determine the lifetime of the electron-nuclear spin system.

We find that the electron-nuclear spin system keeps a memory of up to hundreds of milliseconds, a value not observed before. These extremely long spin lifetimes may be interpreted in terms of the formation of a self-consistent electron-nuclear spin complex in which the polarised electron spin and the nuclear spin ensemble mutually stabilise each other. Such a complex is known as a nuclear spin polaron (NSP) [24, 25, 117].

In the theoretical model describing the polaron state the concept of nuclear spin temperature plays an important role [24]. When the spin-lattice relaxation time T_1 is much larger than the time T_2 characteristic for equilibration of the nuclear spins by the dipole-dipole interaction, the spin system is well isolated from the lattice. $T_2 \approx 10^{-4}$ s is also short compared to the time T_{1e} describing the relaxation due to electrons. Therefore, the nuclear spin system can to a good approximation considered to be in thermodynamical equilibrium. The equilibrium state can be described by a single parameter, the nuclear spin temperature Θ [16, 90]. The pumping of the system with oriented electrons lowers Θ. If a magnetic field is present, the spin temperature gives rise to a nuclear polarisation $\rho_c \propto B/\Theta$. In the absence of an *external* magnetic field the field necessary to obtain nuclear polarisation can also be provided by the Knight field of the electron. The condition for the polaron formation is that the nuclear spin temperature decreases below a value of the order of 10^{-7} K [24].

The predominant and most striking signature of the appearance of a nuclear

and reinitialisation of the electron spin.

spin polaron is the giant increase in nuclear spin relaxation time. The spin relaxation time of the nuclear spins configuring the total polaron spin $\mathbf{J}_\Sigma$ scales with the number of nuclear spins forming the polaron, N_B, which means that the nuclear spin relaxation time could be a factor 10^5 larger than the dipole-dipole interaction time $T_2 \approx 10^{-4}$ s which normally defines the timescale of nuclear spin relaxation [24, 118]. Thus, the nuclear spin polaron relaxation time may be as large as seconds.

What is even more important, though, is the fact that such a nuclear spin polaron state also affects the spin relaxation time of the resident electron. While the nuclear spins generally provide the main depolarising mechanism of the resident electron spin, the possible formation of a nuclear spin polaron drastically increases the electron spin relaxation time of the resident electron spin $\mathbf{S}$ in the spin polaron. For optical orientation parallel to the z axis the macroscopic nuclear polaron spin $\mathbf{J}_\Sigma$ as well as the nuclear magnetic field associated with $\mathbf{J}_\Sigma$ is parallel to z. The nuclear magnetic field of the polaron state can be so strong, that the Zeeman splitting of the resident electron spin induced by it can become larger than the thermal energy of the lattice. In our experiments with $T \approx 1.9$ K a nuclear magnetic field $|B_N| \gtrsim 5.7$ T is needed in order to obtain a spin splitting E_Z of the resident electron fulfilling $E_Z > k_B T$. In this case the electron spin freezes on the lower Zeeman level, the resident electron's spin relaxation becomes depressed. This in turn impedes the relaxation of the nuclear spins by the electron leading to a mutual stabilisation of nuclear and electron spin polarisation. As we have estimated in chapter 5.4 a nuclear magnetic field of the required magnitude could possibly be generated in a fraction of the quantum dots. We thus can expect that at least in some quantum dots an extremely stable electron-nuclear spin state may be generated.

Recently the dynamics of a central spin (the resident electron spin) in a spin bath (the nuclear spin ensemble) was calculated [26, 119]. These calculations also revealed that the central spin retains its initial magnitude for an infinite time if the bath is fully polarised in either direction parallel to the central spin.

We are going to study the polaron formation at zero external magnetic field in our heterostructure by studying the most prominent property of the nuclear spin polaron, the greatly enhanced spin lifetime of the electron-nuclear spin system, with the help of a specially designed excitation-detection scheme.

8.2 Polarisation Memory Measurements

To investigate the dynamics of the electron-nuclear spin system at zero externally applied magnetic field we use an excitation-detection scheme which is again based on the illumination of the sample by pulse trains. This time, however, a dark time Δt_d is introduced between the excitation cycles. Figure 8.1 depicts the scheme.

Each period consists of illumination by a first pulse train "*pump 1*", an ensuing

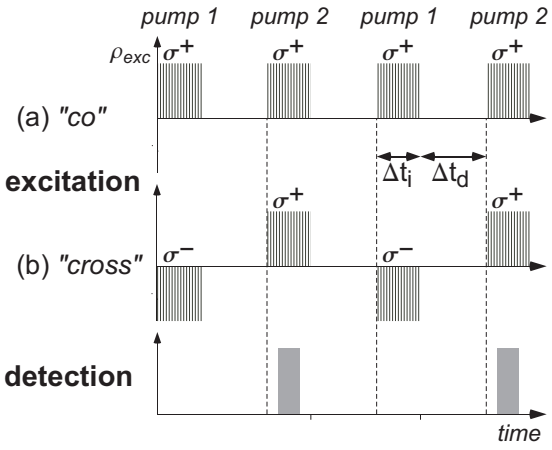

Figure 8.1: The excitation-detection scheme for spin lifetime measurements: The excitation is performed with pulse trains "*pump 1*" and "*pump 2*" of duration Δt_i with a dark time of duration Δt_d between them. (a) In the "co" polarised scheme all pulse trains have the same helicity. (b) In the "cross" polarised scheme the helicity of *pump 1* is inverted with respect to the one of *pump 2*. The read out (grey) of the NCP is always performed during excitation cycle *pump 2* so that all changes observed are induced by *pump 1*. 100 μs $< \Delta t_{d(i)} <$ 500 ms.

dark time[2] Δt_d and a second illumination period "*pump 2*" with $\Delta t_{i,p1} = \Delta t_{i,p2}$. The duration of Δt_d as well as Δt_i can be varied between 100 μs and 500 ms. The helicity of *pump 2* was kept constantly σ^+ and the negative circular polarisation of the photoluminescence was monitored during *pump 2* throughout. The helicity of *pump 1* on the other hand was either also kept σ^+ or changed to σ^- so that a co-polarised ($\sigma^+\sigma^+$) and a cross-polarised ($\sigma^+\sigma^-$) excitation could be realised. The excitation power was kept in the saturation regime of the negative circular polarisation where the maximum circular polarisation degree was obtained at continuous excitation.

We have seen in chapter 7.2 that the build up of electron polarisation occurs on a sub microsecond timescale and can therefore not be resolved in the experiment presented here. Nuclear polarisation, however, takes tens to hundreds of milliseconds to accumulate[3] [99]. During the illumination cycles *pump 1* and *pump 2* nuclear polarisation is generated. At fixed excitation density the degree of nuclear polarisation achievable only depends on the times Δt_i and Δt_d. If more nuclear polarisation is generated during the illumination time Δt_i than decays in the dark time Δt_d, nuclear polarisation becomes accumulated. In the co-polarised scheme the excitation of *pump 1* and *pump 2* therefore reinforce each other. In the cross-polarised scheme though, *pump 2* will start to reverse the nuclear polarisation generated during *pump 1*.

In the dark time Δt_d the nuclear polarisation established during the illumination decays. If the nuclear polarisation is completely decayed during the dark time, *pump 1* and *pump 2* are independent of one another. Each excitation cycle

[2]Experimentally the dark time is realised with the help of an acousto-optical modulator. For a detailed description of the experimental setup refer to chapter 4.

[3]c. f. chapter 7.3

begins to polarise the electron-nuclear spin system starting from an unpolarised initial state. In this case, the circular polarisation ρ_c measured during *pump 2* for the co-polarised and the cross-polarised scheme are obviously identical.

If, however, the measured circular polarisation for cross-polarised excitation is smaller than for co-polarised excitation, this can only be due to a memory of the nuclear polarisation generated during *pump 1* which is retained by the system over the dark time. We therefore associate "memory" with the difference between the circular polarisation obtained for the co-polarised scheme and the circular polarisation measured with the cross-polarised scheme. By increasing Δt_d and monitoring the difference in circular polarisation between co and cross-polarised excitation we are therefore able to determine the time a spin memory is kept by the system.

In a first step we keep $\Delta t_i = \Delta t_d$ and gradually increase these times. In this experiment both the degree of nuclear polarisation achievable during Δt_i and the time it is given to decay increase simultaneously.

In a second step, we keep the illumination time constant and only increase Δt_d until the memory vanishes, i. e. until co-polarised and cross-polarised excitation yield the same circular polarisation. This method is, however, more time-consuming than the first, due to the lower duty cycle. First, this experiment is performed for different Δt_i in order to find the illumination time needed to generate a state of maximal stability. For this particular Δt_i it is then possible to measure the maximum electron-nuclear spin memory time.

In order to obtain a reasonable signal to noise ratio the read out gate in *pump 2* for the detection of the circular polarisation had a width of $\Delta t_i/2$. We thus have to keep in mind that we observe a time integrated circular polarisation. Some spin memory might be erased during the read out.

8.3 Long Spin Lifetimes

To study the memory retained by the electron-nuclear spin system over a dark time during which the excitation is switched off, we start with an excitation scheme where the duration of the illumination is equal to the duration of the dark time, $\Delta t_i = \Delta t_d = \Delta t$ (see figure 8.1). Figure 8.2 (a) shows the circular polarisation of the photoluminescence vs. Δt for co-polarised (full circles) and cross-polarised (open circles) excitation.

Let us first focus on the data obtained with the *co-polarised* protocol (full circles in figure 8.2 (a)). The negative circular polarisation saturates for $\Delta t > 500$ μs at $\rho_c \approx 28$ %, the value for continuous excitation without a darktime. The illumination time is then long enough to allow nuclear polarisation to be generated during the pulse trains so that $B_N > B_f$ and the random nuclear fluctuations are overcome. As illumination time Δt_i and dark time Δt_d are increased in parall, the fraction $\Delta t_i/\Delta t_d$ stays constant. For short Δt not much nuclear polarisation

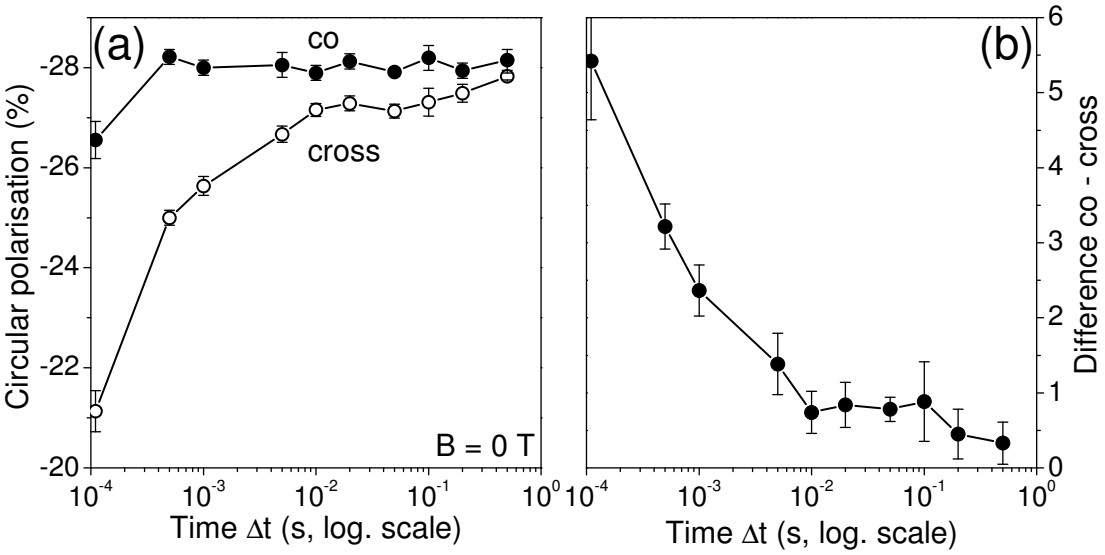

Figure 8.2: (a) Circular polarisation of the PL for co-polarised excitation (full circles) and cross-polarised excitation (open circles) in dependence of $\Delta t_i = \Delta t_d = \Delta t$ at $B = 0$, logarithmic scale. A difference between co and cross suggests that a memory has been retained by the electron-nuclear spin system during the dark time. A difference is still resolvable at $\Delta t = \Delta t_d = 0.2$ s. Power in the saturation regime of the NCP, $T = 1.9$ K.

can be accumulated during a single pulse train. However, as the dark time is also short, there is not much decay between the excitation cycles either. Therefore, nuclear polarisation can accumulate over the pulse trains. For long Δt a large degree of nuclear polarisation can be already generated during each pulse train which then in turn also is given more time to decay during the dark time. In order to obtain a low noise level and to keep the time it takes to perform the measurement reasonably short, we have to chose a long enough time duration for the read out of the photoluminescence during *pump 2*. The decay of nuclear spin polarisation which might have been occured during the darktime is then compensated again in the course of the read out period. Therefore, using the co-polarised protocol, a polarisation memory of the electron-nuclear spin system can only be observed indirectly: from studying the accumulation dynamics of the nuclear polarisation one would expect that an illumination of $\Delta t < 20$ ms is not enough to polarise the nuclear spins to a degree which is enough to fully switch off the influence of the nuclear frozen fluctuation field[4]. The fact that ρ_c already saturates for $\Delta t > 500$ μs therefore means that nuclear polarisation is accumulated which is only possible if some of the polarisation is still present after the darktime.

[4]In chapter 7.2 it was shown that the nuclear spin system needs $\Delta t > 50$ ms until it is polarised to a degree where the frozen fluctuation field is fully overcome.

The situation is, however, completely different for the *cross-polarised* protocol (open circles in figure 8.2 (a)). Now, the excitation helicity of *pump 1* is inverted with respect to the one of *pump 2*. *pump 1* now acts detrimentally on *pump 2*. Nuclear polarisation is only allowed to accumulate in one direction during a single excitation cycle. This is evidenced by the increase of the negative circular polarisation from initially -21 % at $\Delta t = 110$ μs to finally -28 % at $\Delta t = 500$ ms.

Let us inspect the difference in circular polarisation between the co-polarised and the cross-polarised excitation more closely. Figure 8.2 (b) shows this difference $\rho_c^{\mathrm{co}} - \rho_c^{\mathrm{cross}}$ as a function of the dark time. A difference between the circular polarisation for co and cross-polarised excitation larger than the error is observed for all values of Δt up to 0.2 s. This is three orders of magnitude longer than the time characteristic for the dipole-dipole interaction, $T_2 \approx 10^{-4}$ s, which determines the time for the nuclear spin relaxation. The excitation helicity of *pump 2* during which the negative circular polarisation is always measured, does not change in either excitation protocol. Any difference in circular polarisation between the co and the cross-polarised scheme thus has to be caused by the spin memory of the polarisation induced during *pump 1*. This difference is a clear evidence of spin memory in the system, not only of polarisation but also of sign. Times greatly exceeding T_2 are characteristic for the spin-lattice relaxation leading to the equilisation of a nuclear spin temperature Θ. However, in the case of nuclear polarisation by optically oriented electrons at zero external field $1/\Theta \propto \mathbf{B}_e \cdot \langle \mathbf{S} \rangle \propto b_e \langle S \rangle^2$. The square of the electron spin does not hold any information about the excitation photon helicity. The spin cooling would hence be the same for both excitation schemes. It is thus not merely a memory of spin temperature but also of the polarisation *direction*, we really observe spin memory of 0.2 s.

In order to obtain a more direct measure of the spin memory, we use a slightly modified excitation protocol. The illumination time Δt_i is kept constant and only the dark time Δt_d is increased. We first investigate the influence of the *illumination time* on the spin memory. For that purpose we study the circular polarisation plotted over the darktime for different Δt_i. Then, we chose a Δt_i where we can expect maximal memory. For this specific illumination time we analyse the darktime data obtained with respect to the lifetime of the electron-nuclear spin system.

Figure 8.3 shows data sets for illumination times $\Delta t_i = 10, 30, 70$ and 100 ms, again each one measured using both the co-polarised protocol (full circles) and the cross-polarised protocol (open circles). The memory times are again revealed by the data taken for the cross-polarised scheme (figure 8.3, open circles). We analyse the measurements again in terms of the difference between the negative circular polarisation measured with the co-polarised and the one obtained with the cross-polarised protocol. Again, any difference between the co- and cross-polarised protocols indicates a spin memory that has persisted during the dark time. This difference is shown in figure 8.3 by the open diamonds. We observe

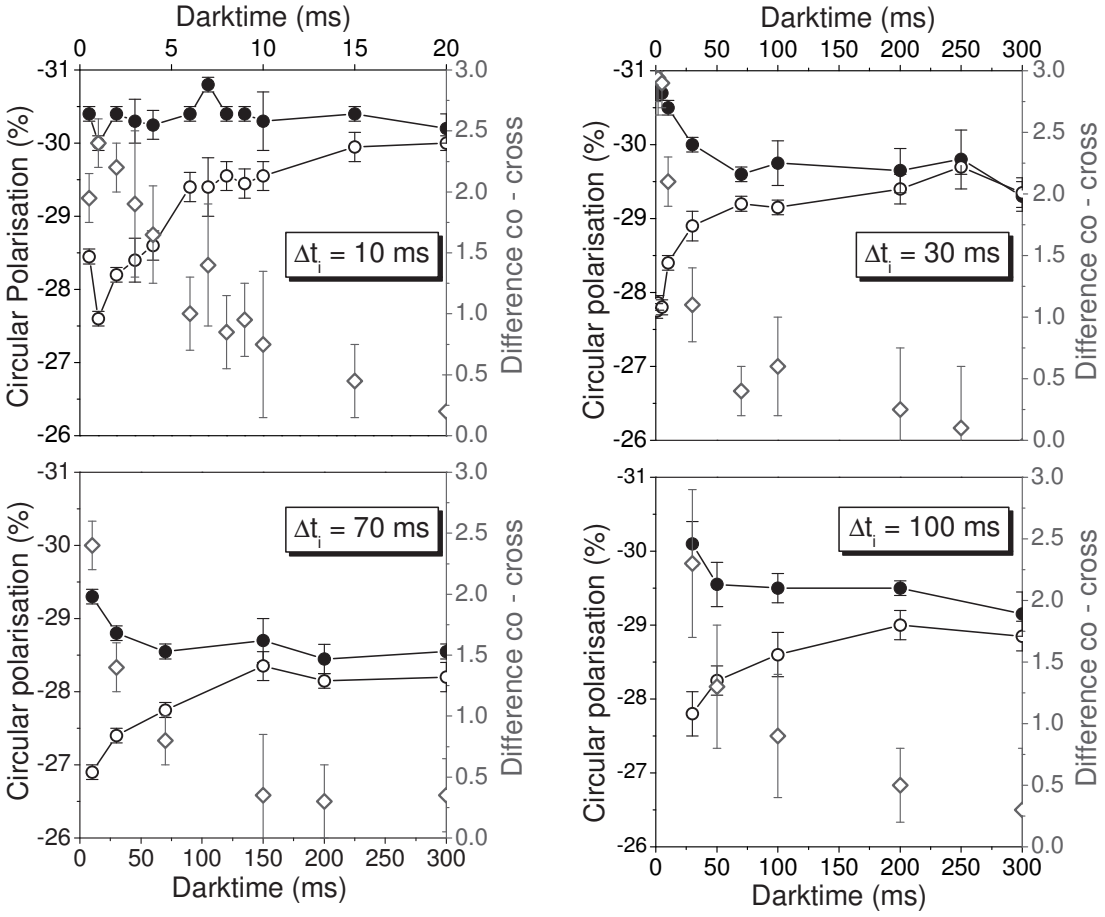

Figure 8.3: Circular polarisation of the PL for co-polarised excitation (full circles) and cross-polarised excitation (open circles) in dependence of the dark time Δt_d, for different illumination times Δt_i: 10 ms, 30 ms, 70 ms, 100 ms. Open diamonds, grey scales: The circular polarisation difference between co and cross. For shorter illumination time the difference approaches 0 earlier, the memory in the electron-nuclear spin system decays faster. $B = 0$, power in the saturation regime of the NCP, $T = 1.9$ K.

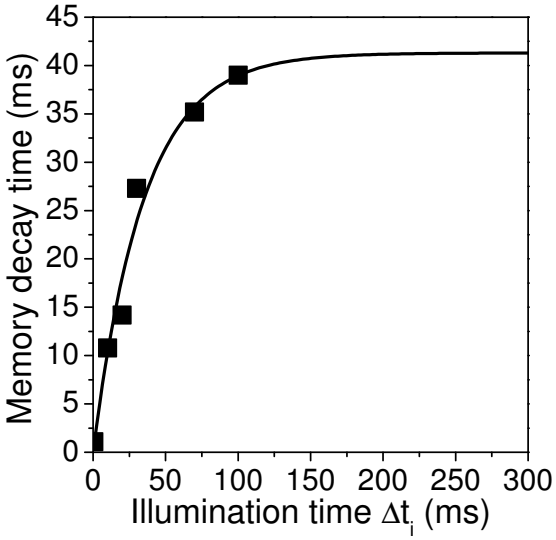

Figure 8.4: Black squares: Time constants of exponential fits to the circular polarisation difference between co-polarised and cross-polarised excitation, $\rho_c^{\mathrm{co}}(\Delta_d) - \rho_c^{\mathrm{cross}}(\Delta_d)$, (red diamonds in figure 8.3) vs. the respective illumination time. Solid line: Exponential asymptotic fit to the data. At $\Delta t_i = 100$ ms the memory decay time is almost saturated.

that the spin memory time increases with increasing illumination duration as for longer excitation more nuclear polarisation can be generated in each excitation cycle.

Before we can ascertain how long spin memory can persist in the nuclear spin system, we have to find out which illumination time we have to use to obtain the maximum spin memory time. The exact dynamics of the electron-nuclear spin system is clearly complicated, e. g. due to the presence of three different types of nuclei in the samples. However, we can phenomenologically fit an exponential decay as a function of darktime to the circular polarisation *difference* between co and cross-polarised excitation (diamonds) for each Δt_i from figure 8.3. The decrease of the difference with growing darktime corresponds to the decay of the spin memory. The time constants obtained by these fits assign the data sets for each Δt_i a phenomenological spin memory decay time. Figure 8.4 shows these time constants plotted vs. the illumination time Δt_i.

As a guide to the eye the function $f(\Delta t_i) = a(1 - \exp(-\Delta t_i/c))$ was fitted to the data. We diagnose that for $\Delta t_i = 100$ ms the memory decay time is almost saturated. This illumination time is long enough so that a stable state of the electron-nuclear spin system can be formed exhibiting the maximum spin memory. This agrees with our previous findings that the nuclear spins require at least some tens of milliseconds to become maximally polarised.

We thus chose $\Delta t_i = 100$ ms for studying the maximum lifetime of the electron-nuclear spin system. Figure 8.5 shows the polarisation of the photoluminescence plotted versus the darktime for illumination time $\Delta t_i = 100$ ms.

A difference of polarisation between co and cross-polarised excitation larger than the error bars is still observable for a dark time of 0.5 s. As discussed before, the difference in polarisation between co- and cross-polarised excitation is a signature for spin memory of the system that is longer than the dark time. The

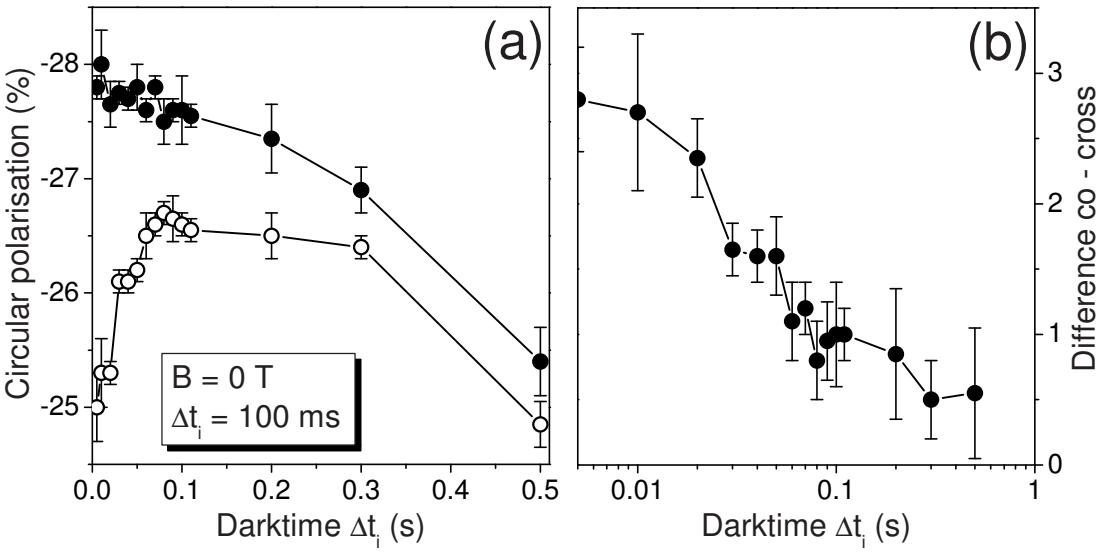

Figure 8.5: (a) Circular polarisation of the PL for co-polarised excitation (full) and cross-polarised excitation (open) as a function of the dark time Δt_d, $\Delta t_i = 100$ ms. A memory in the electron-nuclear spin system is still resolvable after a dark time $\Delta t_d = 0.5$ s. (b) The circular polarisation difference between co and cross polarised excitation. Even at $\Delta t_d = 0.5$ s there is still memory observable. $B = 0$, $T = 1.9$ K.

spin memory of the electron-nuclear spin system thus lasts at least 0.5 s. It is remarkable that at zero external magnetic field the electron-nuclear spin system retains not only a memory about its exposure to circularly polarised light over a sub-second time scale but also to the sign of the light polarisation. This means that the transverse relaxation time T_2 of the nuclear spin system polarisation vector in our quantum dots should be in the sub-second range. Furthermore, the time determined here is only a lower limit to the memory time of the system because during the duration of the polarisation read out in the course of *pump 2* some memory might be erased. The memory times observed here are three orders of magnitude longer than the depolarisation time of the nuclear dipole-dipole interaction. A dramatically increased spin relaxation time was predicted to be the main signature of the nuclear spin polaron formation in a nuclear spin system. We thus have strong evidence that a nuclear polaron builds up in our case.

In the next section we are going to discuss further evidence for the formation of a nuclear spin polaron in the quantum dots under study and address the question of the lifetime of the resident *electron* spin.

8.4 Discussion: Formation of a Nuclear Spin Polaron

The giant deceleration of the electron-nuclear spin relaxation is the predominant signature for the formation of a nuclear spin polaron. The directional relaxation time of the polaron was estimated in references [24, 25]. The macroscopically large spin of such a polaron state, $\mathbf{J}_\Sigma$, changes under the influence of dipole interactions among the nuclei. If a nuclear spin polaron is present, its relaxation time T_2^{NSP} considerably exceeds the dipole-dipole relaxation time $T_2 \approx 10^{-4}$ s of the nuclear spins. T_2^{NSP} scales like $N_B T_2$, where N_B is the number of nuclei establishing the polaron [24, 25, 118]. With N_B being of the order of 10^5, T_2^{NSP} is of the order of seconds which agrees well with the memory times observed in our experiments.

Further support for the nuclear spin polaron model may be provided by studying the temperature dependence of the spin memory. Figure 8.6 (a) once more shows darktime dependencies of the negative circular polarisation, again measured using the excitation scheme with $\Delta t_i = \Delta t_d = \Delta t$. The figure contains data measured at 6.6 K with co- and cross-polarised excitation (red). For comparison additionally the data from figure 8.2 taken at zero magnetic field and 1.9 K (black) are plotted.

We first analyse the data measured at 6.6 K with the co-polarised excitation scheme. We observe that the negative circular polarisation clearly decreases with increasing Δt. In the excitation protocol used the illumination time increases parallel to the darktime. Thus more and more nuclear spin polarisation may be generated during each excitation cycle with increasing Δt. Nevertheless, nuclear spin polarisation does obviously not accumulate as evidenced by the decrease of circular polarisation with increasing Δt for $\Delta t_d > 500$ μs. This behaviour is a sign that for darktimes exceeding these 500 μs more nuclear polarisation decays during the dark time than is generated during illumination.

The circular polarisation measured using *cross-polarised* excitation increases with increasing Δt. If we investigate the difference in circular polarisation between the co and cross-polarised data it becomes obvious, that the memory time is quenched in comparison to the measurement at $T = 1.9$ K. The spin memory already becomes smaller than the errors at $\Delta t = 5$ ms. Figure 8.6 (b) shows the polarisation difference between co and cross-polarised excitation plotted vs. Δt on a logarithmic timescale. The dashed lines represent exponential fits to the data[5]. The fits reveal that the time constant of the exponential decay belonging to the data taken at 6.6 K is a factor 100 shorter than the time constant of the long lived component appearing with the data taken at 1.9 K.

[5] We emphasise again that the exponential fits only phenomenologically describe the behaviour of the system. The time constants therefore may only serve to characterise the dynamics in terms of the order of magnitude of the memory decay.

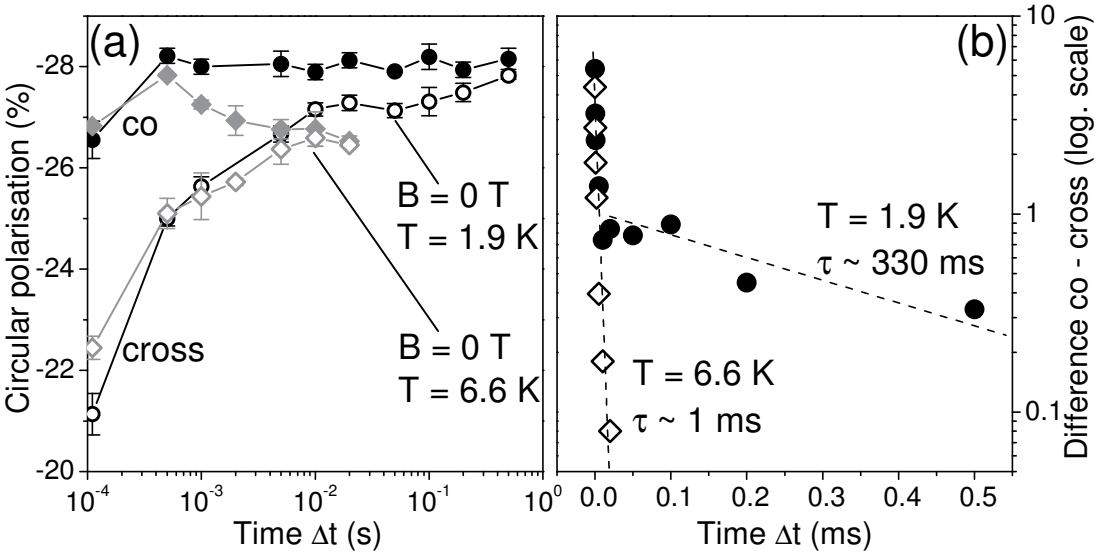

Figure 8.6: (a) Δt dependence of the negative circular polarisation at $B = 0$ T, where $\Delta t_i = \Delta t_d = \Delta t$. Full symbols: co-polarised protocol; open symbols: cross-polarised protocol. Temperature $T = 1.9$ K (circles) and $T = 6.6$ K (diamonds).

The generation of nuclear polarisation should not be affected by the increase in temperature from 1.9 K to 6.6 K [98, 120–122]. Also, the nuclear spin relaxation by the dipole-dipole interaction and the relaxation by the resident electrons are not expected to exhibit such a pronounced temperature dependence. We interpret the quench in memory time appearing with the measurements at 6.6 K in terms of the nuclear spin polaron. To induce a spin splitting of the resident electron which is greater than the thermal energy at 6.6 K a magnetic field of almost 20 T would be needed. Thus, the resident electron spin cannot freeze out. The condition for the polaron formation of a nuclear spin temperature of the order of 10^{-7} K cannot be met at a lattice temperature of 6.6 K.

Possible long memory times in the nuclear spin system have also been explained by the quadrupole splittings of nuclear spin levels [16, 123, 124] instead of the formation of a nuclear spin polaron. It was argued that the quadrupole interaction suppresses nuclear spin flips which keeps the direction of the nuclear spin vector fixed. This in turn would lead to depression of the electron spin depolarisation. The fact that the memory time of the electron-nuclear spin system strongly depends on the temperature, however, cannot be explained by the quadrupolar interactions.

On the other hand, in the model of the nuclear spin polaron presented in section 8.1 the possibility that the polaron state is formed sensitively depends on the electron spin temperature which exceeds the lattice temperature defined by the experimental conditions. Our estimations showed that the temperature of $T = 1.9$ K in our experiments would just be low enough to allow the nuclear

spin polaron to arise. An increase of the temperature to $T = 6.6$ K would thus inevitably destroy the nuclear spin polaron. The quenching of memory time of the electron-nuclear spin system consequently is another strong evidence for the formation of a nuclear spin polaron in the studied quantum dots.

The nuclear spin polaron is a self consistent electron-nuclear spin complex where its constituents, the resident electron spin and the ensemble of the nuclear spins contributing to the polaron state, mutually prevent relaxation. While long lasting nuclear spin polarisation is a remarkable but not completely unexpected feature, an electron spin memory of hundreds of milliseconds is a real novelty indeed at $B = 0$ T. Let us therefore now discuss evidence for the resident electron spin also retaining a memory whose duration is comparable to the one of the nuclei.

A nuclear magnetic field of ≈ 6 T leads to a splitting of the electron spin levels of 2 K. Our calculations showed[6] that the nuclear magnetic field in the studied quantum dots could be as large. For the temperatures $T < 2$ K present in our experiments and high nuclear polarisation, the resident electron spin would thus freeze. Therefore, the spin oriented nuclei induce a considerable quasi-equilibrium polarisation of the resident electrons. The polarised resident electron spin in turn supports the spin polarisation of the nuclei.

If the resident electron spin relaxed, the nuclear spins would precess on a microsecond timescale about the Knight field of the electron. This should cause the depolarisation of the nuclear spins within microseconds. It has in fact been estimated that nuclear depolarisation caused by the indirect coupling of nuclear spins via the resident electron occurs on a timescale of $T_{Ne}^{-1} \sim A^2 N^{3/2} \Omega_e$, where A is the total hyperfine coupling constant in a unit cell, N the number of nuclei in the quantum dot and Ω_e the electron spin splitting [125]. This yielded a timescale of a few microseconds for the nuclear spins to become depolarised [99].

Furthermore, it was measured, that in a quantum dot charged with an electron, nuclear spin polarisation generally decays with a time constant of ≈ 2 ms due to depolarisation by the resident electron [99]. That the spin memory in the negatively charged quantum dots under study persists over hundreds of millisecond is another evidence that the nuclear spin polaron state is formed. If the resident electron in the studied quantum dots was not part of a polaron state we would expect a depolarisation of the nuclear spin system with the help of the resident electron on at most a millisecond time scale. We thus attribute the observation that a polarisation memory is sustained for hundreds of milliseconds to the fact that a coupled electron-nuclear complex is formed. Not only the nuclear polarisation but also a significant fraction of the electron spin projection S_z retains a memory of the excitation with circularly polarised light over a sub-second timescale.

The results presented in this chapter were published in references [25, 126].

[6] c. f. section 5.4

9 Summary

For a long time, the nuclear spins in quantum dots were virtually ignored. It was thought that the interaction strength was so small that the interaction between the nuclei and electrons could only be observed under very specific optical pumping conditions. Then, in the pursuit of long living electron spins as a building block for quantum information storage and processing, their destructive action on the lifetime of the electron spin became apparent. The nuclear spin system increasingly gained the attention of the quantum dot community. It seemed that the randomly oriented, fluctuating nuclear spins can only be counteracted by strong magnetic fields suppressing the depolarising effect of the random nuclear spin fluctuation fields on a single electron spin. Gradually, however, the work done thirty years before on the electron-nuclear spin system in bulk semiconductors attracted the notice of scientists again. Some of the old experiments could be performed with quantum dots as well. It could be shown that the nuclear spins in quantum dots may well be polarised by optical orientation and that their action is not always destructive at all. The nuclear spins in quantum dots are increasingly used in order to create and tailor a specific environment for a single electron in a quantum dot. In this way quantum dots contain their own "nuclear nanomagnet". This might be the future of the studies on the electron-nuclear spin system.

The aim of this work is to shed some more light on the complex interdependent system formed of an electron spin and the nuclear spin ensemble in quantum dots. The effects are manifold, often unexpected, sometimes miraculous. Nevertheless, I believe that this work is another tiny step towards the understanding of this challenging system.

I have shown that the randomly polarised nuclear spin system always affects the electron spin of a single electron in quantum dots. Further we have seen, however, that the nuclear spin system can easily be polarised by optically oriented electrons also in the studied sample, so that it is even a task to keep the nuclear spins randomly oriented. An important finding was to confirm that the nuclear spins can be significantly polarised also at zero external field. I showed that the polarised nuclear spin system can have a supporting effect on the electron spin polarisation or – when the direction of the nuclear field gains a large transverse component – may depolarise the resident electron spin further than the unpolarized nuclear fluctuation field. I demonstrated that the direction of the Overhauser field may indeed be directed by very small external fields. By determining the internal fields acting on the nuclear spins, the Knight field and

the nuclear dipole-dipole field, it could be estimated that the nuclear spin system can in principle be polarised to a degree close to unity. The accumulation dynamics of the electron spins polarised via the effect of negative circular polarisation was found to occur on a timescale of hundred nanoseconds. The nuclear spin system becomes polarised by optical orientation within tens of milliseconds. Finally, I observed spin memory times in the system persisting over up to 0.5 s after the excitation had been switched off. This extremely long spin lifetimes were explained in terms of a coupled electron-nuclear spin state, the nuclear spin polaron.

A The Eponyms

In the present thesis I have used various eponyms[1]. One of them is the *Knight field* which plays a particularly important role in this work. However, who is Knight? I was asking myself – and others – that question for some time, but nobody knew who he or she was. Finally, I found out that it is the American Walter David Knight who lingers on in the world of science as an eponym and who has kept me on the go for the last three years with his tiny magnetic field. In this final chapter I therefore briefly wish to give the names a face and introduce the people appearing in this work as eponyms.

Léon Brillouin

Eponym used: *Brillouin function* – ✻ Aug 7, 1889, Sèvre, France ; ✝ Oct 4, 1969, New York, USA. 1912 with Sommerfeld in Munich, military service in WW I 1914 - 1919, 1920 PhD, developed the *WentzelKramersBrillouin* approximation (WKB), introduced the *Brillouin zone*, 1940 USA, solid state theory, quantum statistics, information theory, also worked for IBM.

Charles-Augustin de Coulomb

Eponym used: *Coulomb interaction* – ✻ Jun 14, 1736, Angoulême, France; ✝ Aug 23, 1806, Paris, France. Attended a military engineering school, had to spend nine years in Martinique reconstructing a fort, after his return development of the torsion balance, proved with it the inverse-quadratic relation between force and distance (*Coulomb law*).

---

[1]Greek: epi - upon, onyma - name; "named after"

Paul Glan

Eponym used: *Glan-Thompson* prism – ✻ Feb 26, 1846 Berlin, Germany; † Aug 8, 1898, Berlin, Germany. 1870 PhD thesis "Über die absoluten Phasenveränderungen durch Reflexion" at Friedrich-Wilhelms-University (today: Humboldt Univerity) Berlin, later private lecturer ibidem, 1880 principle of birefringence and total reflection, translated Hamiltons "Elements of Quaternions" into German, various polarising prisms are named after him: G.-Thompson prism, G.-Taylor prism, G.-Foucault prism, G.-laser prism.

Michael Faraday

Eponym used: *Faraday geometry* – ✻ Sep 22, 1791, Newington Butts, England; † Aug 25, 1867, Hampton Court, London, England. Started an bookbinding apprenticeship at the age of 13, later lab assistant with chemist Sir Humphry Davy, never attended university, first scientific publication 1816, elected member of the Royal Society, director of the laboratory of the Royal Institution, discovered benzol, butylene, laws about the chemical effect of current, first construction of a simple electric motor, first transformer, discovered electro-magnetic induction, formed the concept of force fields (lines of force, made visible with iron filings), found that charge is always on the surface (*Faraday cage*), existence of diamagnetism, rotation of polarisation axis in glass (*Faraday effect*), 1862 last experiment: influence of magnetic field on light, not successful but later led to the discovery of the Zeeman effect. Introduced the Friday Night Lectures of the Royal Institution which still exist today.

"Nothing is too wonderful to be true if it be consistent with the laws of nature, and in such things as these, experiment is the best test of such consistency."

William Rowan Hamilton

Eponym used: *Hamilton operator* – ✻ August 4, 1805 Dublin, Ireland; ✝ Sep 2, 1865 near Dunsink, Ireland. Started learning Latin and Greek at the age of five, spoke Hebrew at the age of seven, 15 languages when 13, among them Sanskrit, Malay, Persian, Arabic and Hindustani, entered Trinity College, Dublin, at the age of 18, four years later professor of astronomy – before his final exam, works on optics developing the function later known as *eikonal*, 1834/35 "On a General Method in Dynamics" introducing the principle of varying action, removed the i in complex numbers writing them as pairs of real numbers, tried to generalise this to three dimensions – which was later proven to be impossible – the generalisation to four dimensions lead to the discovery of the quaternions. First foreign member of the National Academy of Science of the USA. He was an alcoholic in the last third of his life.
"And how the One of Time, of Space the Three, Might in the Chain of Symbols girdled be."

Wilhelm Hanle

Eponym used: *Hanle effect, Hanle curve* – ✻ Jan 13, 1901 Mannheim, Germany; ✝ Apr 29, 1993 Gießen, Germany. Studied in Heidelberg, PhD "Über magnetische Beeinflussung der Polarisation der Resonanz-Fluoreszenz von Quecksilber" with James Franck in Göttingen, thoughts about the development of a reactor ("Uranmaschine"), after WW II he worked on coherence effects of light emission, luminescence, spectroscopy of radioactive gases, developed scintillation counters and dosimeters, governmental expert on "questions of the atomic energy and the protection from ionising radiation in the case of a nuclear war".

Hermann Ludwig Ferdinand v. Helmholtz

Eponym used: *Helmholtz coil* – ✻ Aug 31, 1821 Potsdam, Germany; † Sep 8, 1894 Charlottenburg, Germany. Physiologist and physicist, "universal scientist", studied medicine at the Military Academy in Berlin, PhD in medicine, then military physician, taught anatomy in Berlin, professor for physiology in Königsberg, then Bonn, Heidelberg, finally chair for physics in Berlin, proved the origin of nerves from ganglions, measured the propagation speed of neural excitations, for the first time made the retina of the eye visible using his invention, the ophthalmoskop (eye mirror), mathematical theory for the tone colour of overtones, resonance theory of hearing, mathematical foundation of energy conservation, worked on the foundations of hydrodynamics, foundation of scientific meteorology, electrodynamics, epistemological discussions. Together with W. v. Siemens founder of the "Physikalisch-Technischen Reichsanstalt".
"Jedoch das Gebiet, welches der unbedingten Herrschaft der vollendeten Wissenschaft unterworfen werden kann, ist leider sehr eng, und schon die organische Welt entzieht sich ihm größtenteils."

L. von Krastanow

Eponym used: *Stranski-Krastanow growth.*
He remained a phantom.

William Thomson, 1st Baron Kelvin

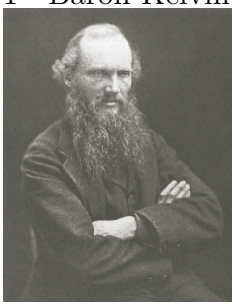

Eponym used: *Kelvin* (unit) – ✻ Jun 26, 1824 Belfast, Northern Ireland; † Dec 17, 1904 Netherhall, Scotland. Read Lagrange and Fourier at the age of 15, chair of natural philosophy at the University of Glasgow at the age of 22, first mathematical formulation of the law of induction, works on the conversion of heat and mechanical work, introduced the absolute temperature scale, the absolute zero temperature, calculation of the data rate through a cable, telegraph equation, took part in submarine cable laying expeditions; calculation of tides, tide predicting machine, adjustable compass, works on electricity: quadrant electrometer, current balance, mirror galvanometer; calculated the age of the earth, hydrodynamics, saw the limits of classical physics. Knighted 1866, 1892 Baron Kelvin, of Largs in the County of Ayr, the title goes back to the river of Kelvin. 661 publications and 70 patents. 1871 he bought a 129 tons yacht.

Walther David Knight

Eponym used: *Knight field* – ✻ October 14, 1919, raised in New York City, USA; † June 28, 2000 Marlborough, USA. During WW II service as a Navy electronics officer, during the work on his PhD he discovered a frequency shift of the NMR in metals due to the paramagnetism of conduction electrons, the *Knight shift* (1949), 1950 Berkeley, pioneering investigations in on conducting solids, first observation of a nuclear quadrupole resonance in a metal, 1967 – 1972 principal dean of the College of Letters and Science, work on the physics of small metal clusters, low-temperature NMR studies of nano-particles, works on cluster beams, measured "magic number" mass distribution of sodium clusters leading to the discovery of size quantisation in small clusters, cluster polarisabilities and ionization potentials, landmark discovery of giant electronic resonances in small clusters.

Sir Joseph Larmor

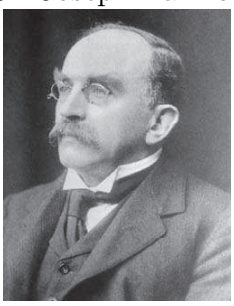

Eponym used: *Larmor precession frequency* – ✻ 11 Jul, 1857 Magheragall, Northern Ireland; ✝ 19 May, 1942, Holywood, Northern Ireland. Professor in Cambridge, he worked on special relativity which was not yet called like this, developed Lorentz transformations before Lorentz (1897), already predicted time dilation and length contraction, studying the electron he introduced the oscillation now called the *Larmor precession*.

Albert W. Overhauser

Eponym used: *Overhauser field* – ✻ Aug 17, 1925, San Diego, USA. PhD at University of California , Berkeley (1951), 1951 – 1958 University of Illinois where he discovered the dynamic polarisation of nuclear spins by electrons, the *Overhauser effect*, Cornell University, 1958 – 1973 Manager, Assistant Director and Director, Physical Science Laboratory, Ford Motor Co., since 1973 Professor of Physics, Purdue University; worked on various subjects among them theory of superconductivity, broken symmetry in metals, lattice dynamics, supercooling of atoms in optical molasses, collective effects in optical absorption, neutron diffraction. Superconductivity, muon depolarization, nuclear and paramagnetic resonance, magneto-transport theory, many-electron theory, imperfections in solids, neutron interferometry, microcalorimetry, modulation spectroscopy, exciton theory, ultrasonic generation, magnetism in metals and alloys.

Wolfgang Ernst Pauli

Eponym used: *Pauli blocking* – ✻ Apr 25 1900, Vienna, Austria; † Dec 15, 1958, Zurich, Switzerland. 1919 started to study physics at Ludwig-Maximilians-Universität Munich at Arnold Sommerfeld, 1921 PhD at the age of 21 about the hydrogen molecule ion, 1921/22 assistant of Max Born in Göttingen, 1922/23 Kopenhagen with Niels Bohr, professor in Hamburg, ETH Zurich, Princeton; explanation of the hyperfine structure by the nuclear spin, introduced a new degree of freedom in quantum mechanics, later identified as "spin", postulated the neutrino, pioneering work in quantum field theory. Nobel prize 1945. He was said to be technically extremely unskilled. His godfather was Ernst Mach.
"Ich kann es mir leisten, nicht zitiert zu werden."

Iwan Nicola Stranski

Eponym used: *Stranski-Krastanow growth* – ✻ Jan 2, 1897, Sophia, Bulgaria; † 1979, Sophia, Bulgaria. Studied chemistry in Vienna and Sophia, 1925 PhD in Berlin, professor for physical chemistry in Sophia, returned to Berlin in 1944, there director of the Institute for Physical Chemistry, 1951-53 President of the Technical University of Berlin. Worked on crystallographic chemistry and physics and on crystal growth.

Nikola Tesla

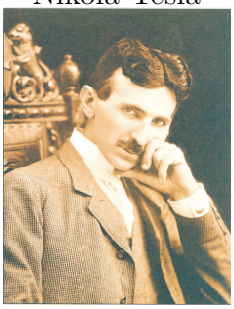

Eponym used: *tesla* (unit) – ✻ Jul 10, 1856, Smiljan, today Croatia; † Jan 7, 1943, New York, USA – He studied in Graz, Prague and Budapest, worked for Thomas Edison in Paris, since 1884 in New York, as well as for Edison's competitor Westinghouse, his works are the foundation of the modern AC power systems, AC generator, AC motor, first radio transmitter, first remote control, high frequency lamp and hundreds patents more. His unusual personality and his science-fiction like "theoretical inventions" as beam weapons, anti-gravitation, teleportation, ion-propelled flying machines in his late years inspired various conspiracy theories after his belongings where confiscated by the US government after his death.

Silvanus Phillips Thompson

Eponym used: *Glan-Thompson prism* – ✻ June 19, 1851, York, England; † June 12, 1916. Professor in Bristol, principal and professor at Finsbury Technical College of the City and Guilds of London Institute for the Advancement of Technical Education, one of his favourite topics was the technical and scientific education which he also studied on journeys through Europe.

Woldemar Voigt

Eponym used: *Voigt geometry* – ✻ Sep 2, 1850, Leipzig, Germany; † Dec 13, 1919 Göttingen. Professor in Königsberg, rector of the University Göttingen, works on magneto- and electro optic, introduced the term "tensor", theory of optics of moving bodies, transformation equations under which the wave equation is invariant, an early form of the Lorentz transformation (1887 *Voigt transformations*, correct up to a constant), theory of light for moving media, "Lehrbuch der Kristallphysik", discovered the *Voigt effect* where the polarisation of light is rotated when traveling through a medium in a magnetic field perpendicular to the light wave. Took part in the German-French war 1870/71, loved music and conducted Bach pieces.

Alessandro Volta

Eponym used: electron *Volt* (unit) – ✻ Feb 18, 1745 Como, Italy; † Mar 5, 1827 Camnago, Italy. Director of a school in Como, professor in Pavia, constructs an "electrophor" to separate charges, discovered methane, electroscope, introduced unit for "tension" ("voltage"), charge-voltage relation in capacitors, invention of the battery (*Voltaic pile*).

Pieter Zeeman

Eponym used: *Zeeman splitting* – ✻ May 25, 1865 Amsterdam, Netherlands; † October 9, 1943, Amsterdam, Netherlands. Student of Hendrik A. Lorentz, 1896 repeated an experiment of Faraday which has not been successful at that time because of the resolution of the instruments: the effect of a magnetic field on the light of a sodium lamp, observed a splitting of the lines, the Zeeman effect; determination of e/m, the sign of the charge before the electron was actually discovered. 1902 Nobel Prize in Physics together with Lorentz.

Bibliography

[1] A. Ekimov, A. A. Onushchenko, *Quantum Size Effect in 3-Dimensional Microscopic Semiconductor Crystals*, JETP Lett. **34**, 345–349 (1981).

[2] A. Ekimov, A. A. Onushchenko, *Quantum Size Effect in the Optical Spectra of Semiconductor Micro Crystals*, Soviet Physics Semiconductors **16**, 775–778 (1982).

[3] A. Ekimov, A. A. Onushchenko, *Size Quantization of the Electron Energy Spectrum in a Microscopic Semiconductor Crystal*, JETP Lett. **40**, 1136–1139 (1984).

[4] A. Ekimov, A. Efros, A. A. Onushchenko, *Quantum Size Effect in Semiconductor Microcrystals*, Sol. Stat. Comm. **56**, 921–924 (1985).

[5] K. Brunner, U. Bockelmann, G. Abstreiter, M. Walther, G. Böhm, G. Tränkle, G. Weimann, *Photoluminescence from a Single GaAs/AlGaAs Quantum Dot*, Phys. Ref. Lett. **69**, 3216 (1992).

[6] J. Y. Marzin, J. M. Gerard, A. Izrael, D. Barrier, G. Bastard, *Photoluminescence of Single InAs Quantum Dots Obtained by Self-Organized Growth on GaAs*, Phys. Rev. Lett. **73**, 716 (1994).

[7] A. Zrenner, *A Close Look on Single Quantum Dots*, J. Chem. Phys. **112**, 7790 (2000).

[8] G. Lampel, *Nuclear Dynamic Polarization by Optical Electronic Saturation and Optical Pumping in Semiconductors*, Phys. Rev. Lett. **20**, 491 (1968).

[9] A. I. Ekimov, V. I. Safarov, *Optical Detection of Dynamic Polarization of Nuclei in Semiconductors*, ZhETF Pis. Red. **15**, 257, 453 (1972), [JETP Lett. **15**, 179, 319 (1972)].

[10] M. I. D'yakonov, V. I. Perel', V. L. Berkovits, V. I. Safarov, *Optical Effects Due to Polarization of Nuclei in Semiconductors*, Zh. Eksp. Teor. Fiz. **67**, 1912 (1974), [Sov. Phys. JETP [**40**, 950 (1975)].

[11] V. L. Berkovits, C. Hermann, G. Lampel, A. Nakamura, V. I. Safarov, *Giant Overhauser Shift of Conduction-Electron Spin Resonance Due to*

Optical Polarization of Nuclei in Semiconductors, Phys. Rev. B **18**, 1776 (1978).

[12] V. L. Berkovits, A. I. Ekimov, V. I. Safarov, *Optical Orientation in a System of Electrons and Lattice Nuclei in Semiconductors - Experiment*, Zh. Eksp. Teor. Fiz. **65**, 346 (1973), [Sov. Phys. JETP **38**, 169 (1974)].

[13] M. I. D'yakonov, V. I. Perel', *Optical Orientation in a System of Electrons and Lattice Nuclei in Semiconductors - Theory*, Zh. Eksp. Teor. Fiz. **65**, 362 (1973), [Sov. Phys. JETP **38**, 177 (1974)].

[14] V. A. Novikov, V. G. Fleisher, Pis'ma Zh. Tekh. Fiz. **20**, 935 (1975).

[15] D. Paget, G. Lampel, B. Sapoval, V. I. Safarov, *Low Field Electron-Nuclear Spin Coupling in Gallium Arsenide under Optical Pumping Conditions*, Phys. Rev. B **15**, 5780 (1977).

[16] F. Meier, B. P. Zakharchenya (Editors), *Optical Orientation*, *Modern Problems in Condensed Matter Sciences*, volume 8, North-Holland, Amsterdam (1984).

[17] I. A. Merkulov, A. L. Efros, M. Rosen, *Electron Spin Relaxation by Nuclei in Semiconductor Quantum Dots*, Phys. Rev. B **65**, 205309 (2002).

[18] P.-F. Braun, X. Marie, L. Lombez, B. Urbaszek, T. Amand, P. Renucci, V. K. Kalevich, K. V. Kavokin, O. Krebs, P. Voisin, Y. Masumoto, *Direct Observation of the Electron Spin Relaxation Induced by Nuclei in Quantum Dots*, Phys. Rev. Lett. **94**, 116601 (2005).

[19] S. W. Brown, T. A. Kennedy, D. Gammon, E. S. Snow, *Spectrally Resolved Overhauser Shifts in Single GaAs/$Al_xGa_{1-x}As$ Quantum Dots*, Phys. Rev. B **54**, 17339 (1996).

[20] A. Imamoglu, E. Knill, L. Tian, P. Zoller, *Optical Pumping of Quantum-Dot Nuclear Spins*, Phys. Rev. Lett. **91**, 017402 (2003).

[21] B. Eble, O. Krebs, A. Lemaître, K. Kowalik, A. Kudelski, P. Voisin, B. Urbaszek, X. Marie, T. Amand, *Dynamic Nuclear Polarization of a Single Charge-Tunable InAs/GaAs Quantum Dot*, Phys. Rev. B **74**, 081306 (2006).

[22] A. I. Tartakovskii, T. Wright, A. Russell, V. I. Fal'ko, A. B. Van'kov, J. Skiba-Szymanska, I. Drouzas, R. S. Kolodka, M. S. Skolnick, P. W. Fry, A. Tahraoui, H.-Y. Liu, M. Hopkinson, *Nuclear Spin Switch in Semiconductor Quantum Dots*, Phys. Rev. Lett. **98**, 026806 (2007).

[23] P.-F. Braun, B. Urbaszek, T. Amand, X. Marie, O. Krebs, B. Eble, A. Lemaitre, P. Voisin, *Bistability of the Nuclear Polarization Created Through Optical Pumping in $In_{1-x}Ga_xAs$ Quantum Dots*, Phys. Rev. B **74**, 245306 (2006).

[24] I. A. Merkulov, *Formation of a Nuclear Spin Polaron under Optical Orientation in GaAs-Type Semiconductors*, Phys. Solid State **40**, 930 (1998).

[25] R. Oulton, A. Greilich, S. Y. Verbin, R. V. Cherbunin, T. Auer, D. R. Yakovlev, M. Bayer, I. A. Merkulov, V. Stavarache, D. Reuter, A. D. Wieck, *Subsecond Spin Relaxation Times in Quantum Dots at Zero Applied Magnetic Field Due to a Strong Electron-Nuclear Interaction*, Phys. Rev. Lett. **98**, 107401 (2007).

[26] M. Bortz, J. Stolze, *Exact Dynamics in the Inhomogeneous Central-Spin Model*, Phys. Rev. B **76**, 014304 (2007).

[27] A. Greilich, D. R. Yakovlev, A. Shabaev, A. L. Efros, I. A. Yugova, R. Oulton, V. Stavarache, D. Reuter, A. Wieck, M. Bayer, *Mode Locking of Electron Spin Coherences in Singly Charged Quantum Dots*, Science **313**, 341 (2006).

[28] A. Greilich, R. Oulton, E. A. Zhukov, I. A. Yugova, D. R. Yakovlev, M. Bayer, A. Shabaev, A. L. Efros, I. A. Merkulov, V. Stavarache, D. Reuter, A. Wieck, *Optical Control of Spin Coherence in Singly Charged (In,Ga)As/GaAs Quantum Dots*, Phys. Rev. Lett. **96**, 227401 (2006).

[29] A. Greilich, A. Shabaev, D. R. Yakovlev, A. L. Efros, I. A. Yugova, A. D. W. D. Reuter, M. Bayer, *Nuclei Induced Frequency Focusing of Electron Spin Coherence*, Science **317**, 1896–1899 (2007).

[30] V. L. Korenev, *Nuclear Spin Nanomagnet in an Optically Excited Quantum Dot*, Phys. Rev. Lett. **99**, 256405 (2007).

[31] A. Zrenner, L. V. Butlov, M. Hagn, G. Abstreiter, G. Böhm, G. Weimann, *Quantum Dots Formed by Interface Fluctuations in AlAs/GaAs Coupled Quantum Well Structures*, Phys. Rev. Lett. **72**, 3382 (1994).

[32] D. Gammon, E. S. Snow, B. V. Shanabrook, D. S. Katzer, D. Park, *Homogeneous Linewidths in the Optical Spectrum of a Single Gallium Arsenide Quantum Dot*, Science **273**, 87 (1996).

[33] O. Schilling, A. Forchel, M. Lebedev, *Deep Etched InGaAs/InP Quantum Dots with Strong Lateral Confinement Effects*, Superlattices and microstructures **16**, 261 (1994).

[34] M. Bayer, A. Schmidt, A. Forchel, F. Faller, T. L. Reinecke, P. A. Knipp, A. A. Dremin, V. D. Kulakovskii, *Electron-Hole Transitions Between States with Nonzero Angular Momenta in the Magnetoluminescence of Quantum Dots*, Phys. Rev. Lett. **74**, 3439 (1995).

[35] U. Woggon, *Optical Properties of Semiconductor Quantum Dots*, *Springer Tracts in Modern Physics*, volume 136, springer, Berlin (1997).

[36] B. Lounis, H. A. Bechtel, D. Gerion, P. Alivisatos, W. E. Moerner, *Photon Antibunching in Single CdSe/ZnS Quantum Dot Fluorescence*, Chem. Phys. Lett. **329**, 399 (2000).

[37] P. Chen, C. Piermarocchi, L. J. Sham, *Control of Exciton Dynamics in Nanodots for Quantum Operations*, Phys. Rev. Lett. **87**, 067401 (2001).

[38] U. Woggon, *Single Semiconductor Nanocrystals: Physics and Applications*, J. Appl. Phys. **101**, 081727 (2007).

[39] G. Schedelbeck, W. Wegscheider, M. Bichler, G. Abstreiter, *Coupled Quantum Dots Fabricated by Cleaved Edge Overgrowth: From Artificial Atoms to Molecules*, Science **278**, 1792 (1997).

[40] I. N. Stranski, L. V. Krastanow, Abhandlungen der Mathematisch-Naturwissenschaftlichen Klasse. Akademie der Wissenschaften und der Literatur in Mainz **146**, 797 (1939).

[41] L. Goldstein, F. Glas, J. Y. Marzin, *Growth by Molecular Beam Epitaxy and Characterization of InAs/GaAs Strained Layer Superlattices*, Appl. Phys. Lett. **47**, 1099 (1985).

[42] E. H. C. Parker, *The Technology and Physics of Molecular Beam Epitaxy*, Kluwer Academic / Plenum Publishers (1985).

[43] P. Michler (editor) *Single Quantum Dots: Fundamentals, Applications and New Concepts*, Topics in Applied Physics, Springer, Berlin Heidelberg (2003).

[44] T. Kipp, H. Welsch, C. Strelow, C. Heyn, D. Heitmann, *Optical Modes in Semiconductor Microtube Ring Resonators*, Phys. Rev. Lett. **96**, 077403 (2006).

[45] A. Greilich, M. Schwab, T. Berstermann, T. Auer, R. Oulton, D. R. Yakovlev, M. Bayer, V. Stavarache, D. Reuter, A. Wieck, *Tailored Quantum Dots for Entangled Photon Pair Creation*, Phys. Rev. B **73**, 045323 (2006).

[46] M. Bayer, A. Kuther, A. Forchel, A. Gorbunov, V. B. Timofeev, F. Schäfer, J. P. Reithmaier, T. L. Reinecke, S. N. Walck, *Electron and Hole G Factors and Exchange Interaction from Studies of the Exciton Fine Structure in $In_{0.60}Ga_{0.40}As$ Quantum Dots*, Phys. Rev. Lett. **82**, 1748 (1999).

[47] M. Bayer, G. Ortner, O. Stern, A. Kuther, A. A. Gorbunov, A. Forchel, P. Hawrylak, S. Fafard, K. Hinzer, T. L. Reinecke, S. N. Walck, J. P. Reithmaier, F. Klopf, F. Schäfer, *Fine Structure of Neutral and Charged Excitons in Self-Assembled In(Ga)As/(Al)GaAs Quantum Dots*, Phys. Rev. B **65**, 195315 (2002).

[48] T. Takagahara, *Theory of Exciton Doublet Structures and Polarization Relaxation in Single Quantum Dots*, Phys. Rev. B **62**, 16840 (2000).

[49] J. J. Finley, D. J. Mowbray, M. S. Skolnick, A. D. Ashmore, C. Baker, A. F. Monte, M. Hopkinson, *Fine Structure of Charged and Neutral Excitons in InAs-$Al_{0.6}Ga_{0.4}As$ Quantum Dots*, Phys. Rev. B **66**, 153316 (2002).

[50] K. V. Kavokin, *Symmetry of Anisotropic Exchange Interactions in Semiconductor Nanostructures*, Phys. Rev. B **69**, 075302 (2004).

[51] E. Blackwood, M. J. Snelling, R. T. Harley, S. R. Andrews, C. T. Foxon, *Exchange Interaction of Excitons in GaAs Heterostructures*, Phys. Rev. B **50**, 14246 (1994).

[52] A. Kuther, M. Bayer, A. Forchel, A. Gorbunov, V. B. Timofeev, F. Schäfer, J. P. Reithmaier, *Zeeman Splitting of Excitons and Biexcitons in Single $In_{0.60}Ga_{0.40}As$/GaAs Self-Assembled Quantum Dots*, Phys. Rev. B **58**, R7508 (1998).

[53] M. Grundmann, O. Stier, D. Bimberg, *InAs/GaAs Pyramidal Quantum Dots: Strain Distribution, Optical Phonons, and Electronic Structure*, Phys. Rev. B **52**, 11969 (1995).

[54] C. Pryor, *Eight-Band Calculations of Strained InAs/GaAs Quantum Dots Compared with One-, Four-, and Six-Band Approximations*, Phys. Rev. B **57**, 7190 (1998).

[55] R. Santoprete, B. Koiller, R. B. Capaz, P. Kratzer, Q. K. K. Liu, M. Scheffler, *Tight-Binding Study of the Influence of the Strain on the Electronic Properties of InAs/GaAs Quantum Dots*, Phys. Rev. B **68**, 235311 (2003).

[56] S. Schulz, S. Schumacher, G. Czycholl, *Tight-Binding Model for Semiconductor Quantum Dots with a Wurtzite Crystal Structure: From One-Particle Properties to Coulomb Correlations and Optical Spectra*, Phys. Rev. B **73**, 245327 (2006).

[57] L.-W. Wang, J. Kim, A. Zunger, *Electronic Structures of [110]-Faceted Self-Assembled Pyramidal InAs/GaAs Quantum Dots*, Phys. Rev. B **59**, 5678 (1999).

[58] X. Cartoixà, L.-W. Wang, *Microscopic Dielectric Response Functions in Semiconductor Quantum Dots*, Phys. Rev. Lett. **94**, 236804 (2005).

[59] M. Bayer, T. Gutbrod, A. Forchel, V. D. Kulakovskii, A. Gorbunov, M. Michel, R. Steffen, K. H. Wang, *Exciton Complexes in $In_xGa_{1-x}As/GaAs$ Quantum Dots*, Phys. Rev. B **58**, 4740 (1998).

[60] J. J. Finley, P. W. Fry, A. D. Ashmore, A. Lemaître, A. I. Tartakovskii, R. Oulton, D. J. Mowbray, M. S. Skolnick, M. Hopkinson, P. D. Buckle, P. A. Maksym, *Observation of Multicharged Excitons and Biexcitons in a Single InGaAs Quantum Dot*, Phys. Rev. B **63**, 161305 (2001).

[61] I. A. Akimov, A. Hundt, T. Flissikowski, F. Henneberger, *Fine Structure of the Trion Triplet State in a Single Self-Assembled Semiconductor Quantum Dot*, Appl. Phys. Lett. **81**, 4730 (2002).

[62] I. A. Akimov, K. V. Kavokin, A. Hundt, F. Henneberger, *Electron-Hole Exchange Interaction in a Negatively Charged Quantum Dot*, Phys. Rev. B **71**, 075326 (2005).

[63] S. Cortez, O. Krebs, S. Laurent, M. Sénès, X. Marie, P. Voisin, R. Ferreira, G. Bastard, J.-M. Gérard, T. Amand, *Optically Driven Spin Memory in N-Doped InAs-GaAs Quantum Dots*, Phys. Rev. Lett. **89**, 207401 (2002).

[64] S. Laurent, M. Sénès, O. Krebs, V. K. Kalevich, B. Urbaszek, X. Marie, T. Amand, P. Voisin, *Negative Circular Polarization as a General Property of N-Doped Self-Assembled InAs/GaAs Quantum Dots under Nonresonant Optical Excitation*, Phys. Rev. B **73**, 235302 (2006).

[65] I. E. Kozin, V. G. Davydov, I. V. Ignatiev, A. V. Kavokin, K. V. Kavokin, G. Malpuech, H.-W. Ren, M. Sugisaki, S. Sugou, Y. Masumoto, *Zero-Field Spin Quantum Beats in Charged Quantum Dots*, Phys. Rev. B **65**, 241312 (2002).

[66] R. Ferreira, G. Bastard, *Phonon-Assisted Capture and Intradot Auger Relaxation in Quantum Dots*, Apl. Phys. Lett. **74**, 2818 (1999).

[67] J. Hours, P. Senellart, E. Peter, A. Cavanna, J. Bloch, *Exciton Radiative Lifetime Controlled by the Lateral Confinement Energy in a Single Quantum Dot*, Phys. Rev. B **71**, 161306 (2005).

[68] N. Baer, C. Gies, J. Wiersig, F. Jahnke, *Luminescence of a Semiconductor Quantum Dot System*, Eur. Phys. J. B **50**, 411 (2006).

[69] M. Schwab, H. Kurtze, T. Auer, T. Berstermann, M. Bayer, J. Wiersig, N. Baer, C. Gies, F. Jahnke, J. P. Reithmaier, A. Forchel, M. Benyoucef, P. Michler, *Radiative Emission Dynamics of Quantum Dots in a Single Cavity Micropillar*, Phys. Rev. B **74**, 045323 (2006).

[70] T. Berstermann, T. Auer, H. Kurtze, M. Schwab, D. R. Yakovlev, M. Bayer, J. Wiersig, C. Gies, F. Jahnke, D. Reuter, A. D. Wieck, *Systematic Study of Carrier Correlations in the Electron-Hole Recombination Dynamics of Quantum Dots*, Phys. Rev. B **76**, 165318 (2007).

[71] D. Schwedt, C. Nacke, H. Stolz, S. Eshlaghi, S. Reuter, A. Wieck, *Spectrally Resolved Resonant Rayleigh Scattering from Excitons in GaAs Quantum Wells*, Phys. Rev. B **67**, 195303 (2003).

[72] G. Kocherscheidt, W. Langbein, U. Woggon, V. Savona, R. Zimmermann, D. Reuter, A. D. Wieck, *Resonant Rayleigh Scattering Dynamics of Excitons in Single Quantum Wells*, Phys. Rev. B **68**, 085207 (2003).

[73] V. K. Kalevich, I. A. Merkulov, A. Y. Shiryaev, K. V. Kavokin, M. Ikezawa, T. Okuno, P. N. Brunkov, A. E. Zhukov, V. M. Ustinov, Y. Masumoto, *Optical Spin Polarization and Exchange Interaction in Doubly Charged InAs Self-Assembled Quantum Dots*, Phys. Rev. B **72**, 045325 (2005).

[74] A. S. Bracker, E. A. Stinaff, D. Gammon, M. E. Ware, J. G. Tischler, A. Shabaev, A. L. Efros, D. Park, D. Gershoni, V. L. Korenev, I. A. Merkulov, *Optical Pumping of the Electronic and Nuclear Spin of Single Charge-Tunable Quantum Dots*, Phys. Rev. Lett. **94**, 047402 (2005).

[75] M. Ikezawa, B. Pal, Y. Masumoto, I. V. Ignatiev, S. Y. Verbin, I. Y. Gerlovin, *Submillisecond Electron Spin Relaxation in InP Quantum Dots*, Phys. Rev. B **72**, 153302 (2005).

[76] Y. Masumoto, S. Oguchi, B. Pal, M. Ikezawa, *Spin Dephasing of Doped Electrons in Charge-Tunable InP Quantum Dots: Hanle-Effect Measurements*, Phys. Rev. B **74**, 205332 (2006).

[77] T. C. Damen, L. Via, J. E. Cunningham, J. Shah, L. J. Sham, *Subpicosecond Spin Relaxation Dynamics of Excitons and Free Carriers in GaAs Quantum Wells*, Phys. Rev. Lett. **67**, 3432 (1991).

[78] M. E. Ware, E. A. Stinaff, D. Gammon, M. F. Doty, A. S. Bracker, D. Gershoni, V. L. Korenev, S. C. Badescu, Y. Lyanda-Geller, T. L. Reinecke, *Polarized Fine Structure in the Photoluminescence Excitation Spectrum of a Negatively Charged Quantum Dot*, Phys. Rev. Lett. **95**, 177403 (2005).

[79] P. Le Jeune *et al.*, *Proceedings of the 24th International Conference on the Physics of Semiconductors*, World Scientific Publishing, Singapore (1998).

[80] B. Baylac, X. Marie, T. Amand, M. Brousseau, J. Barrau, Y. Shekun, *Hole Spin Relaxation in Intrinsic Quantum Wells*, Surface Science **326**, 161–166 (1995).

[81] V. K. Kalevich, M. Paillard, K. V. Kavokin, X. Marie, A. R. Kovsh, T. Amand, A. E. Zhukov, Y. G. Musikhin, V. M. Ustinov, E. Vanelle, B. P. Zakharchenya, *Spin Redistribution Due to Pauli Blocking in Quantum Dots*, Phys. Rev. B **64**, 045309 (2001).

[82] B. Pal, M. Ikezawa, Y. Masumoto, I. V. Ignatiev, *Millisecond-Range Electron Spin Memory in Singly-Charged InP Quantum Dots*, J. Phys. Soc. Jpn. **75**, 54702 (2006).

[83] B. Pal, S. Y. Verbin, I. V. Ignatiev, M. Ikezawa, Y. Masumoto, *Nuclear Spin Effects in Negatively Charged InP Quantum Dots*, Phys. Rev. B **75**, 125322 (2007).

[84] M. Sénès, B. Urbaszek, X. Marie, T. Amand, J. Tribollet, F. Bernardot, C. Testelin, M. Chamarro, J. M. Gérard, *Exciton Spin Manipulation in InAs/GaAs Quantum Dots: Exchange Interaction and Magnetic Field Effects*, Phys. Rev. B **71**, 115334 (2005).

[85] A. L. Ivanov, P. Borri, W. Langbein, U. Woggon, *Radiative Corrections to the Excitonic Molecule State in GaAs Microcavities*, Phys. Rev. B **69**, 075312 (2004).

[86] S. V. Gupalov, E. L. Ivchenko, A. V. Kavokin, *Fine Structure of Localized Exciton Levels in Quantum Wells*, JETP **86**, 388–394 (1998).

[87] R. I. Dzhioev, B. P. Zakharchenya, V. L. Korenev, M. V. Lazarev, *Interaction Between the Exciton and Nuclear Spin Systems in a Self-Organized Ensemble of InP/InGaP Size-Quantized Islands*, Phys. Solid State **41**, 2014 (1999).

[88] M. Grundmann, D. Bimberg, *Theory of Random Population for Quantum Dots*, Phys. Rev. B **55**, 9740 (1997).

[89] K. Gündoğdu, K. C. Hall, T. F. Boggess, D. G. Deppe, O. B. Shchekin, *Efficient Electron Spin Detection with Positively Charged Quantum Dots*, Appl. Phys. Lett. **84**, 2793 (2004).

[90] A. Abragam, *The Principles of Nuclear Magnetism*, Clarendon Press, Oxford (new edition 1983).

[91] A. V. Khaetskii, D. Loss, L. Glazman, *Electron Spin Decoherence in Quantum Dots Due to Interaction with Nuclei*, Phys. Rev. Lett. **88**, 186802 (2002).

[92] D. Litvinov, A. Rosenauer, D. Gerthsen, P. Kratzert, M. Rabe, F. Henneberger, *Influence of the Growth Procedure on the Cd Distribution in CdSe/ZnSe Heterostructures: Stranski-Krastanov versus Two-Dimensional Islands*, Appl. Phys. Lett. **81**, 640–642 (2002).

[93] A. Hundt, J. Puls, F. Henneberger, *Spin Properties of Self-Organized Diluted Magnetic $Cd_{1-x}Mn_xSe$ Quantum Dots*, Phys. Rev. B **69**, 121309(R) (2004).

[94] I. A. Akimov, D. H. Feng, F. Henneberger, *Electron Spin Dynamics in a Self-Assembled Semiconductor Quantum Dot: The Limit of Low Magnetic Fields*, Phys. Rev. Lett. **97**, 056602 (2006).

[95] R. V. Cherbunin, I. V. Ignatiev, T. Auer, A. Greilich, R. Oulton, G. G. Kozlov, D. Reuter, A. D. Wieck, D. R. Yakovlev, M. Bayer, *Manifestation of Hyperfine Interaction Between Electron and Nuclear Spins in Singly-Charged InGaAs/GaAs Quantum Dots* (2007), submitted to Phys. Rev. B.

[96] A. W. Overhauser, *Polarization of Nuclei in Metals*, Phys. Rev. **92**, 411 (1953).

[97] D. Gammon, A. L. Efros, T. A. Kennedy, M. Rosen, D. S. Katzer, D. Park, S. W. Brown, V. L. Korenev, I. A. Merkulov, *Electron and Nuclear Spin Interactions in the Optical Spectra of Single GaAs Quantum Dots*, Phys. Rev. Lett. **86**, 5176 (2001).

[98] D. H. Feng, I. A. Akimov, F. Henneberger, *Nonequilibrium Nuclear-Electron Spin Dynamics in Semiconductor Quantum Dots*, Phys. Rev. Lett. **99**, 036604 (2007).

[99] P. Maletinsky, A. Badolato, A. Imamoglu, *Dynamics of Quantum Dot Nuclear Spin Polarization Controlled by a Single Electron*, Phys. Rev. Lett. **99**, 056804 (2007).

[100] M. I. Darby, *Tables of the Brillouin Function and of the Related Function for the Spontaneous Magnetization*, Brit. J. Appl. Phys. **18**, 1415–1417 (1967).

[101] C. Kittel, *Introduction to Solid State Physics, 8^{th} Edition*, Wiley & Sons (2005).

[102] C. W. Lai, P. Maletinsky, A. Badolato, A. Imamoglu, *Knight-Field-Enabled Nuclear Spin Polarization in Single Quantum Dots*, Phys. Rev. Lett. **96**, 167403 (2006).

[103] M. I. Dyakonov, V. I. Perel, Zh. Eksp. Teor. Fiz. **68**, 1514 (1975).

[104] D. Paget, Ph.D. thesis, Université de Paris Sud (1975).

[105] W. D. Knight, *Nuclear Magnetic Resonance Shift in Metals*, Phys. Rev. **76**, 1259 (1949).

[106] M. Gueron, *Density of the Conduction Electrons at the Nuclei in Indium Antimonide*, Phys. Rev. **135**, A200 (1964).

[107] W. Hanle, *Über Magnetische Beeinflussung der Polarisation der Resonanzfluoreszenz*, Z. Phys. **30**, 93–105 (1924).

[108] R. J. Epstein, D. T. Fuchs, W. V. Schoenfeld, P. M. Petroff, D. D. Awschalom, *Hanle Effect Measurements of Spin Lifetimes in InAs Self-Assembled Quantum Dots*, Appl. Phys. Lett. **78**, 733 (2001).

[109] I. Yugova, A. Greilich, E. A. Zhukov, D. Reuter, A. Wieck, D. R. Yakovlev, M. Bayer, *Exciton Fine Structure in InGaAs/GaAs Quantum Dots Revisited by Pump-Probe Faraday Rotation*, Phys. Rev. B **75**, 195325 (2007).

[110] J. Berezovsky, M. H. Mikkelsen, O. Gywat, N. G. Stoltz, L. A. Coldren, D. D. Awschalom, *Nondestructive Optical Measurements of a Single Electron Spin in a Quantum Dot*, Science **314**, 1916 (2006).

[111] H. Christ, J. I. Cirac, G. Giedke, *Quantum Description of Nuclear Spin Cooling in a Quantum Dot*, Phys. Rev. B **75**, 155324 (2007).

[112] R. V. Cherbunin, S. Y. Verbin, T. Auer, D. R. Yakovlev, D. Reuter, A. D. Wieck, I. Y. Gerlovin, I. V. Ignatiev, M. Bayer, *Dynamics of the Nuclear Spin Polarization by Optically Oriented Electrons in a (In,Ga)As/GaAs Quantum Dot Ensemble*, in preparation (2008).

[113] P. Maletinsky, C. W. Lai, A. Badolato, A. Imamoglu, *Nonlinear Dynamics of Quantum Dot Nuclear Spins*, Phys. Rev. B **75**, 035409 (2007).

[114] A. Russell, V. I. Falko, A. I. Tartakovskii, M. S. Skolnick, *Bistability of Optically Induced Nuclear Spin Orientation in Quantum Dots*, Phys. Rev. B **76**, 195310 (2007).

[115] M. N. Makhonin, A. I. Tartakovskii, A. B. Vankov, I. Drouzas, T. Wright, J. Skiba-Szymanska, A. Russell, V. I. Falko, M. S. Skolnick, H.-Y. Liu, M. Hopkinson, *Long Nuclear Spin Polarization Decay Times Controlled by Optical Pumping in Individual Quantum Dots*, Phys. Rev. B **77**, 125307 (2008).

[116] M. Kroutvar, Y. Ducommun, D. Heiss, M. Bichler, D. Schuh, G. Abstreiter, J. J. Finley, *Optically Programmable Electron Spin Memory Using Semiconductor Quantum Dots*, Nature **432**, 81–84 (2004).

[117] S. I. Vasil'ev, L. A. Kalmykova, I. A. Merkulov, *Numerical Simulation of a Phase Transition in the Nuclear Spin System of Gallium Arsenide with Adiabatic Demagnetization*, JETP Lett. **37**, 77 (1983).

[118] I. A. Merkulov, D. R. Yakovlev, K. V. Kavokin, G. Mackh, W. Ossau, A. Waag, G. Landwehr, *Hierarchy of Relaxation Times in the Formation of an Excitonic Magnetic Polaron in (CdMn)Te*, JETP Letters **62**, 335 (1995).

[119] M. Bortz, J. Stolze, *Spin and Entanglement Dynamics in the Central-Spin Model with Homogenous Couplings*, J. Stat. Mech. **P06018** (2007).

[120] B. Urbaszek, P.-F. Braun, T. Amand, O. Krebs, T. Belhadj, A. Lemaítre, P. Voisin, X. Marie, *Efficient Dynamical Nuclear Polarization in Quantum Dots: Temperature Dependence*, Phys. Rev. B **76**, 201301(R) (2007).

[121] J. Lu, M. J. R. Hoch, P. L. Kuhns, W. G. Moulton, Z. Gan, A. P. Reyes, *Nuclear Spin-Lattice Relaxation in N-Type Insulating and Metallic GaAs Single Crystals*, Phys. Rev. B **74**, 125208 (2006).

[122] M. Paillard, X. Marie, P. Renucci, T. Amand, A. Jbeli, J. M. Gérard, *Spin Relaxation Quenching in Semiconductor Quantum Dots*, Phys. Rev. Lett. **86**, 1634–1637 (2001).

[123] R. I. Dzhioev, V. L. Korenev, *Stabilization of the Electron-Nuclear Spin Orientation in Quantum Dots by the Nuclear Quadrupole Interaction*, Phys. Rev. Lett. **99**, 037401 (2007).

[124] R. I. Dzhioev, V. L. Korenev, *Stabilizing Effect of Nuclear Quadrupole Interaction on the Polarization of Electron-Nuclear Spin System in a Quantum Dot*, arXiv:cond-mat/0702010v4 (2007).

[125] D. Klauser, W. A. Coish, D. Loss, *Nuclear Spin State Narrowing Via Gate-Controlled Rabi Oscillations in a Double Quantum Dot*, Phys. Rev. B **73**, 205302 (2006).

[126] R. Oulton, S. Y. Verbin, T. Auer, R. V. Cherbunin, A. Greilich, D. R. Yakovlev, M. Bayer, D. Reuter, A. Wieck, *Sub-Second Electron Spin Lifetimes in Quantum Dots at Zero Applied Magnetic Field Due to Alignment of QD Nuclei*, phys. stat. sol. (b) **243**, 3922–3927 (2006).

List of Publications

1. G. Baldassarri Höger von Högersthal, D. Fröhlich, M. Kulka, **Th. Auer**, M. Bayer, H. Stolz, *Acoustic and optical phonon scattering of the 1S yellow orthoexciton in Cu_2O*, Phys. Rev. B **73**, 035202 (2006)

2. A. Greilich, M. Schwab, T. Berstermann, **T. Auer**, R. Oulton, D. R. Yakovlev, M. Bayer, V. Stavarache, D. Reuter, A. Wieck, *Tailored Quantum Dots for Entangled Photon Pair Creation*, Phys. Rev. B **73**, 045323 (2006)

3. M. Schwab, H. Kurtze, **T. Auer**, T. Berstermann, M. Bayer, J. Wiersig, N. Baer, C. Gies, F. Jahnke,J. P. Reithmaier, A. Forchel, M. Benyoucef, P. Michler, *Radiative emission dynamics of quantum dots in a single cavity micropillar*, Phys. Rev. B **74**, 045323 (2006)

4. R. Oulton, S. Yu. Verbin, **T. Auer**, R. V. Cherbunin, A. Greilich, D. R. Yakovlev, M. Bayer, D. Reuter, A. Wieck, *Sub-second electron spin lifetimes in quantum dots at zero applied magnetic field due to alignment of quantum dot nuclei*, Phys. Stat. Sol. (b) **243**, 3922 (2006)

5. T. Berstermann, **T. Auer**, H. Kurtze, M. Schwab, D. R. Yakovlev, M. Bayer, J. Wiersig, C. Gies, F. Jahnke, D. Reuter, A. D. Wieck, *Systematic study of carrier correlations in the electron-hole recombination dynamics of quantum dots*, Phys. Rev. B **76**, 165318 (2007)

6. R. Oulton, A. Greilich, S. Yu. Verbin, R. V. Cherbunin, **T. Auer**, D. R. Yakovlev, M. Bayer, I. A. Merkulov, V. Stavarache, D. Reuter, A. D. Wieck, *Subsecond spin relaxation times in quantum dots at zero applied magnetic field due to a strong electron-nuclear interaction*, Phys. Rev. Lett. **98**, 107401 (2007)

7. R. V. Cherbunin, I. V. Ignatiev, **T. Auer**, A. Greilich, R. Oulton, G. G. Kozlov, D. Reuter, A. D. Wieck, D. R. Yakovlev, M. Bayer, *Manifestation of hyperfine interaction between electron and nuclear spins in singly-charged InGaAs/GaAs quantum dots*, submitted to Phys. Rev. B (2007)

8. **T. Auer**, R. Oulton, A. Bauschulte, D. R. Yakovlev, M. Bayer, S. Yu. Verbin, R. V. Cherbunin, D. Reuter, A. D. Wieck, *The Knight field and the local nuclear dipole-dipole field in an (In,Ga)As quantum dot ensemble*, submitted to Phys. Rev. B (2008)

9. R. V. Cherbunin, S. Yu. Verbin, **T. Auer**, D. R. Yakovlev, D. Reuter, A. D. Wieck, I. Ya. Gerlovin, I. V. Ignatiev, M. Bayer, *Dynamics of the nuclear spin polarization by optically oriented Electrons in a (In,Ga)As/GaAs quantum dot ensemble*, in preparation

Danksagung

Zum guten Schluß gebührt zahlreichen Menschen Dank, die auf unterschiedliche Weise dazu beigetragen haben, daß diese Arbeit gelingen konnte.

Ich danke Herrn Prof. Dr. Manfred Bayer für die Aufnahme in seine Arbeitsgruppe, für die Möglichkeit meine Forschungen in seinen herausragend ausgestatteten Laboren durchführen zu dürfen und für die Hilfe und Unterstützung, die ich erfahren habe.
Danke Herrn Prof. Dr. Metin Tolan für die Übernahme der Zweitkorrektur.
Ebenfalls danken möchte ich Herrn Dr. Dmitri R. Yakovlev für die Unterstützung und Herrn Prof. Dietmar Fröhlich, der mich in meinen ersten Monaten in Dortmund in die hohen Künste der optischen Spektroskopie, des Umgangs mit Helium, Stickstoff und Kryostaten und ganz allgemein der experimentellen Forschung einführte.

Ich danke der Sprecherin des Graduiertenkollegs „Materialeigenschaften und Konzepte für die Quanteninformationsverarbeitung“, Frau Prof. Dr. Ulrike Woggon, für die Aufnahme in den Kreis der Stipendiaten des Graduiertenkollegs.

Vielen Dank Herrn Prof. Dr. Andreas D. Wieck und seinen Mitarbeitern am Lehrstuhl für Angewandte Festkörperphysik der Universität Bochum für die „11955-900“. Ich kann sagen: Dieser Pudel hat nicht nur einen Kern.

Spasibo meinen russischen Kollegen, Prof. Dr. Sergey Yu. Verbin und Roman V. Cherbunin mit denen ich im Labor zusammenarbeiten durfte! Es waren lange Winternächte, in denen Sergey und ich versuchten, dem Elektronen-Kernspinsystem seine Geheimnisse abzutrotzen. Wir hatten eine angenehme und fruchtbare Zusammenarbeit – die Daten, die wir gemeinsam gesammelt haben, bilden jetzt den Kern dieser Arbeit.

Auch mit Roman hatte ich eine abwechslungsreiche Zusammenarbeit im Labor. Seine „special box“ ist ein lieb gewonnener Baustein im Kernspin-Aufbau geworden.

Ein dickes Dankeschön an Klaus Wiegers und Michaela Wäscher sowie Thomas Stöhr! Michaela war immer offen für sämtliche Fragen zu Verwaltung, Formularen und Anträgen. Sicherlich hat sie uns das Leben oft erleichtert, ohne daß wir es gemerkt haben!

Immer wenn es Herausforderungen technischer Natur zu lösen galt, war Klaus zur Stelle. Mehr als einmal wurde er mit der Frage konfrontiert: „Warum ist der RTI außen kalt und nicht innen?“ – und Klaus wußte immer eine Antwort. Bei vielen Schwierigkeiten war augenblicklich klar, daß Herrn Fröhlichs Worte einmal mehr zutrafen: „Das kann nur Wiegers!“

Thomas hat in einer im wahrsten Sinne des Wortes brenzligen Situation die verschmorte „special box“ wieder hergerichtet und so die knapp bemessene Meßzeit gerettet.

Danke Ilya Akimov, der sich dafür bereit erklärt hat bei meiner Promotionsprüfung als Vertreter der wissenschaftlichen Mitarbeiter teilzunehmen und für Diskussionen.

Herzlichen Dank an Dr. Ruth Oulton! Ruth, Du hast mich für das Thema Kernspins begeistert und mich immer angespornt und ermutigt. Früh morgens um halb sieben haben wir zusammen die entscheidende Messung mit 500 ms Memory-Zeit gestartet. Danke auch für das Korrekturlesen der Arbeit und die hilfreichen Ratschläge. Vielen Dank für die vielen guten Gespräche, die schönen Unternehmungen und die wertvolle Unterstützung und ganz allgemein für die gute gemeinsame Zeit in Dortmund und darüber hinaus.

Ein Dankeschön meinen Kollegen von der Experimentellen Physik II, den ehemaligen wie den gegenwärtigen. Hannes Kurtze für gute Gespräche, „extrem Voraussetzungsreiches“, Feierabendbiere und das Korrekturlesen der Arbeit, Alex Greilich für die Hilfe in allen Laborfragen, den gemeinsamen Weg zum „Zwei-Stern-Taucher“ und für’s gegenseitige Draufhauen beim Box-Training, Thorsten Berstermann für die Zusammenarbeit bei den nichtexponentiellen Zerfällen, das Korrekturlesen der Arbeit und die gemeinsamen Biere, Michael Gerbracht für abendliche Unternehmungen, Matthias Schwab für die schnelle Aufnahme in das soziale Herz der Gruppe und die Grillpartys, Marko Kulka für die gute Zusammenarbeit in Sachen Kupferoxidul, meinem Diplomanden Ansgar Bauschulte sowie

Martin Kneip, Lucy Fokina, Benjamin Kaminski, Jan Brandt, Christian Sandfort, Gregor Bartsch, Marc Assmann, Stefan Spatzek, Markus Wiemann, Marcel Arlt, Ingo Sänger, Cedric Bardot, Giorgio Baldassarri Höger von Högersthal, Oliver Schöps, Evgeny Zhukov, Alexey Scherbakov.

Vielen Dank meinen Eltern für ihre Unterstützung und Hilfe. Herzlichen Dank auch meinem Bruder Ulrich für unterhaltsame Telefonate, erholsame Ansitze und eine immer hervorragende Bewirtung.

Index